SYNTHESIS OF INDIUM PHTHALOCYANINES FOR PHOTODYNAMIC ANTIMICROBIAL CHEMOTHERAPY AND PHOTO-OXIDATION OF POLLUTANTS

A thesis submitted in fulfilment of the requirements for the degree of

MASTERS IN SCIENCE

Of

RHODES UNIVERSITY

By

AZOLE SINDELO

MARCH 2018

DEDICATION

To my parents:

Nobuntu and Zola

For their unwavering support and love

And to my siblings

Siyaxolisa, Sakhekile and Chulumanco

ACKNOWLEDGEMENTS

I would like to express my deepest appreciation to my supervisor, Distinguished Prof T. Nyokong for her expertise, guidance, patience and support. For teaching us to celebrate small successes. I am grateful for the oppurtunities she has given me and for sending me to Shinshu University in Japan for two months and for the conferences, I attended under her guidance. I would like thank Dr Mack and Dr Britton for their support and assistance throught my studies. I would like to thank Ms Gail Cobus for her patience and amazing her with administrative work.

I would like to thank the S22 research group for being supportive and never producing a dull day. To the lab manager through my studies, thank you for lending a helping hand. To all the administrative, technical and supporting staff of Chemistry department (Rhodes University), thank you for that prompt email, warm coffee and efficient responses.

The Department of Science and Technology (DST) and National Research Foundation (NRF) for funding.

To my friends for motivating when I am feeling down, for the entertainment and the never-ending debates, thank you for being awesome. I am grateful to my family, for being with me in this journey. Finally yet importantly, I would like to thank God for his Grace. Thank you all.

ABSTRACT

Indium (III) octacarboxyl phthalocyanine (ClInOCPc) alone and when conjugated to magnetic nanoparticles (MNP-ClInOCPc), 2(3),9(10),16(17),23(24)-octapyridylsulfanyl phthalocyaninato chloroindium (III) (ClInOPyPc) and its quaternized derivative 2(3),9(10),16(17),23(24)-octamethylpyridylsulfanyl phthalocyaninato chloroindium (III) (ClInOMePyPc) were synthesized. All Pcs were tested for both photodynamic antimicrobial chemotherapy (PACT) of an unknown water sample and photo-degradation of methyl red (MR). The singlet quantum yield (Φ_{Δ}) for the ClInOCPc and MNP-ClInOCPc in PAN polymer fibers were 0.36 and 0.20 respectively using ADMA as a quencher in water. The photo-inactivation of bacteria in a water sample with unknown microbes was tested, with the MNP-ClInOCPc inactivating 90.6 % of the microbes and the ClInOCPc with 84.8 %. When embedded to the polymer, there was 48% bacterial clearance for ClInOCPc and 64% clearance for the MNP-ClInOCPc. The rate of degradation of MR increased with decrease of the MR concentration, with the MNP-ClInOCPc having the fastest rate. For ClInOPyPc and ClInOMePyPc, the singlet quantum yields were 0.46 and 0.33 in dimethylformamide (DMF), respectively. The PACT activity of ClInOMePyPc (containing 8 positive charges) was compared to those of 9(10),16(17),23(24)-tri-N-methyl-4-pyridylsulfanyl-2(3)-(4-aminophenoxy) phthalocyaninato chloro indium (III) triiodide (**1**) (containing 3 positive charges) and 2-[4-(N-methylpyridyloxy) phthalocyaninato] chloroindium (III) iodide (**2**) (containing 4 positive charges). When comparing ClInOMePyPc, **1** and **2**, the largest log reduction for *E. coli* were obtained for complex **2** containing four positive charges hence showing it is not always the charge that determines the PACT activity, but the bridging atom in the phthalocyanine plays a role.

TABLE OF CONTENTS

LIST OF ABBREVIATIONS

A/abs	**-**	**Absorbance**
ADMA	**-**	**Anthracene-9,10-bis-methylmalonate**
AOP	**-**	**Advanced oxidation process**
APTES	**-**	**3-aminopropyl triethoxysilane**
C. albican	**-**	**Candida albican**
CFU	**-**	**Colony forming unit**
ClInOCPc	**-**	**indium (III) octacarboxyl phthalocyanine**
ClInOPyPc	**-**	**octapyridylsulfanyl phthalocyaninato chloroindium (III)**
ClInOMePyPc	**-**	**octamethylpyridylsulfanyl phthalocyaninato chloroindium (III)**
DBU	**-**	**1,8-diazabicyclo[5.4.0]undec-7-ene**
DCM	**-**	**Dichloromethane**
DLS	**-**	**Dynamic light scattering**
DMF	**-**	**N,N-Dimethylformamide**
DMS	**-**	**Dimethyl sulfate**
DMSO-d6	**-**	**Deuterated dimethylsulfoxide**
DPBF	**-**	**Diphenylisobenzofuran**
E. coli	**-**	**Escherichia coli**
EDC	**-**	**1-Ethyl-3-(3-dimethylaminopropyl)carbodiimide**

EDX	-	**Energy dispersive x-ray spectroscopy**
F	-	**Fluorescence**
H_2Pc	-	**Metal Free phthalocyanine**
1H NMR	-	**Proton nuclear magnetic resonance**
HOMO	-	**Highest occupied molecular orbital**
IC	-	**Internal conversion**
IR	-	**Infrared**
ISC	-	**Intersystem crossing**
LUMO	-	**Lowest unoccupied molecular orbital**
MPc	-	**Metallophthalocyanine**
MNPs	-	**Magnetic nanoparticles**
MR	-	**Methyl red**
MRSA	-	**Methicilin-resistant staphylococcus aureus**
NHS	-	**N-hydroxysuccinimide**
NIR	-	**Near infrared region**
NPs	-	**Nanoparticles**
PACT	-	**Photodynamic antimicrobial chemotherapy**
PAN	-	**Polyacrylonitrile**

PBS	**-**	**Phosphate-buffer saline**
Pc	**-**	**Phthalocyanine**
PDT	**-**	**Photodynamic therapy**
PS	**-**	**Photosensitizer**
ROS	**-**	**Reactive oxygen species**
S. aureus	**-**	**Staphylococcus aureus**
SEM	**-**	**Scanning electron microscope**
TCSPC	**-**	**Time-correlated single photon counting**
TEOS	**-**	**Tetraethyl orthosilicate**
TEM	**-**	**Transmission electron microscope**
UV/Vis	**-**	**Ultraviolet/visible**
XRD	**-**	**X-ray powder diffraction**

LIST OF SYMBOLS

α	-	**non-peripheral position**
β	-	**Peripheral position**
ε	-	**Molar extinction coefficient**
λ	-	**Wavelength**
λ_{abs}	-	**Absorbance**
λ_{em}	-	**Emission**
λ_{exc}	-	**Excitation**
τ_F	-	**fluorescence lifetime**
τ_T	-	**triplet lifetime**
Φ_F	-	**fluorescence quantum yield**
Φ_T	-	**triplet quantum yield**
Φ_Δ	-	**singlet oxygen quantum yield**
$^1O_2$	-	**triplet molecular molecular oxygen**
$^3O_2$	-	**triplet molecular molecular oxygen**
t	-	**time**

CHAPTER ONE

INTRODUCTION

1.1 Phthalocyanines

1.1.1 History and Structure

Blue/green organic compounds which were later named phthalocyanines (Pcs) were first observed in 1907 by Bruan and Tcherniac, when a phthalimide was reacted with acetic acid to form a dark and insoluble product that was incorrectly named as *ortho*-cyanobenzamide [1, 2]. Twenty years later at Fribourg University, de Diesbach and von der Weid produced the first metalled Pc (copper phthalocyanine), when an *ortho*-dibromobenzene was reacted with cupper cyanide [2, 3]. In 1928, Scottish Dyes Ltd (later called Imperial Chemical Industries (ICI)) filed the first patent on the preparation of Pcs by reacting phthalic anhydride with ammonia in an enamelled cast-iron crucible that was cracked resulting in the production of a stable and insoluble greenish iron phthalocyanine [4]. At Imperial College, Linstead and co-workers determined the structure of the Pc using various characterization methods such as elemental analysis, Robertson and co-workers using x-ray crystallography determined the correct structure for metal free Pc (H_2Pc) (Fig. 1.1A) and metalloPc (MPc) (Fig. 1.1B) [5]. They showed that the compound is a symmetrical macrocycle consisting of four isoindoline units (Fig. 1.1) linked by aza nitrogen with a central cavity for hosting various metals or metalloids [6]. Linstead coined the term phthalocyanine from the Greek language, where the prefix phthal, arise from naphtha (rock oil) to reiterate the influence of numerous phthalic-acid-derivitives as starting materials, and the suffix cyanine from the blue colour [7].

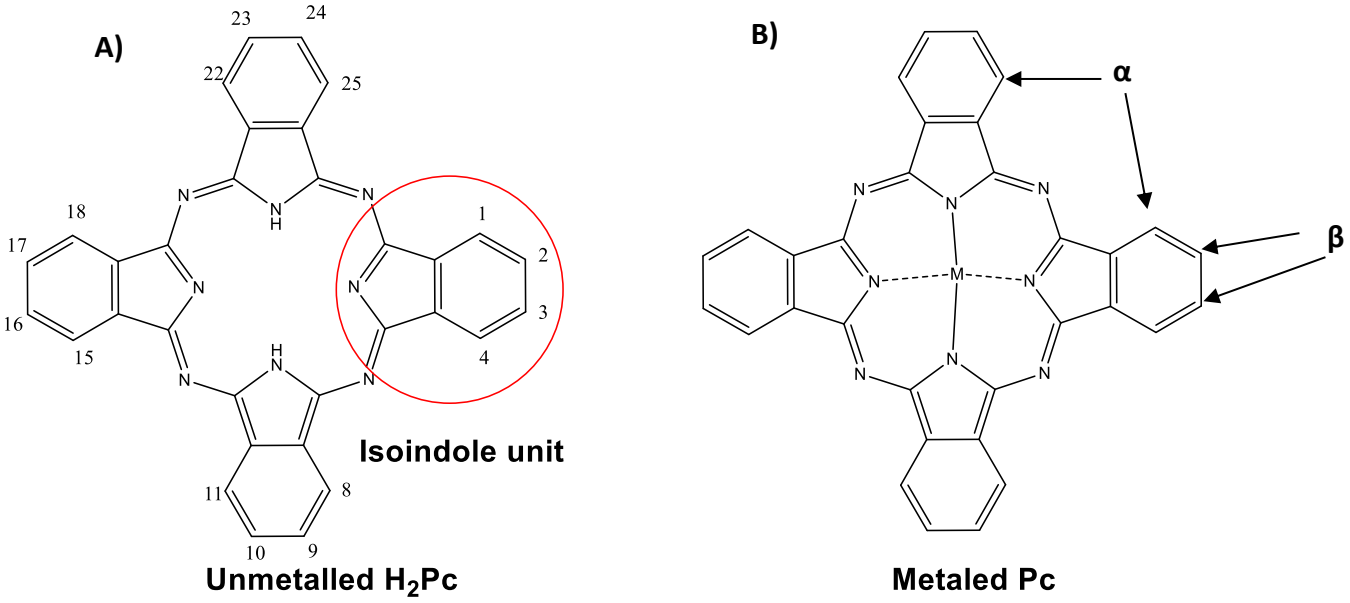

Figure 1.1: Illustration of the structure of phthalocyanines with: A) showing an H_2Pc and each of the possible sites of substitution at the benzo-positions of Pcs and B) showing the co-ordination of metal ions in Pcs.

The non-peripheral positions on the Pc ring are located at 1, 4, 8, 11, 15, 18, 22, and 25 (Fig.1.1A); designate as α-positions, while those located at positions 2, 3, 9, 10, 16, 17, 23, and 24 (Fig. 1.1A) are regarded as β-substituents [8, 9]. In this work, neutral and positively charged octa-substituted phthalocyanines will be synthesized for use in photodynamic antimicrobial chemotherapy (PACT) and degradation of pollutants using methyl red as an example.

1.1.2 Synthesis of Octa-substitued phthalocyanines

Octa-substituted phthalocyanine (Scheme 1.1) may be obtained by the cyclotetramerization of di-substituted phthalonitrile (**a**) in the presence of a metal salt and using a base as a catalyst. Alternatively, octa-subtitute using urea (or a suitable solvent), metal salt and pyromellitic dianhydride (**b**) as the precursor under a reflux, followed by hydrolysis in acid may be employed only for octacarboxyl Pc. The latter method was employed in this work for the synthesis of indium (III) octacarboxyl phthalocyanine (ClInOCPc).

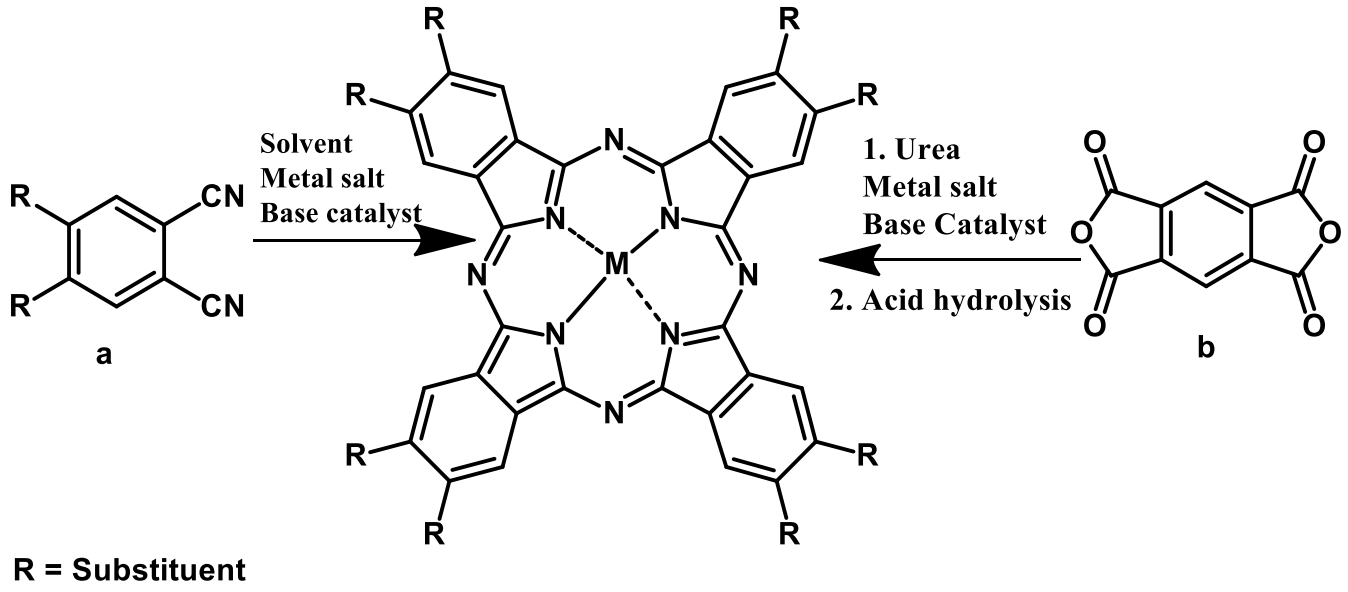

Scheme 1.1: A general synthetic pathway of octa-substituted phthalocyanines.

For water solubility, hydrophilic substituents such as carboxylate and sulfonates are employed as ring substituents [10]. Water-soluble ClInOCPc is employed in this work. Water solubility is important for biological work.

Water solubility can also be achieved by quarternization of Pcs. Phthalocyanines that have amine and pyridine derivatives can be quaternized forming positively charged derivatives. The methylation of these complexs can be achieved using common solvents such as methyl iodide

(or any halogenated alkyl solvent) and dimethylsulfate [11, 12]. Generally, to obtain the cationic phthalocyanines, a neutral Pcs is first formed then the compound is subjected to a methylating agent as the final step of the synthetic pathway (Scheme 1.2) [13]. Novel octamethylpyridylsulfanyl phthalocyaninato chloroindium (III) (ClInOMePyPc) was formed by the quaternization of octapyridylsulfanyl phthalocyaninato chloroindium(III) (ClInOPyPc) in this work. Structures of the complexes used in this work are shown in Fig. 1.2, ClInOCPc is known [14].

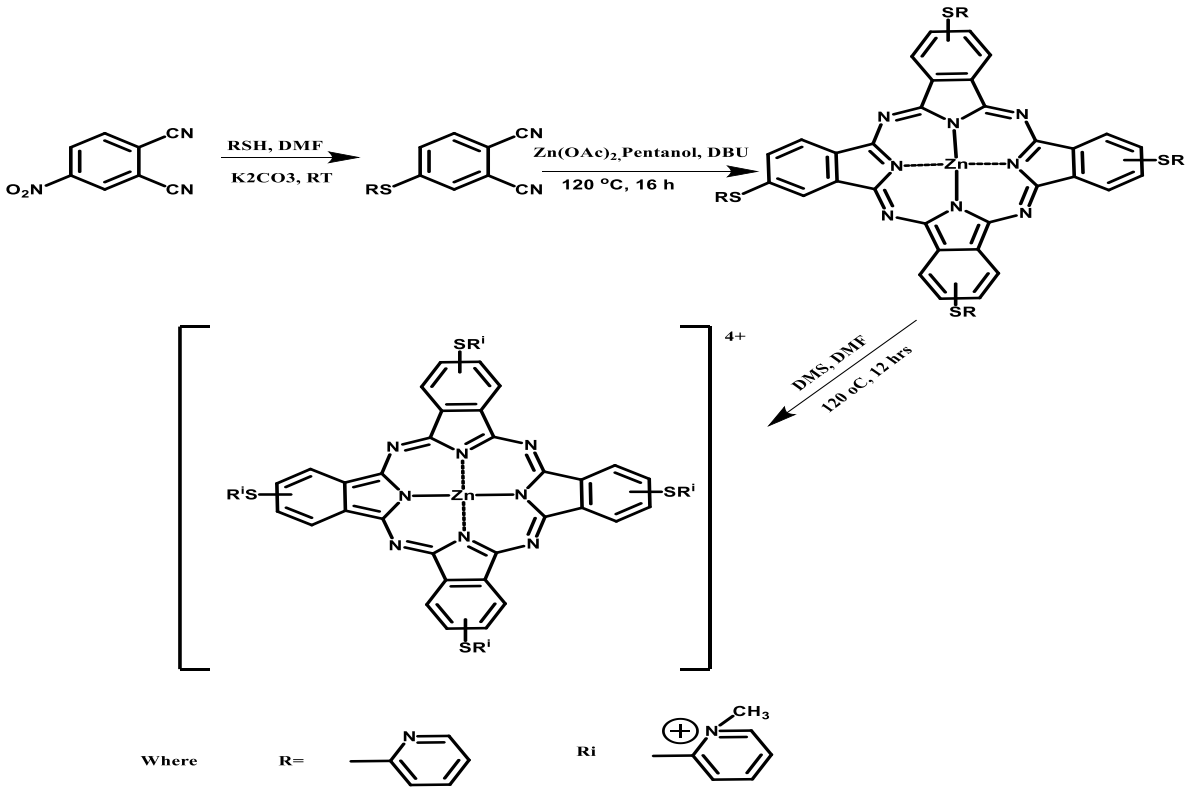

Scheme 1.2: Examples of cationic water-soluble phthalocyanines, where DMS = Dimethyl Sulfate, DMF = N,N-Dimethylformamide and DBU = 1,8-diazabicyclo[5.4.0]undec-7-ene [13].

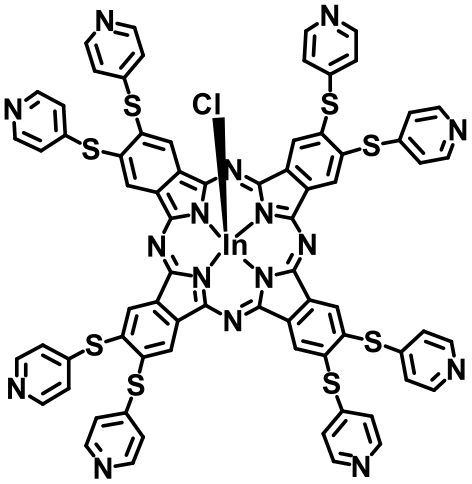

ClInOPyPc

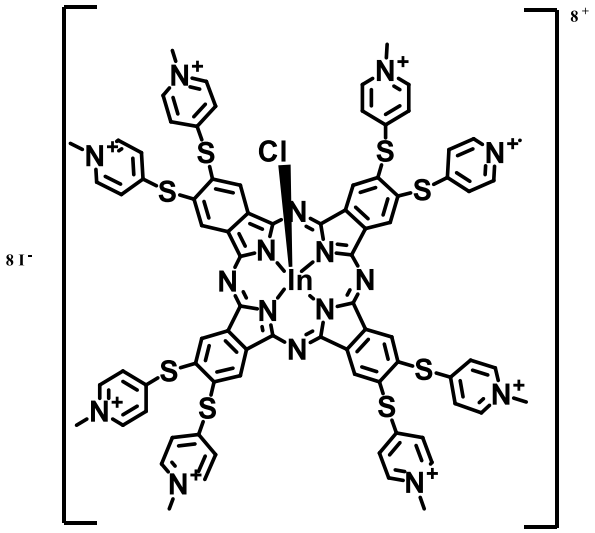

ClInOMePyPc

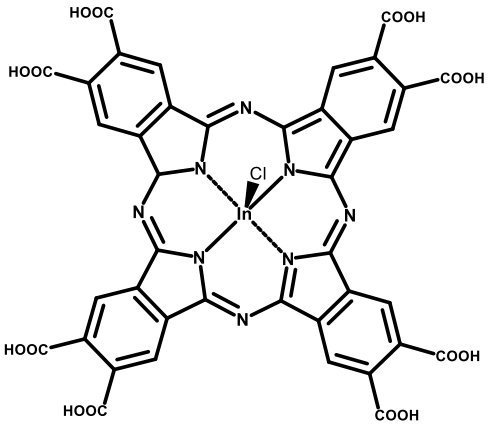

ClInOCPc

Figure 1.2: Complexes used in this thesis.

1.1.3 Electronic absorption spectroscopy

Metalled phthalocyanines are characterised by two pronounced absorption bands, namely the strong, isolated Q-band appearing in the red region in the electromagnetic spectrum and the weaker B (Soret)-band between 300-400 nm (Fig. 1.3) [15]. Typically, the B-band appears to be broad due to the overlapping of two bands (B_1 and B_2).

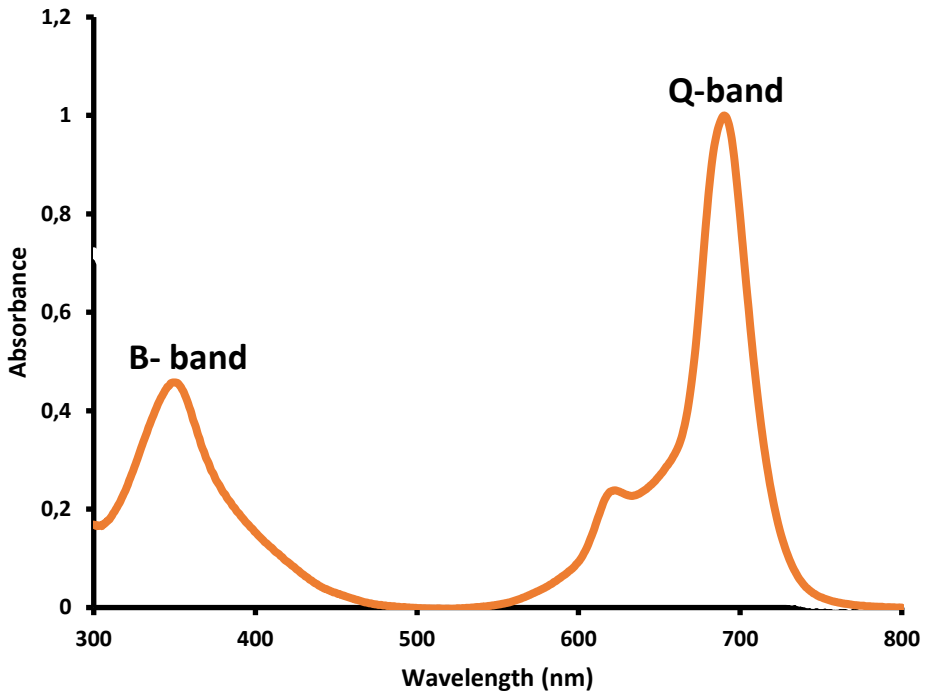

Figure 1.3: Ground state electronic absorption of metallated phthalocyanine.

The linear combination of atomic orbitals model explains the transitions from a_{1u}, a_{2u} and b_{2u}, where the afore-mentioned bands originate. The transition from the a_{1u} of the highest occupied molecular obirtal (HOMO) to a doubly degenerate transition e_g of the lowest unoccupied molecular orbital (LUMO) results in the Q-band while the transition from the a_{2u} or b_{2u} of the HOMO to the e_g of the LUMO result in the B-bands, Fig 1.4 [16]. In the ultra-violet region, there are other absorption bands, namely the N, L, and C bands. They are only observed in transparent solvents.

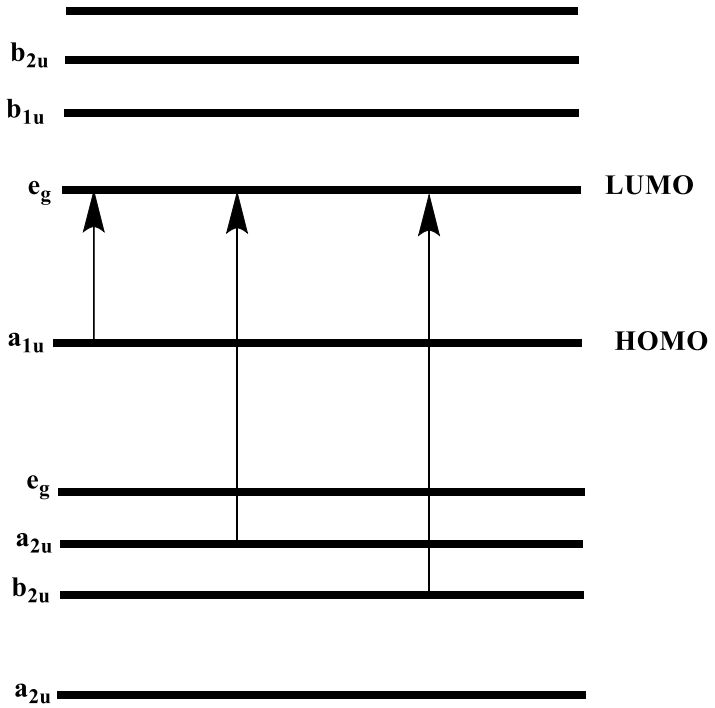

Figure 1.4: Electronic transition in metallated phthalocyanine.

1.1.4 Applications of Phthalocyanines

Pcs have been used in various applications such as imaging [17], electrophotography [18], chemo-sensing [19], dye-sensitized solar cells [20, 21], photodegradation of pollutants [22] and photodynamic antimicrobial chemotherapy (PACT) [23]. The latter two (PACT and pollutant degradation) are the subject of this work and will be discussed separately below. ClInOCPc is linked to magnetic nanoparticles (MNPs), all Pcs (ClInOCPc, MNP-ClInOCPc, ClInOPyPc and ClInOMePyPc) were tested for both PACT and degradation of pollutants (methyl red) when embedded in electrospun fibers. Phthalocyanines are linked to magnetic nanoparticles for ease of separation after use hence the latter will be discussed next.

1.2 Nanoparticles

1.2.1 General background and Synthesis

About 2000 years ago, gold nanoparticles were used as pigments for remedial and artistic purposes [24]. Nanoparticles may be manufactured and can be naturally occurring. The naturally occurring nanoparticles originate from both organic (polysaccharides, proteins to name a few) and inorganic (metals such as aluminosilicates among others) compounds [25]. There are numerous methods that have been reported for the preparation of nanoparticles which are summarized in Fig. 1.5 [26].

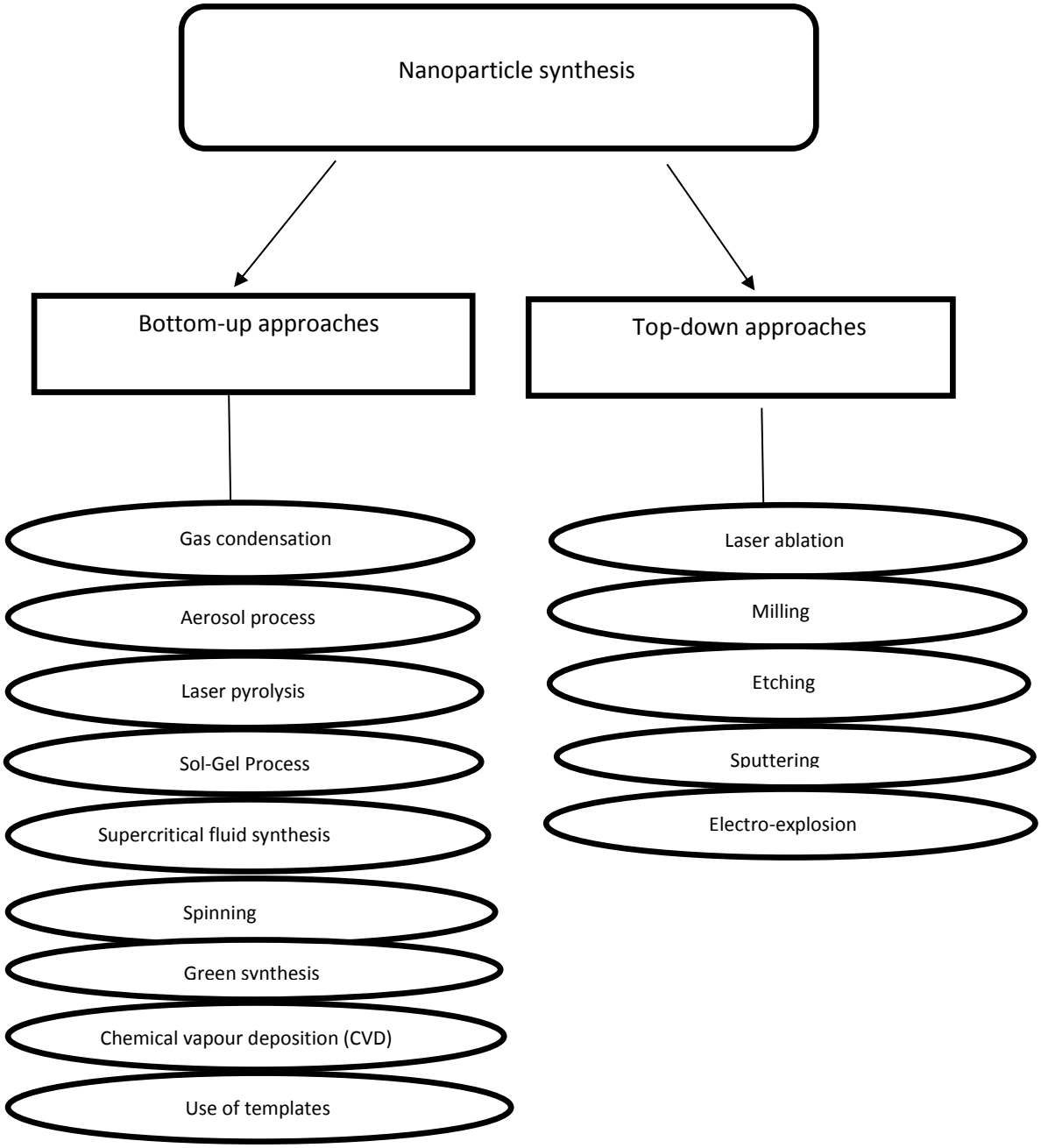

Figure 1.5: Some nanoparticle preparation methods.

There are two approaches for synthesis of NPs, the top down and bottom up approaches [27]. Top down approach involves particle size reduction of large particles into smaller particles using various techniques such as sputtering, laser ablation and milling to name a few [28]. This approach requires no harsh solvents; however, it involves high-energy input. In the bottom-up approach the precursor is dissolved in organic solvent and precipitated with a

stabilizer to produce NPs. Known techniques includes laser pyrolysis, sol-gel process and spinning [29]. The latter was employed in this work for MNPs.

For biological application, the surface of NPs is tuned to reduce cytotoxicity and improve selective binding and drug delivery [30, 31]. Functionality is provided through the introduction of different capping agents and ligands such as surfactants, polymers, biomolecules and small molecules [32-36]. The functionalization allows for covalent and non-covalent conjugation to incorporate multiple compounds for producing the desired activity [37].

1.2.2 Magnetic nanoparticles (MNPs)

Magnetic nanoparticles have been popular amongst researchers for a variety of applications due to their astounding properties such as superparamagnetism, specificity and non-toxicity [37-40]. Like any other NPs, there are multiple methods to synthesize magnetic nanoparticles but for this work, the co-precipitation method with the combination of Stöber method were employed [41-43]. Table 1.1 [44-50] lists the Pcs, which have been linked to MNPs and their applications.

Table 1.1: Phthalocyanine mixed with magnetic nanoparticles that have been applied before

Pc	Conjugated/mixed to	Application	Ref
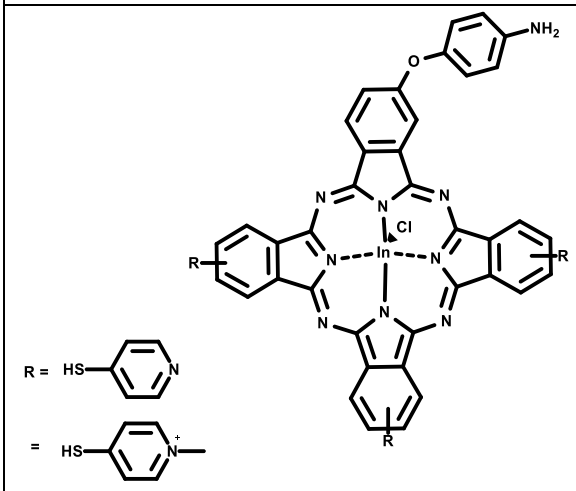	MNP-COOH	PACT (*E.coli)*	44
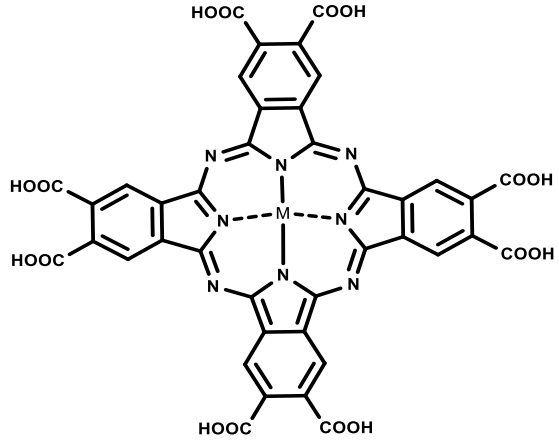 M = Zn	$MNP-NH_2$	Photophysics & Phodegradation (Orange G)	45, 46
M = ClIn	$MNP-NH_2$ Quantum Dots-MNPs	Photophysics	47, 48

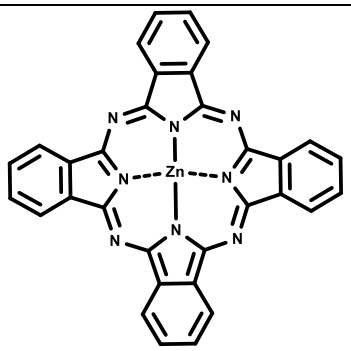	Poly(methyl methacrylate) & MNPs	PDT	49, 50

Table 1.1 shows that MNP-ClInOCPc employed in this work is known but used for PACT for the first time in this research. Table 1.1 also shows some examples of MPc containing three positive charges and used for PACT. This work uses eight positive charges. Effect of charge and bridging ligand on PACT activity will be explored.

1.3 Photodynamic Antimicrobial Chemotherapy (PACT)

1.3.1 Background

Photodynamic antimicrobial chemotherapy (PACT), it is based on the administration of a non-toxic photosensitizer to the microbial cells followed by activation by light of appropriate wavelength. The photo-excited photosensitizer produces reactive oxygen species (ROS) such as singlet oxygen that are cytotoxic to the targeted bacteria [51, 52]. There has been an increase in the number of drug resistant pathogens, such as *Methicillin-resistant staphylococcus aureus* (MRSA) [53]. There are various photosensitisers that have been used for PACT; phthalocyanines are used in this work.

1.3.2 Target micro-organisms

Gram positive (+) and Gram negative (-) bacteria are employed in this work. The significant difference between the two bacterial strains, illustrated in Fig. 1.6 is that the Gram (+) strain such as *Staphylococcus aureus (S. aureus)* has 15–80 nm thick cell wall composed of a thick peptidoglycan layer that is protecting the plasma membrane and has protruding lipoteichoic acid [54]. The Gram (+) strain is more sensitive to photoinactivation than the Gram (-) bacteria such as *Escherichia coli (E.coli)* strain. This is due to the additional cell wall composed of phospholipid double layer and polysaccharides in the latter [55].

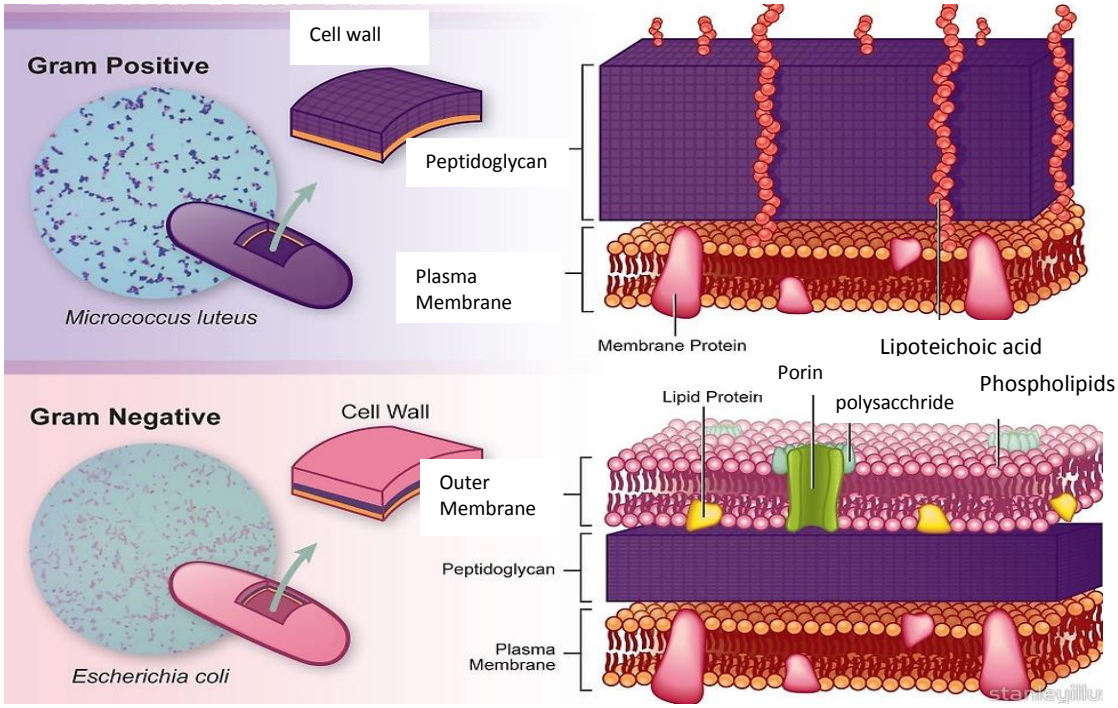

Figure 1.6: Gram (+) and Gram (-) structures [55].

Fungi are more complex in their composition, and classification compared to bacteria. For this work, the focus is on Gram (+) fungi, *Candida albican* (*C. albican*). *C. albican* consists of the outer and inner walls; the outer wall is composed of O- and N-linked mannose polymer (mannans) and protein, Fig. 1.7 [56]. The inner wall is made up of β-1,6-glucan, β-1,3-glucan and chitin, these proteins provide rigidity and structure [56].

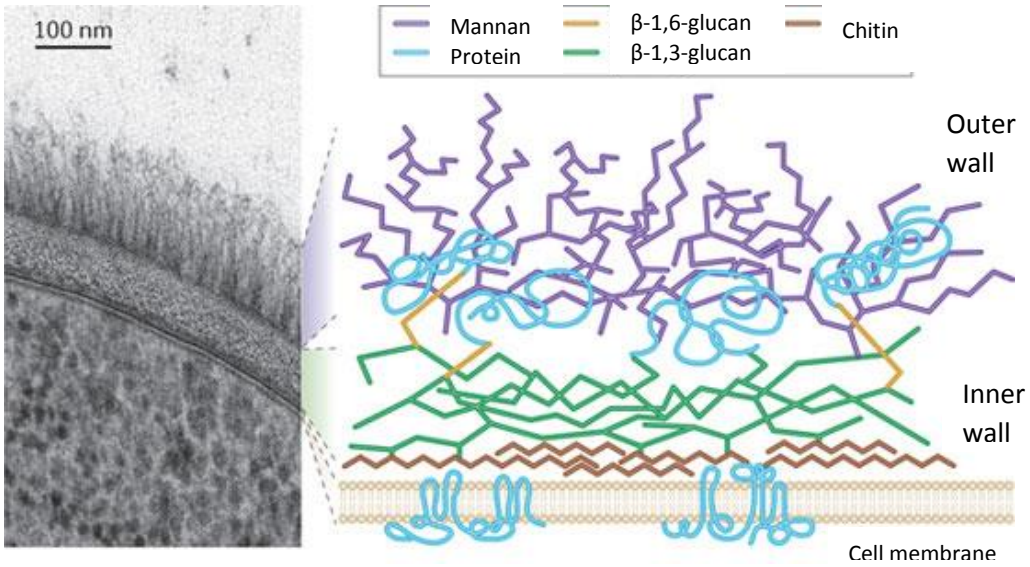

Figure 1.7: Structure of Fungi [56].

Table 1.2 [44, 57-65] summarizes the microorganisms that have been photo inactivated using phthalocyanines alone, or when conjugated to nanoparticles or supported on polymers. Studies have shown that the Gram (+) strain is easily penetrable due to its structure by any phthalocyanines, while Gram (-) strain cannot be penetrated by neutral nor anionic Pcs. Cationic Pcs have demonstrated positive results due to the negative charges on the surface of Gram (-) bacteria. In this work, neutral water soluble ClInOCPc, its conjugate with MNPs as well as quarternized Pc (ClInOMePyPc) are used to treat bacteria *(E.coli* and *S. aureus*), fungi (*C. albican*) and a water sample from a local stream.

Table 1.2 shows that positively charged Pc containing a maximum of four positive charges have been employed for inactivation of bacteria. This thesis describes the synthesis of a Pc with eight positive charges and compares it to Pcs with four and three positive charges. ClInOMePyPc has more positive charges than the Pcs in Table 1.2, hence it is expected to show enhanced activity against bacteria.

Table 1.2: Phthalocyanines that have been used for PACT studies.

Complex	**Support/NPs**	**Micro-organism**	**Ref**
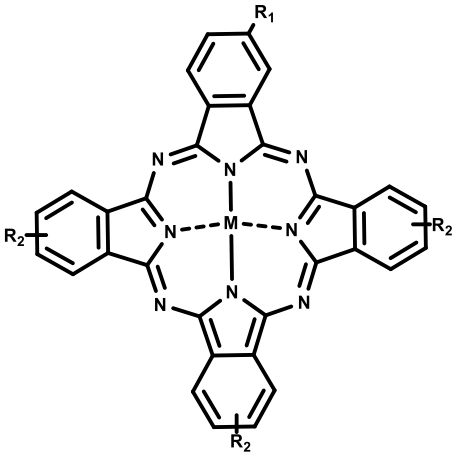			
R_1 = 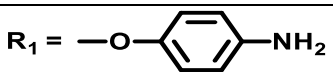 R_2 = 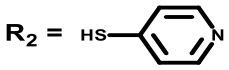 or R_2 = 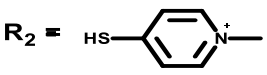	MNP-COOH	*E.coli*	44
R_1 = poly-L-lysine R_2 = 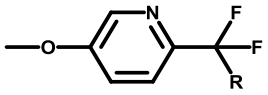 M = Zn	AuNPs, AgNPs	*S. aureus*	57

$R_1 = R_2 =$ 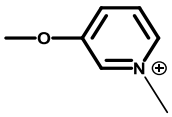 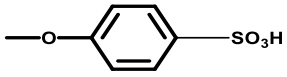 $R_1 = R_2 =$ M =Zn		*S. aureus* *P. aeruginosa* *C. albicans*	58
$R_1 = R_2 =$ 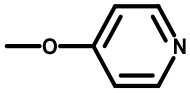 $R_1 = R_2 =$ 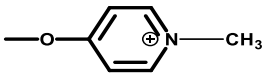 M = Zn M=ClIn		*E. coli*	59 60
$R_1 = R_2 =$ 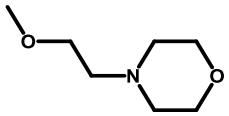 and $R_2 = H, R_1 =$ 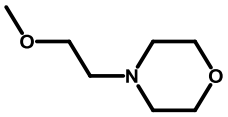 $R_1 = R_2 =$ 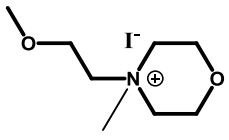 and $R_2 = H, R_1 =$ 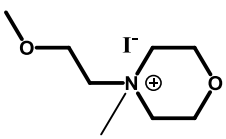		*C. albicans*	61

M = Zn			
$R_1 = R_2 =$ 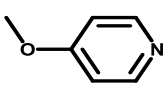 $R_1 = R_2 =$ 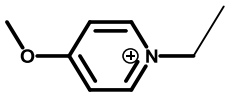 M = Pb		*E. coli*	62
$R_1 =$ 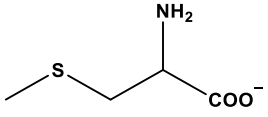 $R_2 =$ 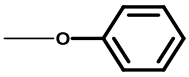 M = Ge $(OH)_2$, TiO, Sn $(OH)_2$& Zn	AgNPs	*S. aureus*	63
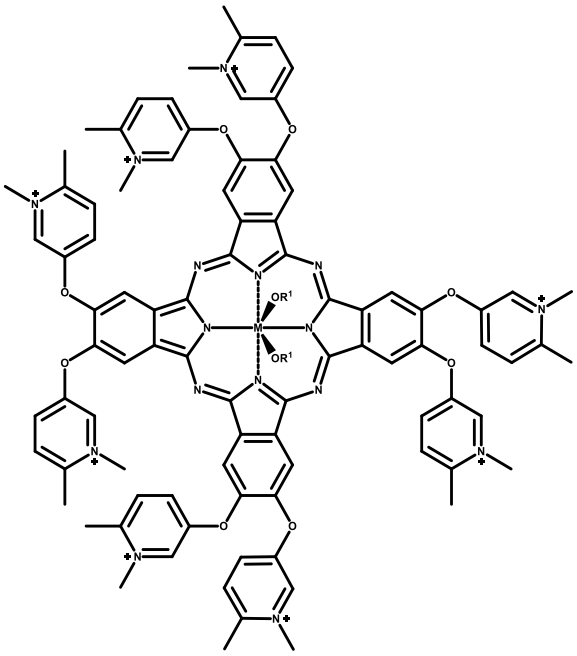			
$R^1 =$ 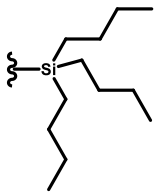		*S. aureus* *Methicillin-resistant*	64

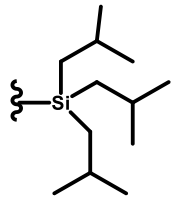 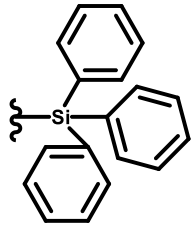 M = Si		*Staphylococcus aureus* *E. coli*	
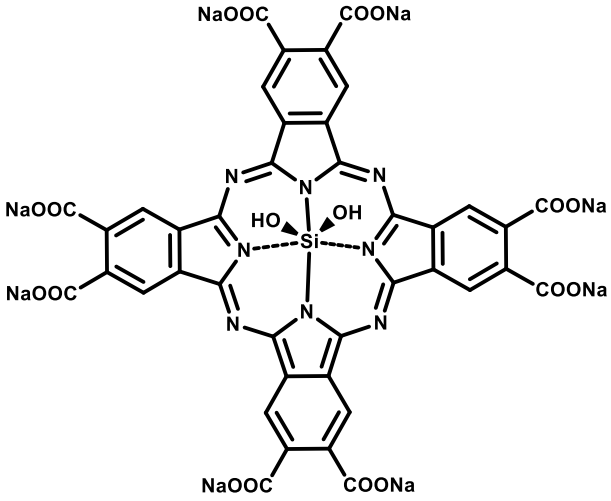	PtNPs	*C. albicans* *S. aureus*	65

1.4 Photo-degradation of pollutants

Advanced oxidation process (AOP) is receiving a great deal of popularity owing to its efficiency in the degradation of recalcitrant dye pollutants in wastewater [66-68]. The method is an alternative technique to chlorination, ozonation and adsorption; it is economically effective for degrading pollutants in wastewaters [66]. There are various methods employed to achieve AOP including, Fenton reagent [69, 70], photo-assisted Fenton [71, 72] and photocatalysis [73]. Photocatalysis is an eminent method for the degradation of organic dyes such as azo dyes, which are a subject of this work. Singlet oxygen production is imperative for oxidative processes; the photo-catalytic behaviour of Pcs relies heavily on their ability to produce reactive oxygen species such as singlet oxygen when excited with light [74-76].

1.4.1 Azo dyes

Azo dyes are the most common group of synthetic colorants and are widely used in industries such as textiles and ink [77, 78]. They consist of the (-N=N-) functional group as a chromophore in their molecular structure. There is a great environmental concern about the fate of these dyes, where large amounts of dyes enter the wastewater streams during industrial operation [79]. When incorporated into the body, azo dyes are converted into the corresponding aromatic amines, which can cause cancer [80]. Table 1.3 [46, 81-88] shows Pcs which have been used for degradation of pollutants. As the table shows, there has been three examples of the use of MNP-Pc for degradation of azo dyes, despite the advantage of magnetic separation. Methyl Red is used as pollutant of interest in this work due to its popularity in paper printing and textile dyeing [89] from which a significant amount is disposed to the environment through wastewaters and can causes irritation of the eye, skin

and digestive tract if inhaled or swallowed [90]. Therefore, it is essential to remove the dye from wastewaters using effective methods.

Table 1.3: Phthalocyanine containing complexes used for degrading Azo dyes and various pollutants.

Complex	**Pollutant**	**Nano-support/particles**	**Ref**
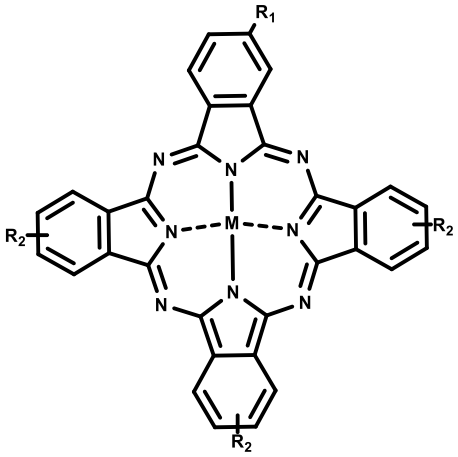			
$R_1 = R_2 =$ 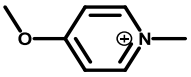 M = Zn	Methyl Orange	Polysulfone	[81]
$R_1 = R_2 =$ 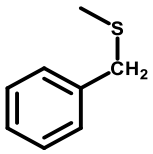 M = Zn	Orange G 4-chlorophenol	Polystyrene AuNPs	[82]
$R_1 = R_2 =$ 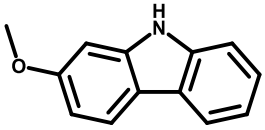 M = Zn	Methyl Orange	Polystyrene AgNPs	[83]

$R_1 = R_2 = NH_2$ M = Zn	Rhodamine 6G	Chitosan AuNPs	[84]
	Acid Orange II	Silk fiber	[86]
$R_1 = R_2 =$ 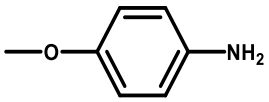 M = Zn	Orange G	Polystyrene $CoFe_2O_4$-COOH NPs (MNPs)	[88]
$R_1 = R_2 =$ 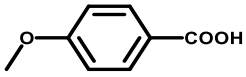 M = Zn	Orange G	$SiGd_2O_3$NPs (MNPs)	[85]
	Orange G	Polystyrene $CoFe_2O_4$-NH_2 NPs (MNPs)	[88]
$R_1 = R_2 = H$ M= Fe	Methyl Orange	Polyacrylonitrile	[87]
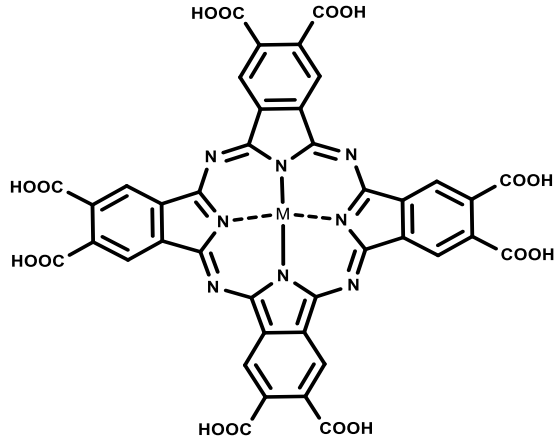 M = Zn	Orange G	MNP-NH_2	[46]

The three reports using MNP-Pc for degradation of pollutants employed Zn as central metal in Pc. This work uses ClInOCPc embedded in electrospun fibers. Indium is a heavy metal and generates high singlet quantum yields compared to Zn used in literature [88], In encourages intersystem crossing in Pcs, which results in high triplet state population from which singlet oxygen is generated.

1.5 Nanofibers

Nanofibers are very thin solid fibers with a diameter in the nanometre range. These are attractive due to their large surface area per unit of mass, small pore size, low cost, ease of processing and high tensile strength [91-94]. Nanofibers have been used in numerous application such in textiles, pharmaceutics and drug delivery. The fibers may be formed by using several techniques such as drawing, template synthesis, self-assembly and electrospinning, [95-98] the latter is employed in this work.

The process of elecrospinning has been known for about 80 years with the first patent issued to Formhals in 1934 [99, 100]. Electrospinning involves passing a charged polymer solution through a high voltage electric field in order to fabricate fibers with nanoscale diameters (Fig. 1.8). Once the polymer solution reaches a certain charge, a jet of polymer is ejected from the droplet that forms at the tip of the needle. The polymer jet travels to the low potential collector were it dries and gathers as a mat of nanofibers. The parameters which affect fiber quality include the distance to the collector, molecular weight of the polymer, viscosity of the solution and potential difference [101, 102]. Polymer nanofibers have been used in wound dressing, drug delivery, protective clothing, cosmetics, sensors and optical sensing [100-107].

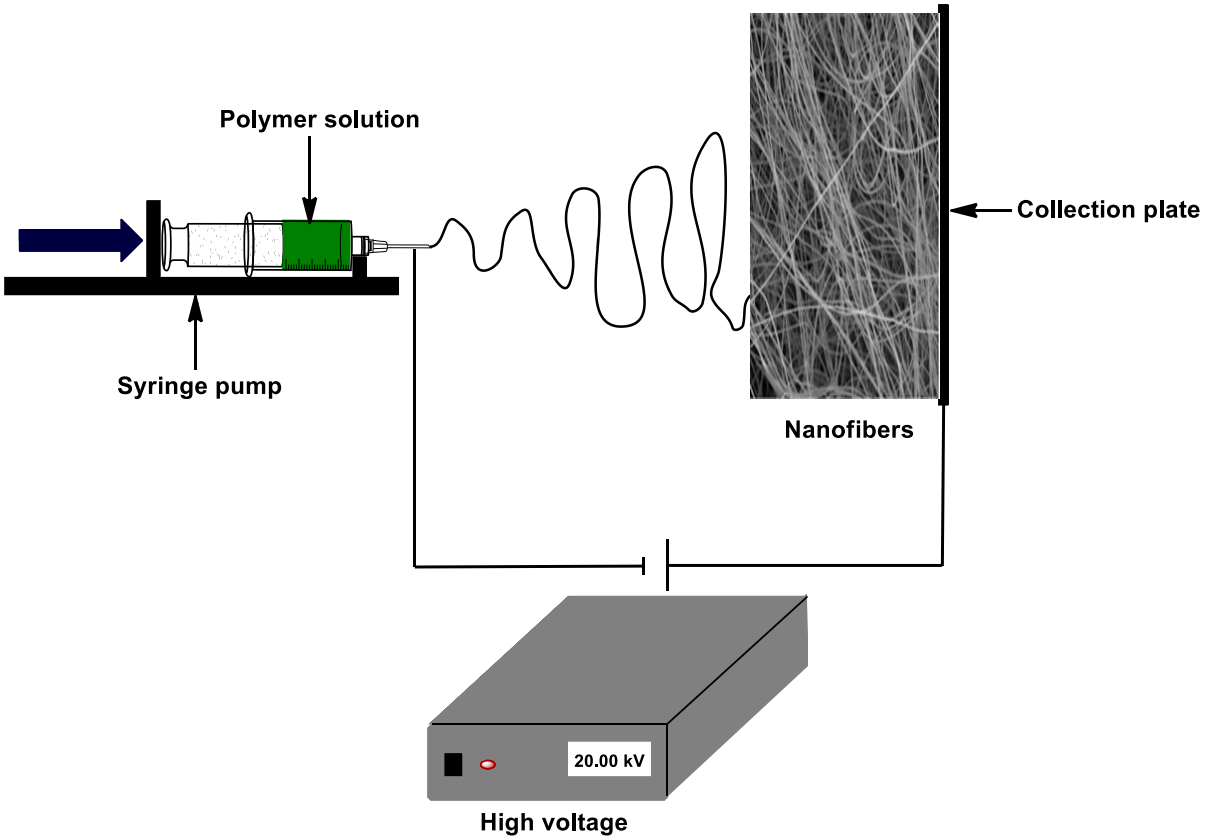

Figure 1.8: Electrospinning set-up.

As Table 1.3 shows, electrospun fibers containing Pcs that have been reported mainly using polystrene; this work uses polyacrylonitrile (PAN). PAN polymer was used in this work for its affordability, versatility (functional group modification), low density, thermal stability, mechanical strength [108, 109]. PAN has been applied in catalysis, clothing, metal ion adsorption and commercial aircraft [108-111]. ZnOCPc/PS was used for degradation of Orange G, but this work uses In heavy central metal for better catalysis.

1.6 Photo-physical and photo-chemical parameters of phthalocyanines

The Jablonski diagram may be used to describe the photophysical parameters of Pcs, Fig. 1.9 [112]. Following absorption of a photon of a particular energy the photosensitizer (PS) such as Pc gets excited from ground level (^{0}PS) to the first excited state. Once the Pc is excited (^{1}PS*) it dissipates its energy either kinetically through a short lived non-radiative vibrations and internal conversion (IC) or emit light via fluorescence or undergoes a spin change through intersystem crossing (ISC) to the triplet state. In the triplet excited state (^{3}PS*) the Pc can undertake 2 types of reactions; type I and type II mechanisms. In type I there is electron transfer between ^{3}PS* and a substrate to produce OH^{-}* radicals. In type II, ^{3}PS* and molecular oxygen interacts to form singlet oxygen which is imperative in the applications of this work [113-115].

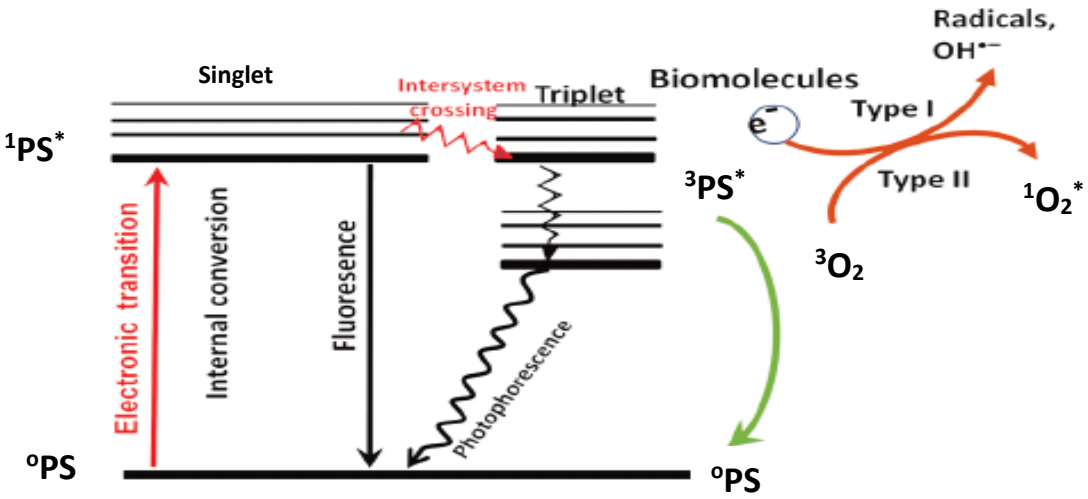

Figure 1.9: Jablonski diagram [112].

1.6.1 Fluorescence Quantum yields and lifetimes

Fluorescence quantum yield (Φ_F) is the measurement of the number of molecules fluorescing per quanta of light. The Φ_F values may be determined using comparative methods [116], Equation 1.1, and ZnPc is used as a standard ((Φ_F= 0.20 in DMSO (dimethyl sulfoxide) [117]) values in DMF corrected using refractive indices or using a standard (Φ_F= 0.23 in DMF (N,N-dimethylformamide) [118]).

$$\Phi_F = \Phi_F^{std} \frac{F A_{std} n^2}{F_{std} A\, n_{std}^2} \qquad 1.1$$

where, *F* and F_{std} are the areas under the fluorescence emission curves of the sample and the standard, respectively. *A* and A_{std} are the respective absorbances of the sample and standard at the excitation wavelength. *n* and n_{std} are the refractive indices of the sample and standard, respectively. The fluorescence lifetime measures the mean time between the absorption and re-emission of a photon through fluorescence. The time-correlated single photon counting (TSCPC) technique is used in this work for determination of fluorescence lifetimes [119, 120]. Fluorescence quantum yields [113] and the lifetimes are influence by many factors including the central metal, electronic energy transfer, the type of solvent used and aggregation to mention a few.

1.6.2 Triplet state quantum yield and lifetimes

Triplet state quantum yield determines the efficiency of intersystem crossing. The population of the triplet state by excited photosensitisizer is paramount for the desired application on this work. The duration of the molecule in the triplet state is referred to as triplet lifetime (τ_T). The triplet quantum yields were determined in DMSO and DMF using a comparative method, and ZnPc as a standard in DMSO (Φ_T = 0.65 [113]), using Equations 1.2 – 1.4

$$\Phi_T = \Phi_T^{std} \frac{\Delta A_T \varepsilon_T^{std}}{\Delta A_T^{std} \varepsilon_T} \quad 1.2$$

$$\varepsilon_T = \varepsilon_s \frac{\Delta A_T}{\Delta A_s} \quad 1.3$$

$$\varepsilon_T^{std} = \varepsilon_s^{std} \frac{\Delta A_T^{std}}{\Delta A_s^{std}} \quad 1.4$$

where ΔA_T^{std} and ΔA_T are the changes in the triplet state absorbances of the standard and the sample, respectively, Φ_T^{std} the triplet quantum yield for the standard. ε_T and ε_T^{std} are the triplet state molar extinction coefficients for the sample and the standard, respectively and are determined using the Equations 1.3 and 1.4, from their respective ground state molar extinction coefficients (ε_s and ε_s^{std}), changes in absorbances of the ground singlet states (ΔA_s and ΔA_s^{std}) and changes in the triplet state absorptions (ΔA_T^{std} and ΔA_T). The ORIGIN 8 software used to fit the triplet lifetimes' kinetic curve.

1.6.3 Singlet oxygen quantum yield

Singlet oxygen quantum yield (Φ_Δ) is defined as the amount of singlet oxygen generated per photon absorbed by the phthalocyanine complex [115]. The photosensitization involves the transfer of energy from the $^3PS^*$ to triplet molecular oxygen ($^3O_2$) as shown in Fig. 1.9 [112]. The singlet quantum yield was calculated using equation 1.5.

$$\Phi_\Delta = \Phi_\Delta^{std} \frac{RI_{Abs}^{std}}{R^{std}I_{abs}} \quad 1.5$$

where Φ_Δ^{std} is the singlet oxygen quantum yield of a known standard (ZnPc $\Phi_\Delta^{std} = 0.58$ in DMF [113] and 0.42 in aqueous media using ClAlPcSmix (a mixture of differently substituted sulfonated phthalocyanines) as the standard) [113], R and R^{std} are the singlet oxygen quencher photobleaching rates in the presence of the respective MPcs and their conjugates and of the standard, respectively. Singlet oxygen generation is monitored spectroscopically by the decrease in the absorption maximum of the quencher [121, 122]. $I_{Abs}$and I_{Abs}^{std} are the rates of light absorption of the sample and standard, respectively, and are defined by Equation 1.6 and 1.7.

$$I_{abs} = \frac{\alpha.A.I}{N_A} \quad 1.6$$

$$I_{Abs}^{std} = \frac{\alpha.A.I}{N_A} \quad 1.7$$

where, $\alpha = 1 - 10^{-A(\lambda)}$, A (λ) is the absorbance of the sensitizer (Pc, conjugate and standard) at the irradiation wavelength, A is the irradiated area (2.5 cm^2). *I* is the intensity of light (expressed as photons $cm^{-2}s^{-1}$), and N_A is the Avogadro's constant. In this work, 1,3-

diphenylisobenzofuran (DPBF) in organic media or anthracene-9,10-bis-methylmalonate (ADMA) in aqueous media were used as quenchers, in a 1:1 ratio with the Pc.

For singlet oxygen quantum yield (Φ_Δ) determinations in fibers, the absolute method used due to lack of a standard. The quantum yields (Φ_{ADMA}) were calculated using Equation 1.8, the extinction coefficient of ADMA in water, log (ε) = 4.1 at 380 nm [113].

$$\Phi_{ADMA} = \frac{(C_0 - C_t)V_R}{I_{abs}.t} \qquad 1.8$$

where C_0 and C_t are the ADMA concentrations prior to and after irradiation, respectively; V_R is the solution volume; t is the irradiation time per cycle and I_{abs}, is the absorbance. The absorbance used in Equation 1.8 is that of the metallophthalocyanines on the fibre. The light intensity measured refers to the light reaching the spectrophotometer cell, and it is expected that some of the light may be scattered, hence the values of the metallophthalocyanines in the fibres are estimates.

The Φ_Δ values were calculated using Equation 1.9 [117]:

$$\frac{1}{\phi_{ADMA}} = \frac{1}{\phi_\Delta} + \frac{1}{\phi_\Delta}.\frac{K_d}{K_a}.\frac{1}{[ADMA]} \qquad 1.9$$

where K_d is the decay constant of singlet oxygen and K_a is the rate constant for the reaction of ADMA with $^1O_2$ ($^1\Delta_g$). The intercept obtained from the plot of $1/\Phi_{ADMA}$ versus 1/[ADMA] gives Φ_Δ.

1.7 Summary of aims

The aims of this project can be summarized as follows:

1. To synthesize and characterize
    - ✓ Novel octapyridylsulfanyl phthalocyaninato chloroindium(III) and octamethylpyridylsulfanyl phthalocyaninato chloroindium (III)

2. Synthesize and characterize NH_2 functionalised magnetic nanoparticle and covalently link them to ClInOCPc.

3. Investigation of the photophysical behavior and PACT studies of:

i) ClInOCPc alone or with MNPs, in solution.

ii) ClInOCPc, MNP-ClInOCPc, ClInOPyPc and ClInOMePyPc in fiber.

4. Investigation of the photodegradation of methyl red using all Pcs.

CHAPTER TWO

EXPERIMENTAL

2. Experimental

2.1 Materials

2.1.1 Solvents

Deuterated dimethylsulfoxide (DMSO-d6), n-pentanol, n-hexanol, methanol, acetone, ammonium hydroxide, tetrahydrofuran (THF) and dichloromethane (DCM) were purchased from SAARCHEM South Africa. Ultra-pure water from the Milli-Q Water system from Millipore Corp, Bedford, MA, USA. Dimethylformamide (DMF) was from Associated Chemical Enterprises.

2.1.2 Reagents for the determination of photophysical parameters

1,3-Diphenylisobenzofuran (DPBF), anthracene-9,10-bis-methylmalonate (ADMA), and ZnPc, were all purchased from Sigma-Aldrich, South Africa. ClAlPcSmix was synthesized as in literature [123].

2.1.3 Reagents for phthalocyanine synthesis and known Pcs

ClInOCPc was synthesized as in literature [14], 1,8-diazabicycloundec-7-ene (DBU), indium (III) chloride, and methyl iodide were purchased from Sigma-Aldrich. Dithiopyridyl phthalonitrile was synthesized as in literature [124].

2.1.4 Reagents for nanoparticle synthesis and linking to Pcs

3-Aminopropyl triethoxysilane (APTES), tetraethyl orthosilicate (TEOS), iron(III) chloride hexahydrate, iron(II) sulphate tetrahydrate, N-hydroxysuccinimide (NHS), and 1-ethyl-3-(3-dimethylaminopropyl)carbodiimide (EDC) were obtained from Sigma-Aldrich.

2.1.5 Reagents for bacterial work and Photocatalysis

Phosphate-buffered saline (PBS) solution pH 7.4 was prepared using appropriate amounts of Na_2HPO_4 and NaOH in ultra-pure water from a Milli-Q Water system (Millipore Corp, Bedford, MA, USA). Nutrient agar and agar bacteriological BBL Muller Hinton broth were purchased from Merck and *E.coli* (ATCC 25922) were obtained from Microbiologic. *S. aureus* (ATCC 25923) and *C. Albican* (ATCC 24433) were from Davies Diagnostics. Polyacrylonitrile (PAN, MW = 150 000 g/mol) and Methyl Red (MR) were purchased from Sigma-Aldrich. The water samples were collected from Rhodes University Botanical Gardens stream situated at 33°18'58.7"S and 26°31'13.5"E. The samples were collected in March 2017.

2.2 Equipment

1. UV–visible absorption spectra of solutions were recorded on a Shimadzu UV-2550 spectrophotometer. Perkin Elmer Lambda 950 UV-vis spectrophotometer was used for solid state spectra.
2. Infrared (IR) spectra were recorded on a Bruker Alpha IR (100 FT-IR) spectrometer with platinum-ATR or Perkin-Elmer Fourier transform-IR (100 FT-IR) spectrophotometer.
3. Mass spectra data were collected with a Bruker AutoFLEX III Smartbeam TOF/TOF Mass spectrometer. The spectra were acquired using dithranol as the MALDI matrix operated on either negative ion or positive mode.
4. ^{1}H nuclear magnetic resonance (^{1}H NMR) spectra recorded on a Bruker AMX 600 MHz NMR spectrometer.
5. Elemental analyses were carried out on Vario EL III MicroCube CHNS Analyzer.

6. Fluorescence excitation and emission spectra were recorded on a Varian Eclipse spectrofluorimeter.
7. Laser flash photolysis system (Fig. 2.1) was used for the determination of triplet decay kinetics and transient curve. EKSPLA NT342N-20-AW tunable wavelength laser with excitation pulses (3-5 ns) was used as the laser. The analyzing beam source was from a Thermo Oriel Xenon arc lamp, and photomultiplier tube (a Kratos Lis Projekte MLIS-X3) was used as a detector. Signals were recorded with a two-channel 300 MHz digital real time oscilloscope (Tektronix TDS3032C).

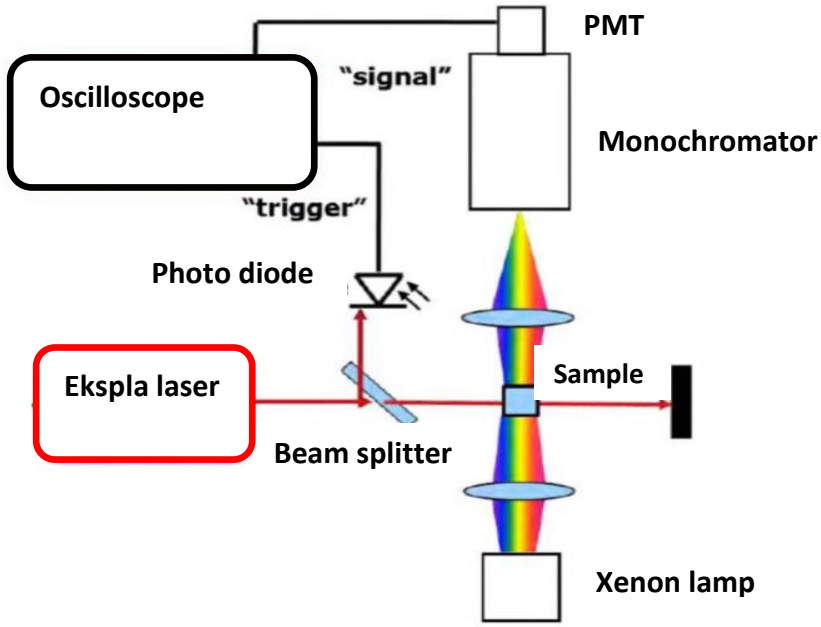

Figure 2.1: Schematic diagram showing the experimental set up for laser flash photolysis.

8. Fluorescence decay lifetimes were measured using a time-correlated single photon counting (TCSPC) apparatus (FluoTime 300, Picoquant GmbH). The excitation source was a diode laser (LDH-P-670 driven by PDL 800-B, 670 nm, 20 MHz repetition rate, 44 ps pulse width, Pico quant GmbH).

9. Photo-irradiations (Fig. 2.2) for singlet oxygen quantum yield determination and antimicrobial studies were performed using a General Electric Quartz lamp (300 W), 600 nm glass (Schott) and water filters were used to filter off ultra-violet and far infrared radiations. Light intensities measured with a POWER MAX 5100 (Molelectron detector incorporated) power meter.

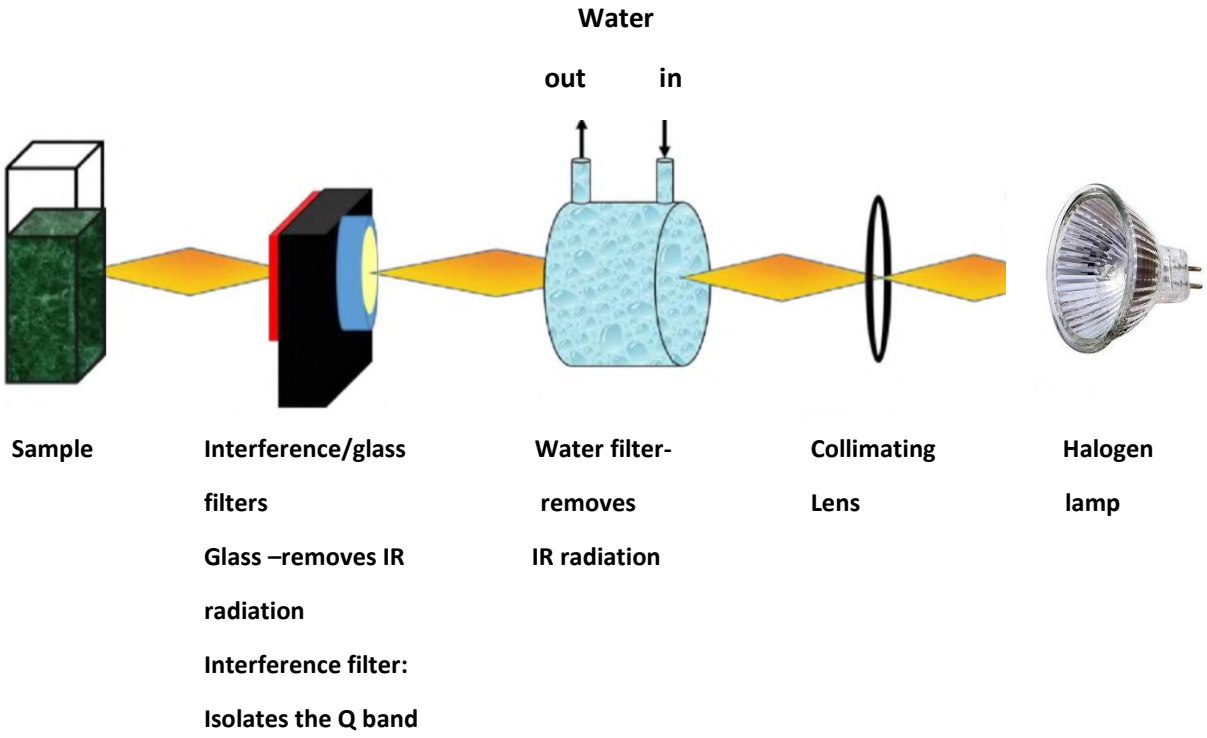

Figure 2.2: Schematic representation of a photo-irradiation apparatus.

10. The optical densities of the bacteria culture were determined using the LEDETECT 96 from LABXIM PRODUCTS.
11. A Metrohm Swiss 827 pH meter was used for pH measurements.
12. Autoclave RAU-530D was used for the sterilization and autoclaving of nutrient broth, nutrient agar and phosphate buffer as well as various apparatus for PACT studies.

13. Vortex mixer and HERMLE Z233M-2 centrifuge from LASIEC were used to mix the bacteria/fungus suspension and for the harvesting of the bacteria/fungus cells, respectively.
14. Scan® 500 automatic color colony counter was used for the evaluation of the colony forming units (CFU)/mL of the bacteria.
15. Electrospun polymer fibers were obtained from a set-up consisting of a high voltage source (Glassman High Voltage. Inc., EL series, 0-40 kV), a pump (Kd Scientific, KDS-100-CE), a plastic syringe connected to a steel needle of the internal diameter of 0.1 mm and aluminium foil as a collector.
16. JEOL JSM 840 scanning electron microscope (SEM) operating at an accelerating voltage of 20 kV was used to examine the morphology of the electrospun nanofibers. Using the Cell D software from Olympus, the average fibre diameter together with the standard deviations were determined from 70 measurements.
17. Nitrogen adsorption/desorption isotherms were measured at 77 K using a Micrometrics ASAP 2020 Surface Area and Porosity Analyzer. Before each measurement, degassing was carried at 900 °C for four days.
18. Transmission electron microscopy (TEM) micrographs were acquired using Zeiss Libra 120 TEM operated at 120 kV using a Megaview Olympus soft imaging.
19. Dynamic light scattering (DLS) experiments were done on a Malvern Zetasizer nanoseries, Nano-ZS90.
20. Photo-degradation of methyl red was performed using Modulight ® Medical Lasersystem (ML) 7710-680 equipped with cylindrical output channels, aiming beams, foot/hand pedal switch, calibration module, fiber sensors (sub miniature version A)

connectors and safety interlocks. The sample holder has a diameter of 2.5 cm, irradiance of 400 mW/cm^2, and a dose of 240 J/cm^2.

21. X-ray powder diffraction (XRD) patterns were recorded using a Cu K radiation (1.5405 °A, nickel filter) on a Bruker D8 Discover equipped with a proportional counter and the X-ray diffraction data were processed using the Eva (evaluation curve fitting) software.

2.3 Syntheses

2.3.1 Synthesis of 2(3), 9(10), 16(17), 23(24)-octapyridylsulfanyl phthalocyaninato chloroindium (III) (ClInOPyPc) (Scheme 3.1)

A mixture of 4,5-dithiopyridyl phthalonitrile (0.370 g, 1.07 mmol) and In (III) chloride (0.059 g, 0.27 mmol) in 5 mL of n-hexanol was heated at reflux temperature under an argon atmosphere for 18 h with constant stirring in the presence of 0.5 mL DBU. The product obtained was precipitated with cyclohexane and subsequently washed with methanol, ethyl acetate, water and acetone and dried in the oven. Yield: 0.27 g (72.01 %). IR [(ATR), V_{max}/cm^{-1}]: 3032 (Ar-H), 1569, 1475, 1401, 1324, 1108, 1066 (C-S-C), 940, 806, 702. ^{1}H NMR (DMSO-δ_6): 7.35-7.34 (d, br, 16H, pyridyl-H), 8.40-8.39 (dd, br, 16H, pyridyl-H), 9.14 (d, 8H, Pc-H). UV/Vis (DMF) λ_{max}/nm (log ε): 712 (5.28), 644 (4.58), 381 (4.87). Calc. for $C_{72}H_{40}ClInN_{16}S_8$: Expected: C 56.30, H 2.62, N 14.59, S 16.70 Found: C 55.56, H 2.88, N 14.87, S 15.84. MALDI TOF MS m/z: Calcd: 1534.01 Found: [M+4H$^+$] = 1538.08.

2.3.2 Synthesis of cationic 2(3), 9(10), 16(17), 23(24)-octamethylpyridylsulfanyl phthalocyaninato chloroindium (III) (ClInOMePyPc) (Scheme 3.1)

ClInOPyPc (0.170g, 1.07 mmol) was dissolved in 5 mL of dry DMF and 15 mL of acetone was added to the mixture followed by addition of 4 mL of methyl iodide. The mixture was heated at reflux temperature for 72 h. The product obtained was precipitated with acetone and subsequently washed with acetone, tetrahydrofuran, diethyl ether and dried in the oven. The solid was dissolved in water and reprecipitated with acetone twice then finally dried under reduced pressure. Yield: 0.18 g (68.05 %). IR [(ATR), V_{max}/cm^{-1}]: 3036 (Ar-H), 1723, 1626, 1569, 1478, 1405, 1166, 1102, 1044 (C-S-C), 851, 810, 699. ^{1}H NMR (DMSO-δ_6); 1.03-0.78 (m, br, 24H, CH_3) 7.85-7.73 (br, 16H, pyridyl-H), 8.13-7.93 (br, 16H, pyridyl-H), 8.32-8.23 (d, br, 8H, Pc-H). UV/Vis (DMF) $\lambda_{max/}$nm (log ε): 699 (5.28), 641 (4.00), 363 (4.38). Calc (%). for $C_{80}H_{64}ClInN_{16}S_8$: C 58.02, H 3.90, N 13.53, S 15.49. Found: C 57.28, H 3.43, N 12.84, and S 15.11.

2.3.3 Synthesis of Magnetic nanoparticles (procedure adopted from [40]) (Scheme 3.2 A)

a) **Bare MNP**: Briefly 4.17 g (25.70 mmol) of iron (III) chloride hexahydrate and 1.95 g (12.84 mmol) of iron (II) sulphate tetrahydrate were dissolved in 80 mL of previously degassed millipore water under argon gas. Then 7.5 mL of liquid ammonia (25%) was added drop-wise. The mixture was stirred for 3 h in an argon atmosphere at the temperature of about 60 °C. A slurry was produced and washed repeatedly with distilled water and then the particles were magnetically separated from the supernatant and re-dispersed in aqueous solution at least three times, until pH 7 was

obtained. The MNPs were then finally dispersed in ethanol, magnetically isolated and dried in vacuum at room temperature.

b) **Silica coated magnetic nanoparticles (MNP-SiOH):** Bare MNPs (0.26 g) were dispersed in a degassed mixture of 80 mL absolute ethanol and water, followed by ultrasonication of the mixture for 30 min. Then, 5 mL of tetraethoxysilane (TEOS) was added to the mixture and pH was adjusted to 9 using ammonium hydroxide. The mixture was stirred in an inert argon environment for 12 h. This was followed by refluxing at 130 °C for 24 h. The brown precipitate was separated and dried.

c) **Amino coated magnetic nanoparticles (MNP-NH_2):** The MNP-SiOH (0.15 g) and 100 mL absolute ethanol were ultrasonicated for 30 min in order to form homogeneous colloid suspension. Then 0.5 mL APTES was added and the mixture heated under reflux in argon atmosphere at 130 °C for 7 h. The precipitate was separated magnetically. The resulting solid product was washed with distilled water and dried in the vacuum for 24 h.

2.3.4 Covalent linking of octa-carboxy Indium (III) phthalocyanine to MNP-NH_2 (procedure adopted from [40]) (Scheme 3.2 B)

The ClInOCPc (15 mg) was dissolved in 5 ml of PBS (pH 7.4). NHS (0.115 g, 1 mmol) and EDC (0.23 g, 1.2 mmol) were added and the solution was stirred for 3 h at room temperature. The MNP-NH_2 (5 mg) was dissolved in PBS and the mixture was added to the solution above and was stirred for 12 h at room temperature under Ar gas. The product was washed with ethanol, then separated and dried, it is represented as MNP-ClInOCPc.

2.4 Electrospinning method

Polyacrylonitrile (PAN) powder was dissolved in DMF and stirred for 24 h at room temperature. The electrospun unfunctionalised PAN fibres were prepared by placing the solution in a 5mL syringe fitted with a hypodermic needle (inner diameter of 0.1 mm). Electrospining was then conducted at a flow rate of 0.05 mL/ h, voltage = 15 kV, tip to collector distance of 12 cm at room temperature and with relative humidity of 48%. The same parameters were maintained for the Pc/PAN solutions represented as ClInOCPc/PAN, MNP-ClInOCPc/PAN, ClInOPyPc/PAN and ClInOMePyPc/PAN.

2.5 Antimicrobial studies

The microorganisms used (*S. aureus, C. albican and E. coli*) were grown on agar plate according to manufacturer's specifications to obtain individual colony. The colony was inoculated into nutrient broth and agitated on a rotary shaker (~200 rpm) overnight at 37 °C (*E. coli* and *S. aureus*) or 30 °C (*C. albican*). Aliquots of the culture were transferred to 4 ml of fresh broth and incubated at 37 °C or 30 °C to mid logarithmic phase (OD 620 nm ≈ 0.6). The bacteria/fungus culture in the logarithmic phase of growth were harvested through the removal of broth culture by centrifuging for 15 min at 3000 rpm and washed three times in PBS. Then, the bacteria/ fungus cultures were diluted to 1/1000 in PBS as the working stock solution.

PACT activities of the bacteria were performed using methods previously reported [44]. In all the experiments, the bacterial/fungal suspensions were incubated in an oven equipped with a shaker for 30 min in the dark at 37 °C (bacteria) or 30 °C (fungus and water sample). Then, half (3 mL) of the incubated bacterial/fungal suspensions were irradiated at the Q-band

maximum of the photosensitizers in 24 well plate, using the set-up described above and the other half was kept in the dark. After irradiation, 100 µL samples inoculated and the plates incubated at the above mentioned temperature. The experiments were done in triplicates.

2.6 Photo-degradation studies

Fibres were immersed in the methyl red solutions for 30 min prior to the photocatalytic experiments being carried out, to eliminate adsorption effect. The photodegradation of the methyl red was monitored by viewing the spectral changes in 8 min intervals using Uv-vis spectrum.

2.7 Experimental conditions for photophysical/chemical studies

For $\Phi_{f,}$ all samples excitation wavelength were fixed to approximately 0.05 to minimise the inner filter effect, both the sample and standard were excited at the same wavelength. For fluorescence lifetimes, the Pcs were also excited at the excitation wavelengths with the TCSPC used to monitor the results.

For Φ_T, the experiments were conducted using a 1 cm quartz cell that filled with a Pc solution, which was degassed using argon to remove any oxygen before each reading. The absorbance of sample solutions and that of the standard were adjusted to be at approximately 1.5 at their crossover wavelength.

For Φ_Δ, the solutions used were not degassed with the Q band absorbance of each Pc solution recording being about 1. DPBF and ADMA were used as quenchers with an absorbance of 2 at 417 nm and 380 nm, respectively. Equal volume (1.5 ml) of both the Pc and quencher were

mixed and irradiated using the Q-band wavelength. UV-Vis spectra was used to monitor the spectral changes at 30 s intervals for DPBF and 3 min for ADMA.

Publications

1) Azole Sindelo, Olawale L Osifeko and Tebello Nyokong. Synthesis, Photophysicochemical and Photodynamic Antimicrobial Chemotherapy studies of indium pyridyl phthalocyanines: charge versus bridging atom. Inorganica Chim. Acta. 476 (2018) 68-76.
2) Azole Sindelo and Tebello Nyokong. Polymer-embedded Indium octacarboxyphthalocyanines possible multi-functional application. Polymer. **Submitted.**

CHAPTER THREE

Synthesis and characterization of phthalocyanines and conjugate

This chapter discusses the synthesis and characterization of MPcs (ClInOPyPc and ClInOMePyPc and ClInOCPc), MNPs and a conjugate of MNP-ClInOCPc.

3.1 Synthesis and characterization of octapyridylsulfanyl indium phthalocyanine (ClInOPyPc) and cationic octapyridylsulfanyl indium phthalocyanine (ClInOMePyPc)

3.1.1 Synthesis (Scheme 3.1)

The peripherally octa substituted indium phthalocyanine was produced by template cyclization of the phthalonitrile in the presence of $InCl_3$ in an inert atmosphere using n-hexanol (Scheme 3.1). ClInOMePyPc was obtained via quaternization of ClInOPyPc using methyl iodide as the quaternizing agent. Both complexes were characterized by elemental analysis and several spectroscopic techniques.

^{1}H NMR spectrum (Fig. 3.1) of ClInOPyPc exhibited the aromatic protons at δ = 9.14 ppm as a doublet and δ = 8.40-8.39 as broad doublet of doublets, and δ = 7.35-7.34 ppm as a doublet. The same trend was observed for ClInOMePyPc with an additional CH_3 multiplet at δ = 1.03-0.78 ppm. Large molecules possess a variety of heavy isotopes which decrease the chances of obtaining a monoisotopic peak, thus the isotopic distribution model has been reported before [125] as an accurate method to assign isotopic distribution. The resulting simulated model was compared to the experimental MALDI-TOF showed a fragmentation of $[M+4H]^+$, for ClInOPyPc.

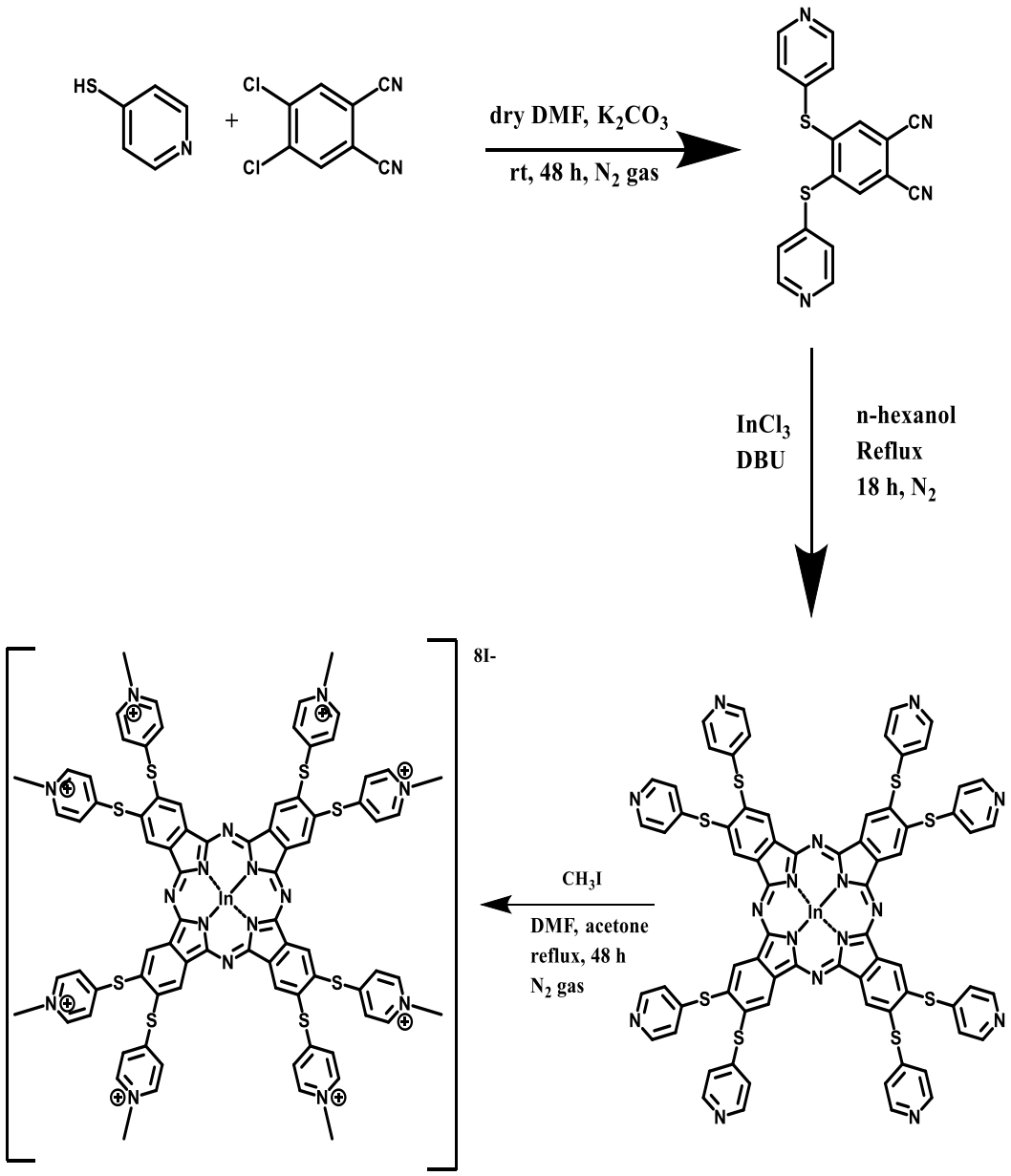

Scheme 3.1: Synthetic route for ClInOPyPc and ClInOMePyPc.

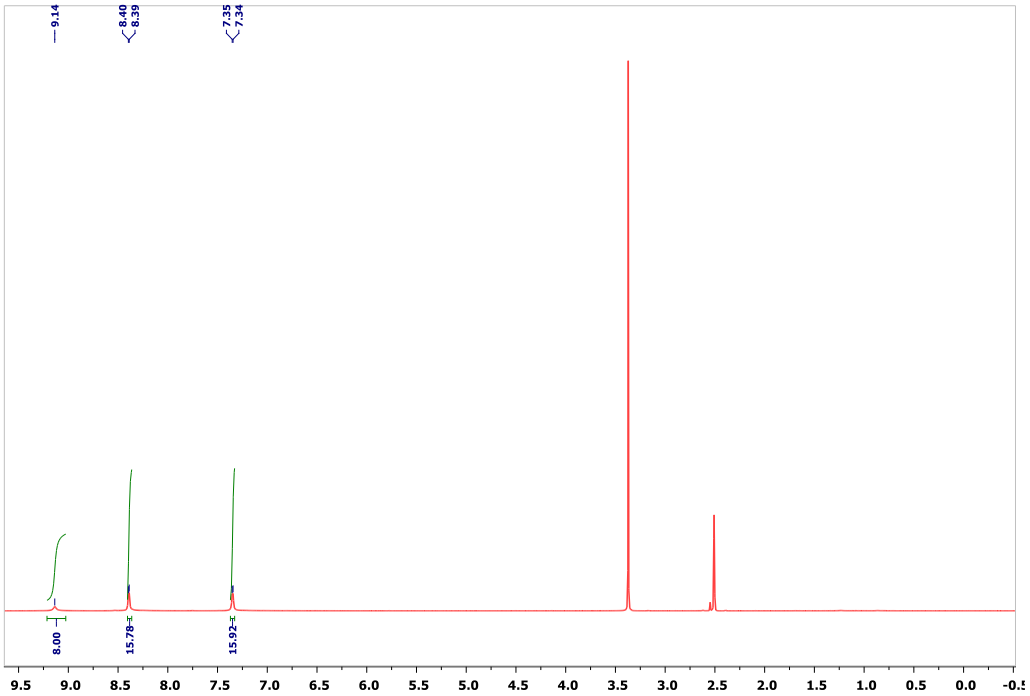

Figure 3.1:^{1}H NMR spectrum of ClInOPyPc.

3.1.2 Ultra-violet visible spectra

The absorbance spectra of ClInOPyPc and the quartenized phthalocyanines ClInOMePyPc are shown in DMF, Fig. 3.2 A and water (Fig. 3.2 B) for the latter. In DMF, ClInOPyPc and ClinOMePyPc have sharp Q bands with no aggregation. The Q band for ClInOMePyPc (699 nm) is blue shifted compared to ClInOPyPc (712 nm) in DMF Table 3.1. Nitrogen groups result in red shifting in phthalocyanines [126]. Hence, the blue shift could be because of the reduction in the electronic properties of the nitrogen groups due to quartenisation.

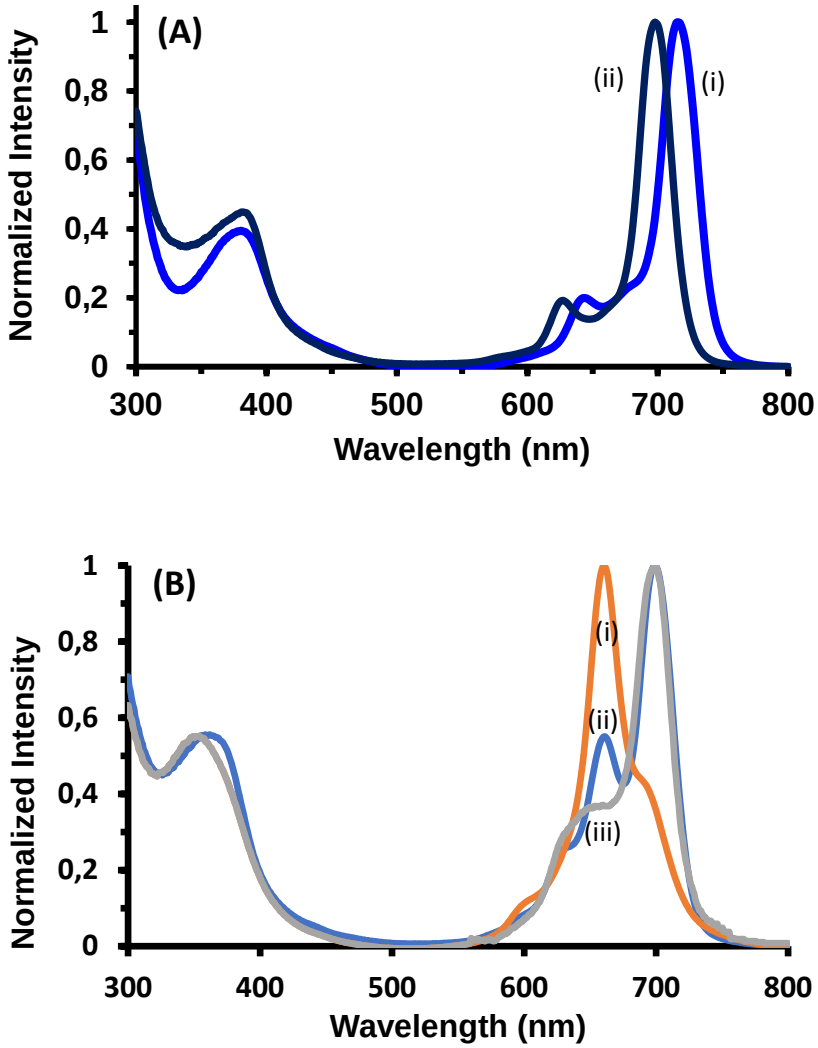

Figure 3.2: UV-Vis absorption spectra of (A) ClInOPyPc (i) and ClInOMePyPc (ii) in DMF, and (B) ClInOMePyPc in (i) water (ii) water plus Triton-X 100 and (iii) 0.2% DMF.

In water, the ClInOMePyPc showed a split Q band which is the indication of H aggregation (Fig. 3.2 B(i)). Aggregation in MPc complexes is judged by broadening or split in the Q band, with the high energy band being due to the "H" aggregate [127]. Addition of Triton-X 100 as a surfactant resulted in the reduction of the intensity of the high energy band and increase in the intensity of the monomer band (at 699 nm), showing reduction in aggregation, Figure 3.2 B(ii). However, Triton-X 100 did not break the aggregates completely since the high energy

band is still present, Figure 3.2 B(ii). The spectrum of ClInOMePyPc in 0.2% DMF in pH 7.4 buffer shows less aggregation, Fig. 3.2 B(iii), but with some broadening in the 630 nm where the aggregate absorbs. ClInOPyPc is insoluble in PBS (pH 7.4)), but was slightly soluble in the pH 7.4 buffer in the presence of 0.2% DMF with sonication and maxima shown in Table 3.1. It is important to determine aggregation behaviour in 0.2% DMF in water since this medium will be used for cell studies.

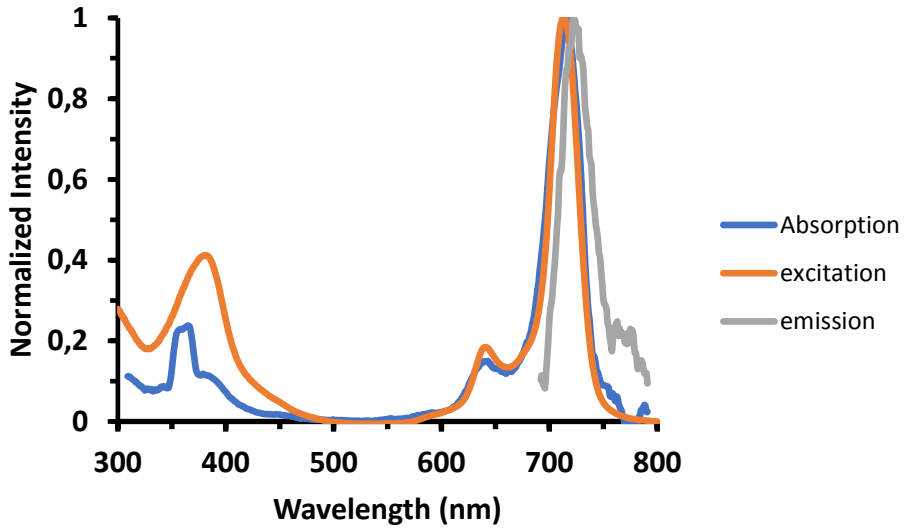

Figure 3.3: Absorption, excitation and emission spectra for ClInOPyPc in DMF.

Emission and excitation spectra for complex ClInOPyPc are shown in Fig. 3.3. The emission spectra were mirror images of the excitation spectra and the latter was the same as the absorption spectra for ClInOPyPc, indicating a non-aggregation of phthalocyanine in solution. The closeness of the Q-band absorption maxima to that of excitation shows that the absorbing molecule is the same as the emitting molecule.

3.2 Characterization for magnetic nanoparticle and their conjugate with ClInOCPc

The synthesis of NH_2 containing MNPs involves functionalization with silica using tetraethoxysilane (TEOS) followed by addition of 3-aminopropyltriethoxysilane (APTES) [44], Scheme 3.2 A. Even though the conjugation of ClInOCPc to MNPs has reported before [47], a new batch of MNPs was synthesized with different defects and sizes, hence the nano-conjugates were characterized in this work.

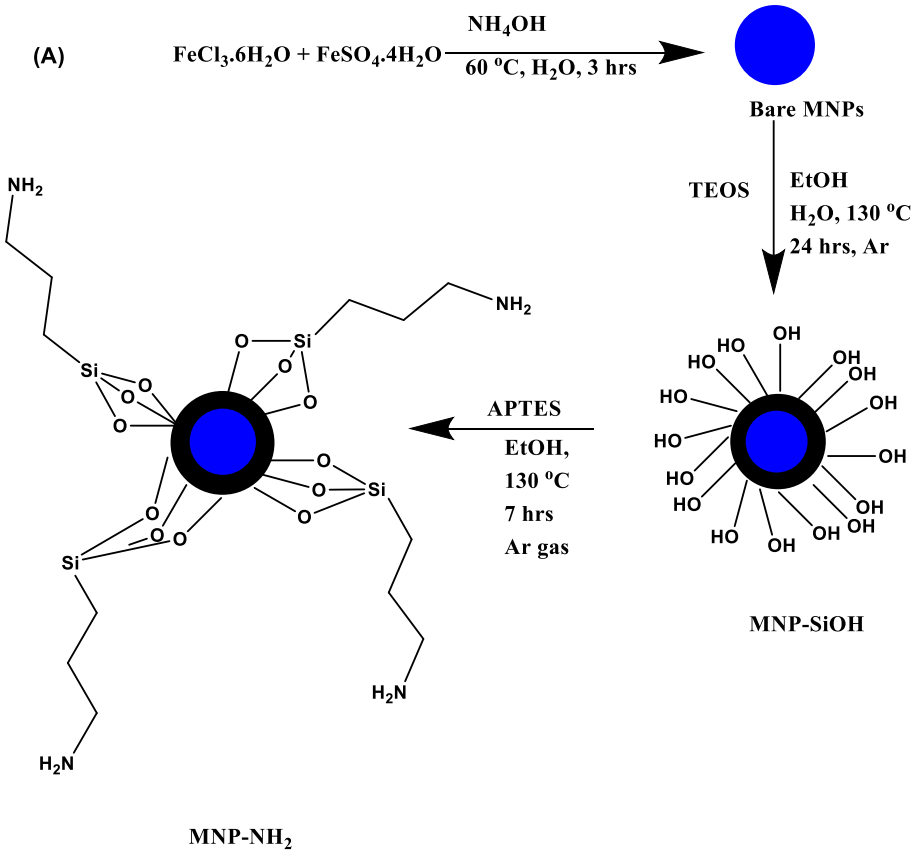

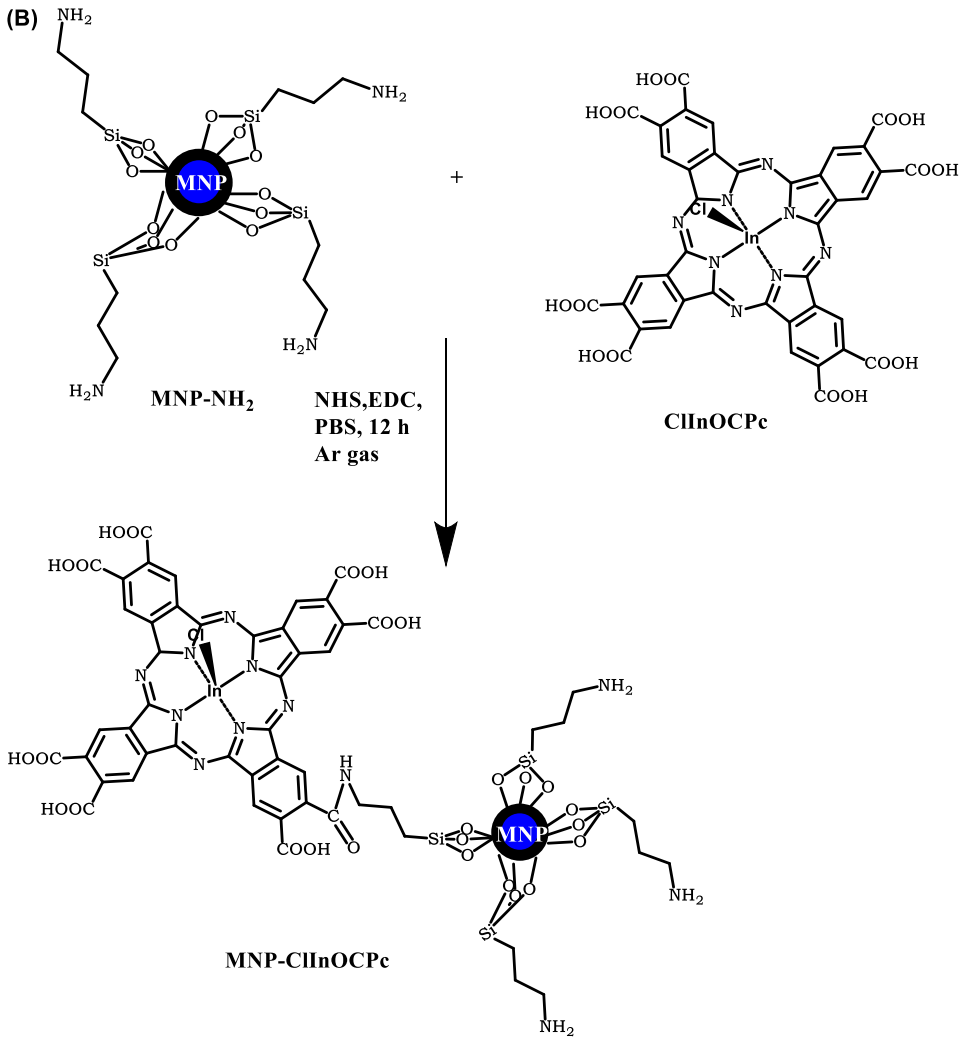

Scheme 3.2: A) Synthesis of MNPs using the co-precipitation method and B) Synthetic route for MNP-ClInOCPc.

3.2.1 Energy-Dispersive X-ray Spectra (EDX)

The EDX spectra of MNP-NH_2, ClInOPc and MNP-ClInOCPc are shown in Fig. 3.4. The MNP-NH_2 (Fig. 3.4 (a)), had Fe and O from the bare MNP, and Si, N and C from the capping agents (TEOS and APTES). ClInOCPc had the expected peaks, namely In, C, O and N which were obtained and for the MNP-ClInOCPc, 3.4 (c) peaks originating from both the ClInOCPc and MNPs were observed. The intense Cl is from the axial ligand in both the ClInOCPc and MNP-ClInOCPc.

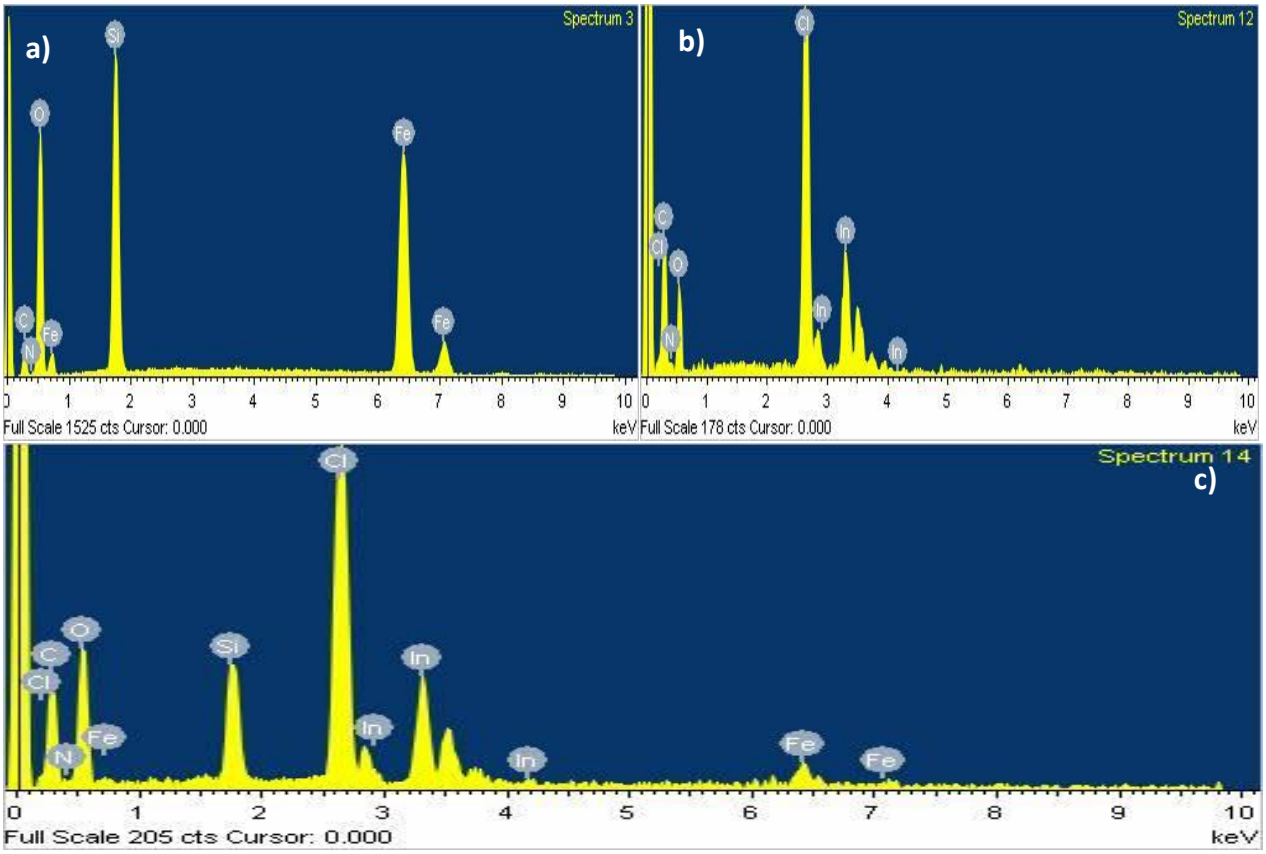

Figure 3.4: EDX data for illustrating the composition of a) MNP-NH_2, b) ClInOCPc, and c) MNP-ClInOCPc conjugate.

3.2.2 Transmission electron microscopy

The TEM images of the MNP-NH_2 (Fig. 3.5) show that they are spherical in nature with a size ranging from 30-35 nm and are mono-dispersed as reported in literature [44]. The TEM image of the MNP-ClInOCPc conjugates shows aggregation, which was not observed in the nanoparticle alone. Aggregation upon conjugation could also be due to $\pi\pi$ interaction from adjacent Pc [127].

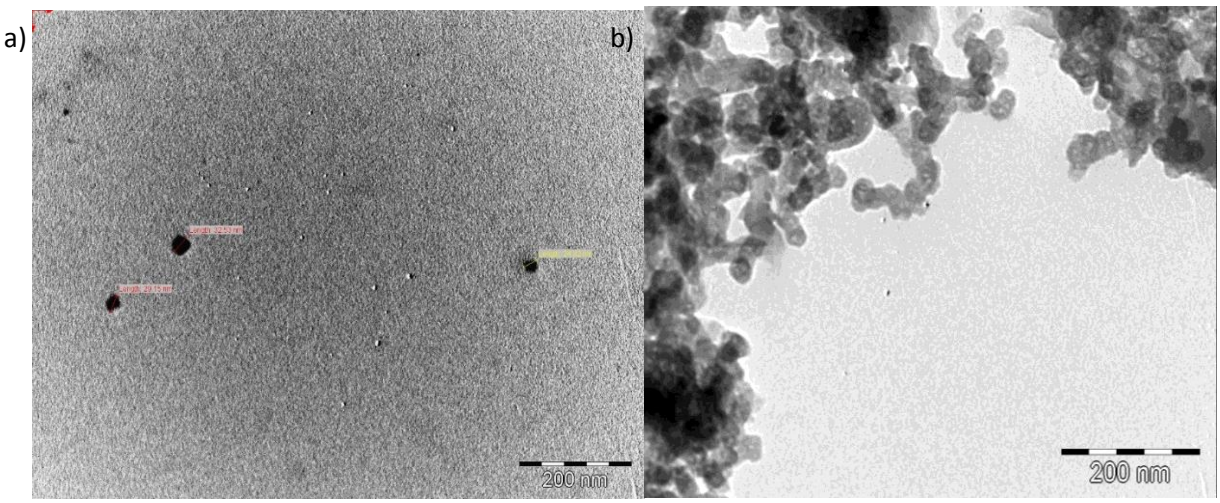

Figure 3.5: TEM images of a) MNP-NH_2 and (b) MNP-ClInOCPc conjugate.

3.2.3 Dynamic light scattering (DLS)

DLS was employed to determine the hydrodynamic sizes, Fig. 3.6. The sizes for MNP-NH_2 and MNP-ClInOCPc were 38.0 nm and 43.8 nm, respectively. The size for DLS is slightly higher than the range obtained from TEM. The sizes determined by DLS have been reported to be larger than those determined by other techniques since DLS results tend to be skewed toward larger particles [128]. There is an increase in size of the MNP-NH_2 nanoparticles upon conjugation due to aggregation as discussed above.

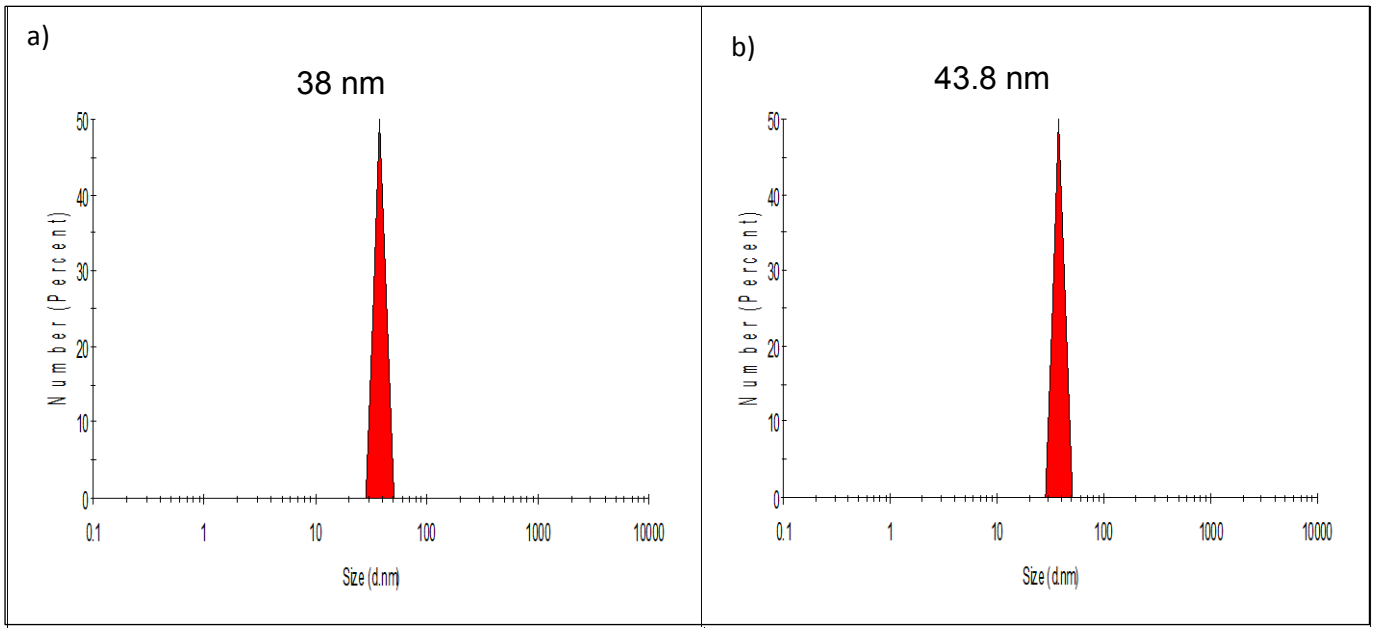

Figure 3.6: DLS plots of (a) MNP-NH_2 and (b) MNP-ClInOCPc in DMSO.

3.2.4 X-ray Powder Diffraction

The XRD diffractograms (Fig. 3.7), show peaks characteristic of magnetite at (220),(311), (400),(422), (511) and (440) as reported before [44]. The XRD pattern for ClInOCPc shows sharp peaks. Sharp XRD peaks are not unusual in phthalocyanines [129, 130]. The conjugate retains the crystallinity of both the ClInOCPc and MNP-NH_2. Upon the formation of the amide bond between the MNP-NH_2 and ClInOCPc, the XRD peaks shifted slightly.

The XRD data was also used to determine the size of the nanoparticles and conjugate employing the Debye-Scherrer [131] equation (3.1):

$$d(\mathring{A}) = \frac{k\lambda}{\beta Cos\theta} \qquad 3.1$$

where k is an empirical constant equal to 0.9, λ is the wavelength of the X-ray source, (1.5405 Å), β is the full width at half maximum of the diffraction peak, and θ is the angular position of the peak. The MNP-NH_2 nanoparticle has a size of 33.8 nm, this value is within the range for TEM. After conjugating with the ClInOCPc there was a size increase to 47.03 nm, thus contradicting the DLS results.

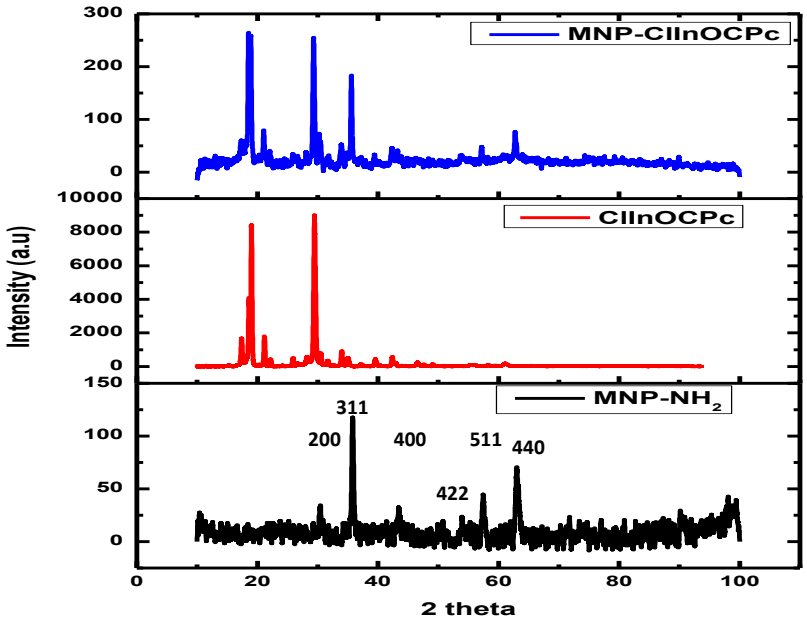

Figure 3.7: XRD diffractograms of MNP-ClInOCPc, ClInOCPc and MNP-NH_2.

3.2.5. X-ray photoelectron spectroscopy (XPS)

The survey spectra for MNP-NH_2, ClInOCPc and the MNP-ClInOCPc are shown in Fig. 3.8. The MNP-NH_2 showed that the nanoparticle had all the expected peaks such as the O 1s, C 1s, N 1s, Si 1s and Si 2s. The ClInOCPc and the MNP-ClInOCPc spectra were similar with MNP-ClInOCPc having an additional Si peaks from the MNPs, the intensity of the In peak was low for the ClInOCPc alone and was not visible in the MNP-ClInOCPc survey spectrum.

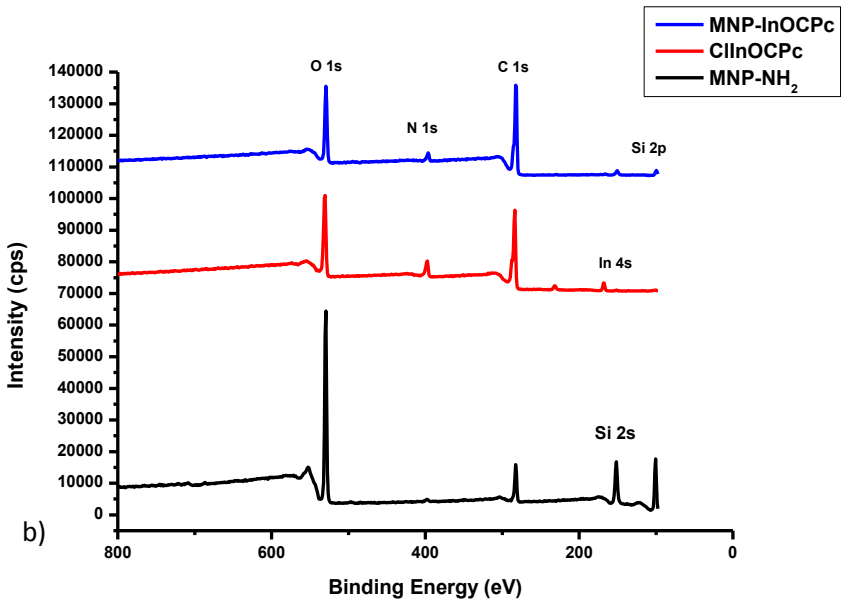

Figure 3.8: Survey spectra of MNP-NH_2, ClInOCPc and MNP-ClInOCPc conjugate.

To further confirm the formation of amide linkage between the MNP-NH_2 and ClInOCPc, high resolution N 1s XPS was employed, Fig. 3.9. The spectra of MNP-NH_2 (Fig 3.9 A) exhibits only two peaks, namely N-C (398.1 eV) and N-H (400.3 eV) from the capping agent (APTES). For the ClInOCPc, the high resolution N1s was resolved into two components at 398.5 and 401.3 eV corresponding to N-C, N-In, Fig. 3.9 B. The conjugate showed four components at 396.6,

397.95, 399.8 and 402.0 eV corresponding to N-C, N-H, N-In and N-C=O (Fig. 3.9 C), with In present. The N-C=O peak confirms amide linkage and therefore a successful conjugation.

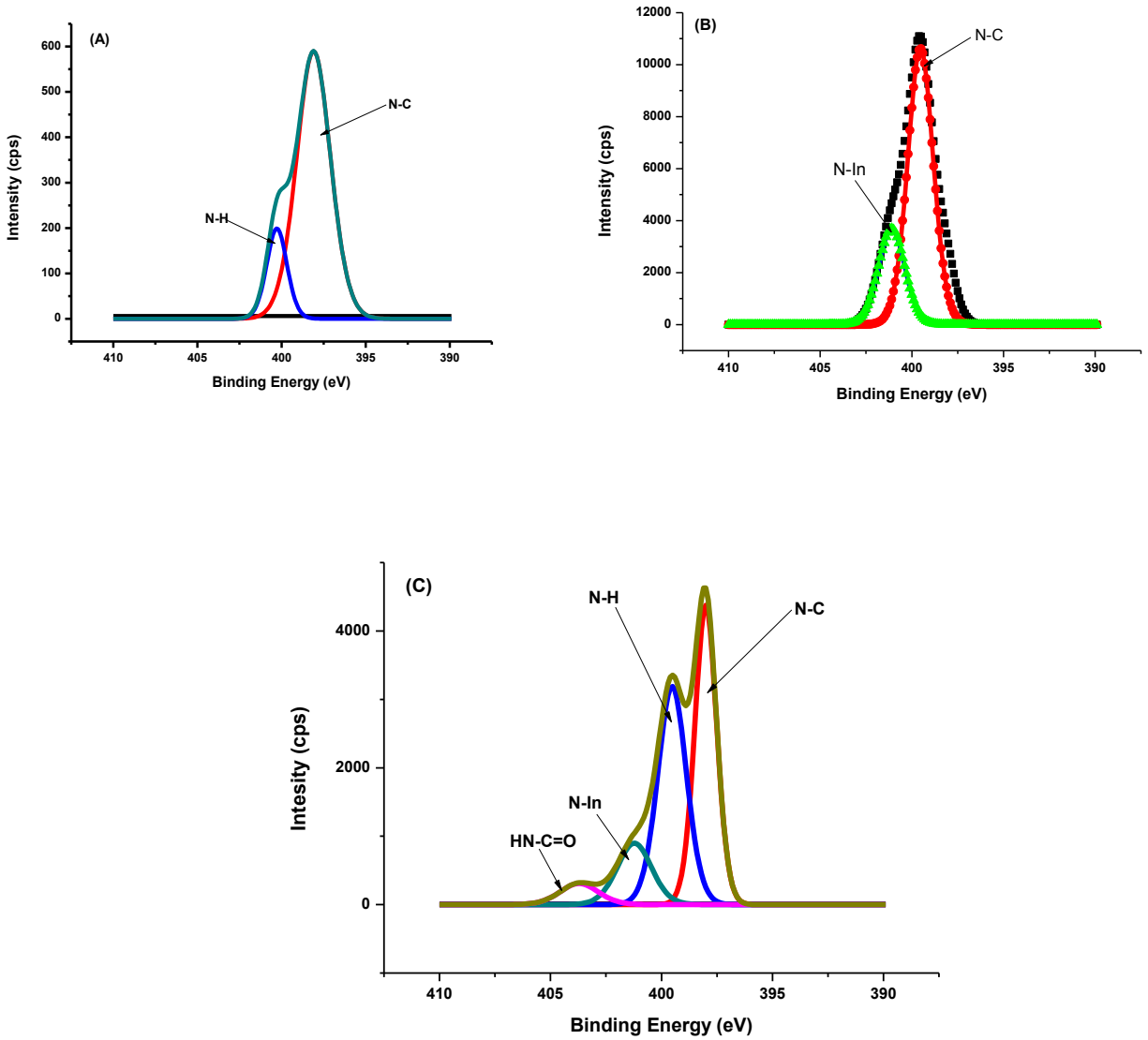

Figure 3.9: High resolution of N 1s for (A) MNP-NH_2 (B) ClInOCPc and (C) MNP-ClInOCPc conjugate.

3.2.6 UV-vis spectra

The spectrum of ClInOCPc were recorded in DMF and there were no shifts in the Q band for ClInOCPc in the presence of MNPs, Table 3.1 and Fig. 3.10.

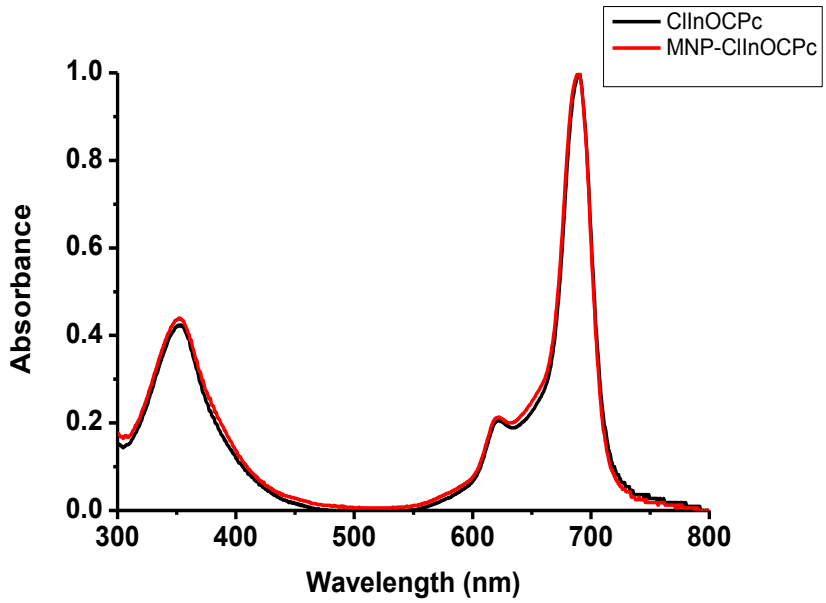

Figure 3.10: UV spectra for ClInOCPc and MNP-ClInOCPc in DMF.

3.3 Photophysical and photochemical parameters

The fluorescence (Φ_F) (eq 1.1) and triplet (Φ_T) (eq 1.2) quantum yields were obtained using a comparative method, using ZnPc as a standard with the following values: Φ_F = 0.2 [117] in DMSO (values in DMF were obtained by correcting for refractive index) and Φ_T = 0.58 for ZnPc [113] in DMF.

Singlet oxygen quantum yields (Φ_Δ) for Pcs in DMF and in PBS (containing 0.2% DMF) were determined using DPBF and ADMA, respectively as chemical quenchers using the relative methods described before [113], eq. 1.5 and ZnPc as a standard in DMF (Φ_Δ = 0.56) [113] and ClAlPcSmix in aqueous media (Φ_Δ = 0.42 [113]). The absorbances of DPBF or ADMA were spectroscopically monitored at 417 nm or 380 nm respectively at a predetermined time course.

3.3.1. Fluorescence quantum yields (Φ_F) and lifetimes (τ_F)

The fluorescence quantum yields (Φ_F) of complexes ClInOPyPc, ClInOMePyPc, ClInOCPc and MNP-ClInOCPc are given in Table 3.1. The low Φ_F value quantum yield observed the Pcs alone, due to the heavy central metal (indium) which encourages intersystem crossing to the triplet state rather than transition back to the ground state. The values decrease further for ClInOCPc in the presence of MNPs due to the additional heavy atom effect of the latter.

The fluorescence lifetimes (τ_F) were determined using the TCSPC method, Fig. 3.11 and biexponential decay processes were observed. Average lifetimes are shown in Table 3.1. The presence of two fluorescence lifetimes for the phthalocyanine have been explained as being due to the formation of aggregates which are non-fluorescent, but which can quench the monomer [132], resulting in quenched and unquenched lifetimes. Values are within those reported for phthalocyanines [121].

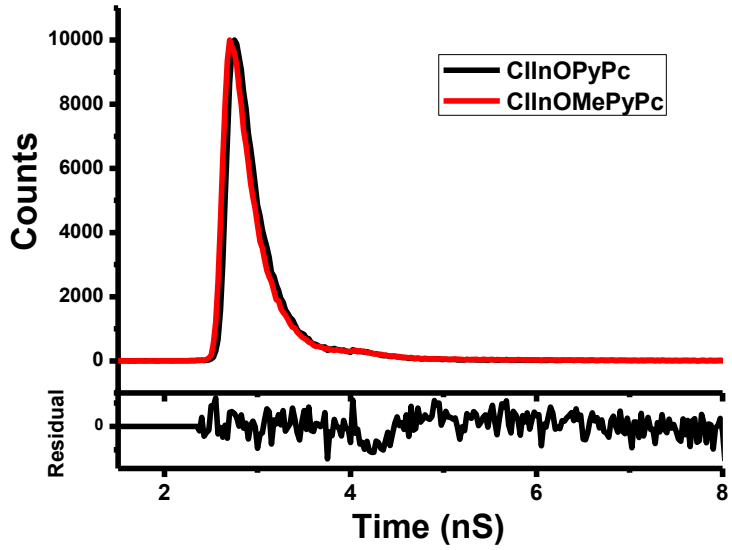

Figure 3.11: Fluorescence lifetime decay curves of ClInOPyPc and ClInOMePyPc in DMF.

3.3.2. Triplet quantum yield (Φ_T) and lifetimes (τ_T)

Table 3.1 shows that MNP-ClInOCPc has a greater Φ_T (at 0.83) compared to ClInOCPc at 0.69. due to the presence of the heavier magnetic nanoparticle. The triplet lifetimes follow the similar trend as flourescences and there is an increase in the lifetime upon conjugating which can be attributed to the protection of the Pc by the MNPs. The transient differential spectrum for complex ClInOPyPc (as an example) in DMF shown in Fig. 3.12 and it shows a triplet absorption maximum at 530 nm. The insert shows the triplet decay curve. The triplet decay curves obeyed second order kinetic which is typical of MPc complexes at high concentration (>1 $\times$ 10^{-4} M) due to the triplet-triplet recombination [133]. For ClInOPyPc (Φ_T = 0.53), ClInOMePyPc (Φ_T = 0.48) larger for the former with corresponding longer τ_T. for the latter.

In general the Φ_T values are high corresponding to low Φ_F values. The Φ_F and Φ_T values in water (0.2 % DMF) are lower due to quenching effect of water [117]. Quantum yields of internal conversion (Φ_{IC}) were obtained from Eq. 3.2, which assumes that only three processes (fluorescence, intersystem crossing and internal conversion), jointly deactivate the excited singlet state of the phthalocyanine complexes.

$$(\Phi_{IC}) = 1- (\Phi_F + \Phi_T) \qquad 3.2$$

These values are generally low as shown in Table 3.1.

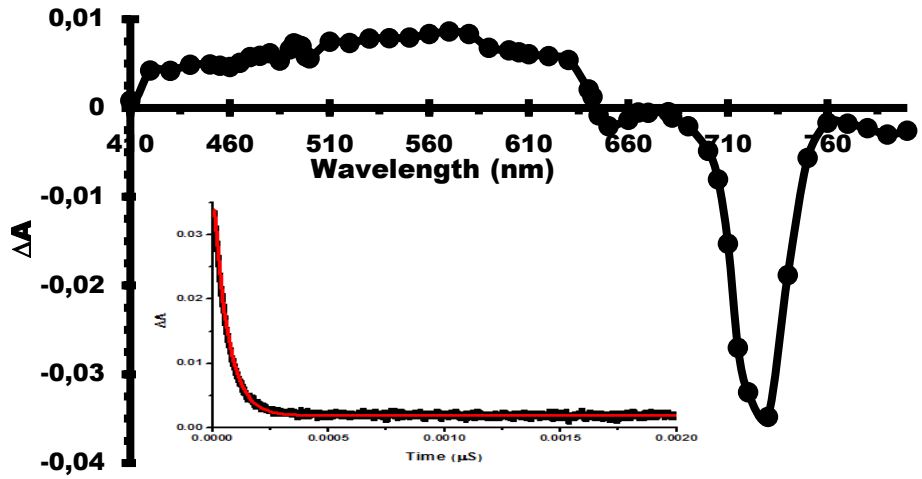

Figure 3.12: Transient differential spectrum of ClInOPyPc, excitation wavelength at 687 nm. Insert= corresponding triplet decay curve. Solvent= DMF.

Table 3.1: Photophysical properties of Indium (III) phthalocyanines in DMF unless otherwise stated.

Complex	$^{a}\lambda_{abs}$ (nm)	$^{a}\lambda_{emm}$ (nm)	$^{a}\lambda_{exc}$ (nm)	Φ_F	τ_F (ns)	Φ_T	Φ_Δ	Φ_{IC}	τ_T (μs)	S_Δ
ClInOPyPc	712 710[b]	723 718[b]	713 711[b]	0.012 0.009[b]	0.25 0.09[b]	0.53 -	0.46 0.33[b]	0.46 -	56 -	0.87 -
ClInOMePyPc	699 698[b]	711 710[b]	703 702[b]	0.013 0.008[b]	0.33 0.33[b]	0.48 -	0.33 0.31[b]	0.51 -	66 -	0.69 -
ClInOCPc	689 693[b]	699 702[b]	691 695[b]	0.018 <0.01[b]	1.94 1.84[b]	0.69 -	0.61 0.41[b]	0.29 -	115 -	0.88 -
MNP-ClInOCPC	689 693[b]	699 704[b]	690 695[b]	0.012 <0.01[b]	1.97 1.67[b]	0.83 -	0.48 0.29[b]	0.15 -	246 -	0.58 -

$^{a}\lambda_{abs}$ = absorption wavelength, λ_{em}= emission wavelength and λ_{exc} = excitation wavelength. [b] in 0.2% DMF/water.

3.3.3 Singlet oxygen quantum yield (Φ_Δ)

Singlet oxygen quantum yield (Φ_Δ) is a measure of singlet oxygen generation and the Φ_Δ values were determined in DMF using DPBF as a singlet oxygen quencher, Fig. 3.13 A and ADMA as a quencher in aqueous media, Fig. 3.13 B. No significant changes in the Q band intensity as the intensity of DPBF peak decreased. The Φ_Δ values are larger for ClInOPyPc compared to complex ClInOMePyPc, corresponding to high triplet yield values in DMF and 0.2% DMF/water.

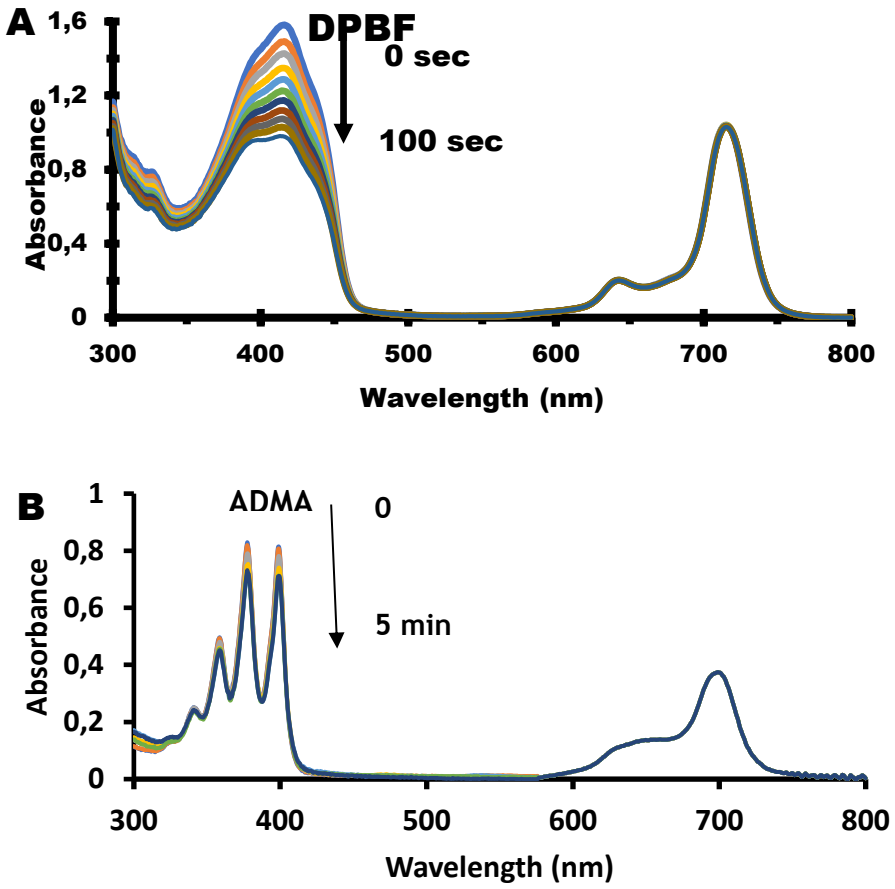

Figure 3.13: Absorption spectral changes during the determination of singlet oxygen quantum yield for (A) ClInOPyPc in DMF and (B) ClInOMePyPc in 0.2% DMF/water using DPBF and ADMA as quenchers, respectively.

Table 3.1 shows Φ_Δ values in DMF are 0.61 and 0.48 for ClInOCPc and MNP-ClInOCPc, respectively. In water (containing 0.2 % DMF, since ClInOCPc and MNP-ClInOCPc are not fully soluble in water) the values are 0.41 and 0.29 for ClInOCPc and MNP-ClInOCPc, respectively. The decrease is surprising since with increase in the Φ_T, the Φ_Δ values are also expected to increase because the more populated the triplet state is, the more singlet oxygen is produced. The decrease in Φ_Δ values maybe attributed to the screening effect caused by the MNPs, which could have prevented the interaction of the excited triplet state of the nanoconjugates and the ground state molecular oxygen [134]. The singlet oxygen quantum yield is lower in water compared to the studies DMF. Water is known to quench the singlet state [117].

The efficiency of energy transfers between the triplet excited state of the phthalocyanines and ground state triplet oxygen to form excited singlet state oxygen (S_Δ) is determined using the ratio ($S_\Delta = \Phi_\Delta/\Phi_T$). S_Δ should be close to unity. The values in S_Δ are all greater than 0.5 but not all are close to unity (Table 3.1).

3.4 Conclusion for the chapter

The Pc complexes were thoroughly characterized with various techniques with the UV/Vis spectra showing that the ClInOPyPc was the most red shifted Pc with a Q-band wavelength at 712 nm, while the ClInOCPc and MNP-ClInOCPc had their bands at 689 nm. The photophysical/chemical studies were conducted in organic and aqueous media. The ClInOCPc had a high Φ_{Δ} of 0.61 and 0.41 in DMF and 0.2 % DMF/Water respectively. Though the MNP-ClInOCPc had a high Φ_{T} of 0.83 there was considerable decrease to 0.48 of Φ_{Δ} in DMF due to the screening effect induced by the MNPs.

CHAPTER FOUR

Characterization of polyacrylonitrile nanofibers

4. Characterization of modified PAN fibers

All complexes were mixed with PAN polymer solution to produce nanofibers. In this chapter, the characterization and singlet oxygen quantum yields of ClInOCPc/PAN, MNP-ClInOCPc/PAN, ClInOPyPc/PAN and ClInOMePyPc/PAN are presented. The PAN fibers were all tested for unknown water sample and all tested for photodegradation of methyl red.

4.1 Solid state UV-Vis spectra

The solid state UV-Vis spectra of ClInOCPc/PAN, MNP-ClInOCPc/PAN and ClInOPyPc/PAN are shown in Fig. 4.1 A and B. The ClInOCPc/PAN and MNP-ClInOCPc/PAN were more red shifted, from 689 nm in solution to ~ 700 nm in the solid state while the ClInOPyPc/PAN and ClInOMePyPc/PAN (the spectra was the same for both, hence the latter not shown) shifted from 712 nm to ~ 722 nm. In Table 4.1, the spectra are broad due to aggregation but showed the presence of the Pc. Aggregation is typical of MPc spectra in the solid state [135]. Aggregation is judged by broadening or split in the Q band, with the high energy band being due to the “H” aggregate [127]. The red-shifting in spectra is common for Pcs in the solid state [136].

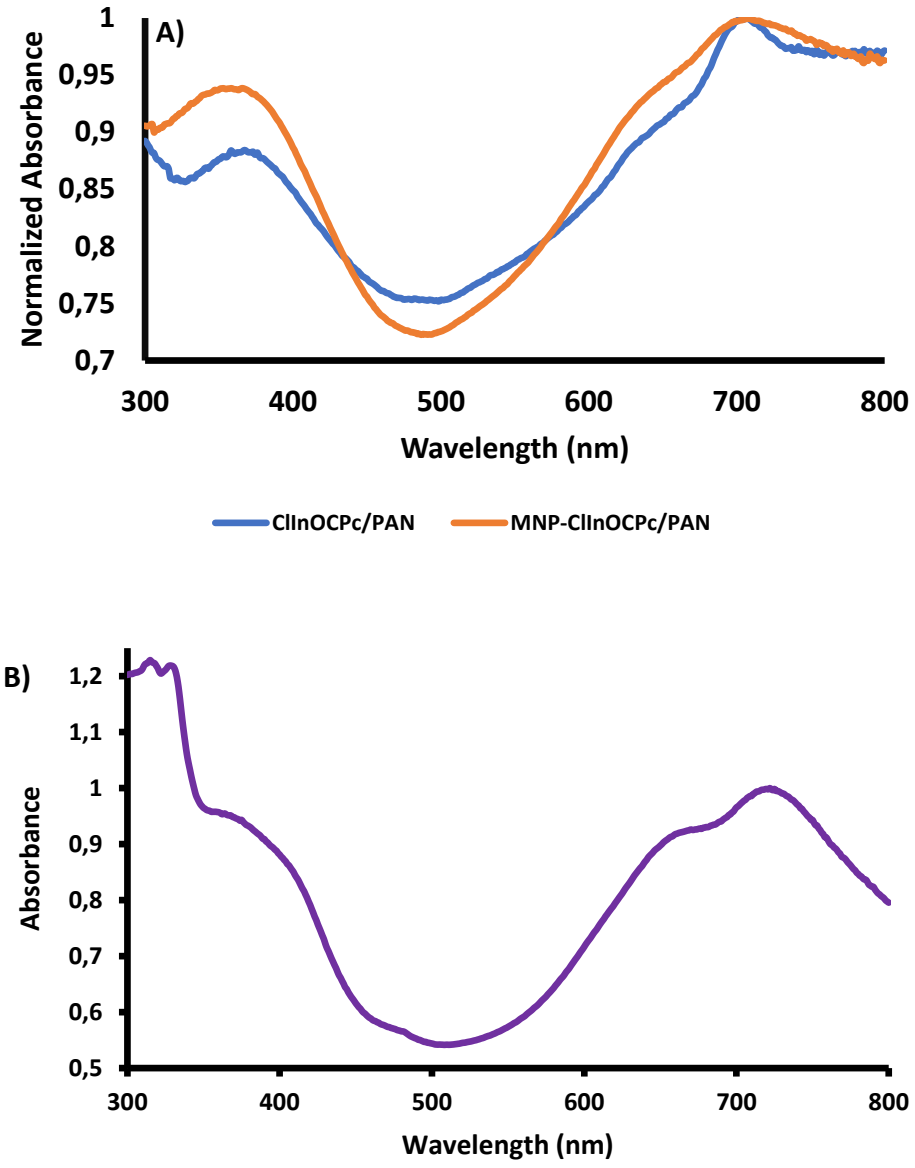

Figure 4.1: UV-Vis spectra of A) ClInOCPc/PAN and MNP-ClInOCPc/PAN, and B) ClInOPyPc/PAN in the solid state.

4.2 Scanning Electron Microscopy (SEM)

The SEM images, Fig 4.2, reveal that the nanofibers are cylindrical and unbranched with relatively smooth surfaces even after incorporation of the Pcs and conjugates. The diameter for PAN alone was 205 nm, upon embedding the complexes there was an increase in diameter for all complexes: ClInOCPc/PAN, MNP-ClInOCPc/PAN, ClInOPyPc/PAN, and ClInOMePyPc/PAN (the latter not shown in Fig 4.2) to 370 nm, 520 nm, 390 nm, and 430 nm respectively. The increase in fiber diameter for Pc/MNPs electrospun fibers has been reported before [88].

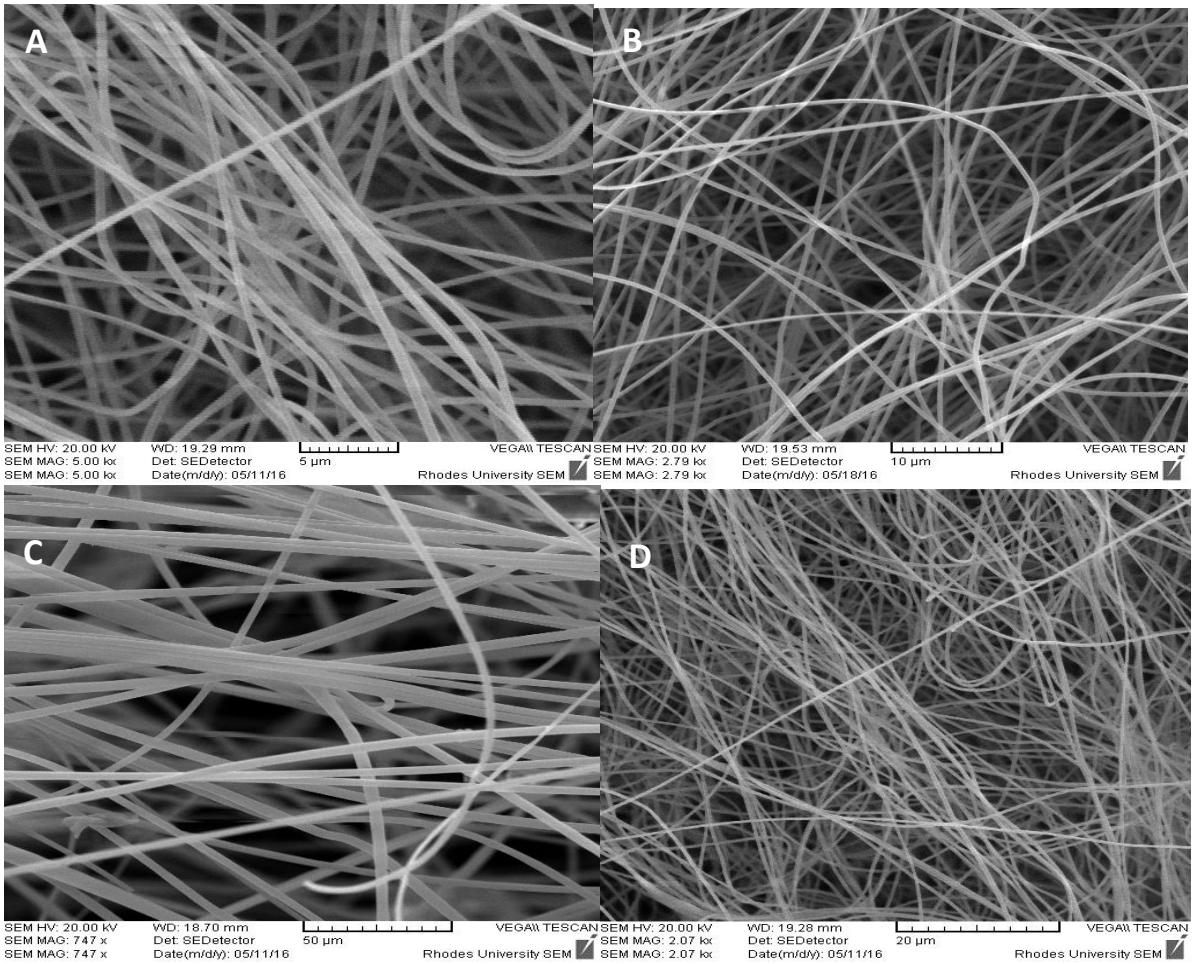

Figure 4.2: SEM images of the nanofibers mats of A. PAN, B. ClInOCPc/PAN, C. MNP-ClInOCPc/PAN, and D. ClInOPyPc/PAN.

4.3 Energy-Dispersive X-ray Spectra (EDX)

The EDX spectrum of the PAN fibre alone, had the expected C, and N peaks with all the conjugates possessing In from the central metal. Additional peaks such as O (in PAN) arise from the aluminium foil (used to collect the fiber) and for ClInOCPc/PAN and MNP-ClInOCPc, it is not clear where S comes from. For ClInOPyPc/PAN had the expected elements. EDX spectrum was similar for ClInOMePyPc/PAN (hence not shown).

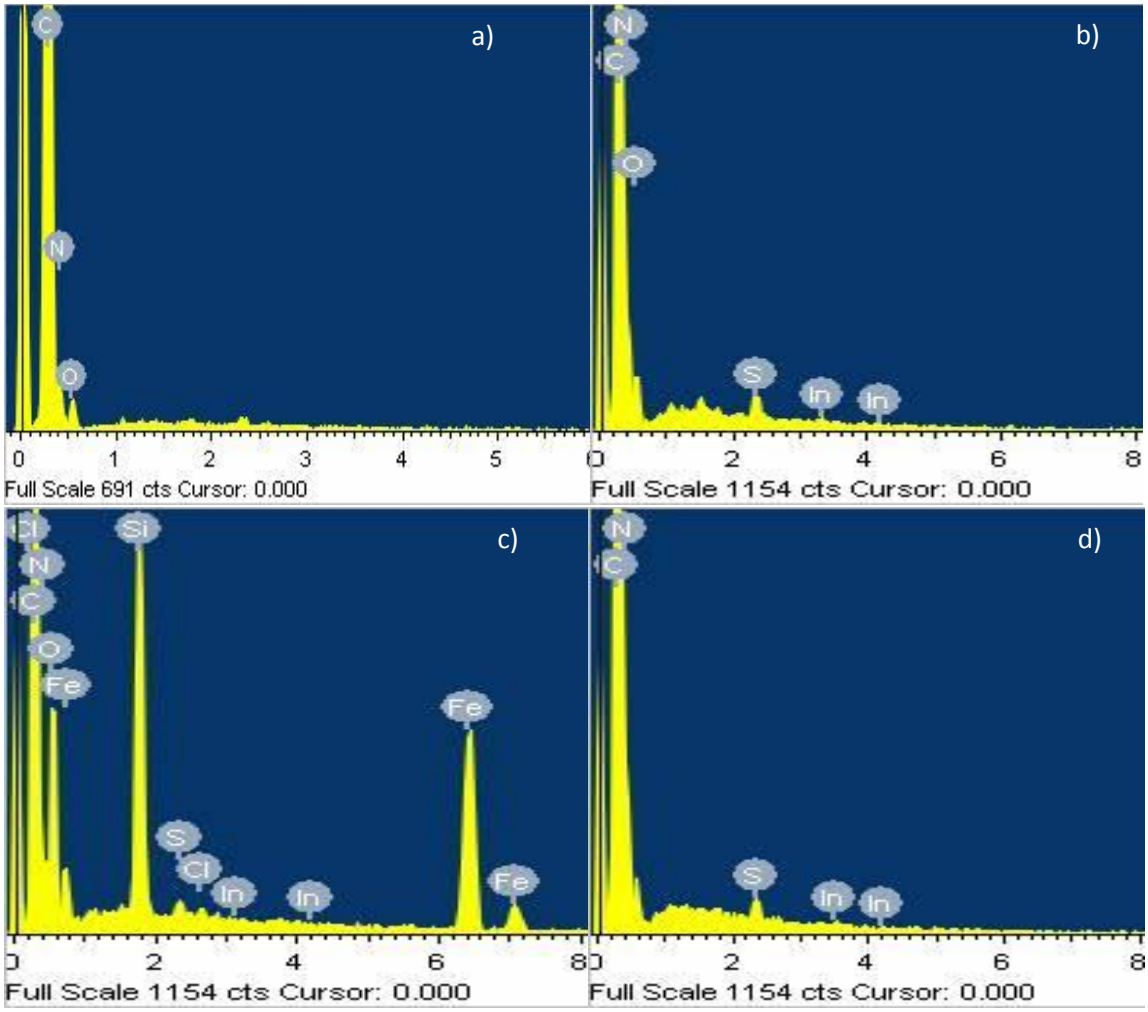

Figure 4.3: EDX data for illustrating the composition a) PAN, b) ClInOCPc/PAN c) MNP-ClInOCPc/PAN, and d) ClInOPyPc/PAN.

4.4 X-ray Diffraction

The XRD patterns for PAN fibres shows one prominent peak at approximately 17° and a weaker peak at 24°, Fig. 4.4 (using ClInOCPc/PAN and MNP-ClInOCPc/PAN as examples). It has been reported that the electrospun fibres produce amorphous peak due to the rapid process of formation leading to the loss of crystals [137]. Following electrospinning, the sharp peaks (Fig. 3.7) of the ClInOCPc are lost. This was also observed for the MNP-ClInOCPc/PAN with an additional peak at 38° which is a prominent peak in magnetite.

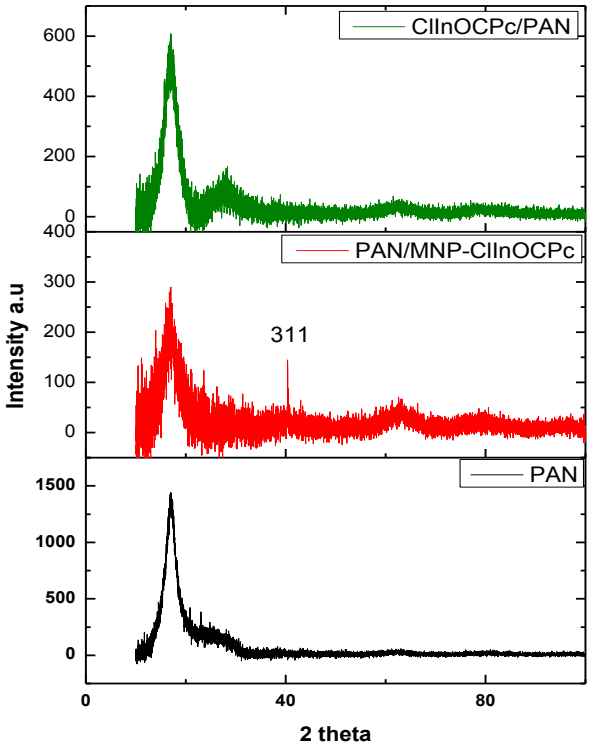

Figure 4.4: XRD diffractograms of PAN, MNP-ClInOCPc/PAN and ClInOCPc/PAN.

4.5 Brunauer-Emmett-Teller isotherm

The nitrogen adsorption-desorption isotherms for the modified PAN fiber mats are shown in Fig. 4.5 using ClInOCPc/PAN and MNP-ClInOCPc/PAN (as examples). The BET of electrospun fibres consistently showed an initial adsorption loop indicating the presence of a monolayer and classified as type IV sorption isotherms. This suggests a wide distribution of pore sizes within the multi-layered fibres [138]. The surface area for PAN was 17.0 m^2/g, upon embedding the photosensitizers, there was an increase to 22.6 m^2/g, 25.3 m^2/g and 37.3 m^2/g for ClInOCPc/PAN, ClInOPyPc/PAN and MNP-ClInOCPc/PAN, respectively, Table 4.1. There was no difference between PAN and ClInOCPc/PAN pore volume of 0.11 cm^3/g, but there was an increase for ClInPyPc/PAN with 0.13 cm^3/g and MNP-ClInOCPc/PAN observing 0.18 cm^3/g, Table 4.1. This increase of both surface area and pore volume for MNP-ClInOCPc/PAN, is due to the presence of large magnetic nanoparticles. There was also an increase in the pore sizes from 204.6 Å for PAN to 247.5 Å, 250.6 Å and 261.9 Å, (Table 4.1) for ClInOCPc/PAN, ClInOPyPc/PAN and MNP-ClInOCPc/PAN respectively, promoted by the change in viscosity brought by the addition of complexes. ClInOMePyPc is left out since it gave unsatisfactory BET results.

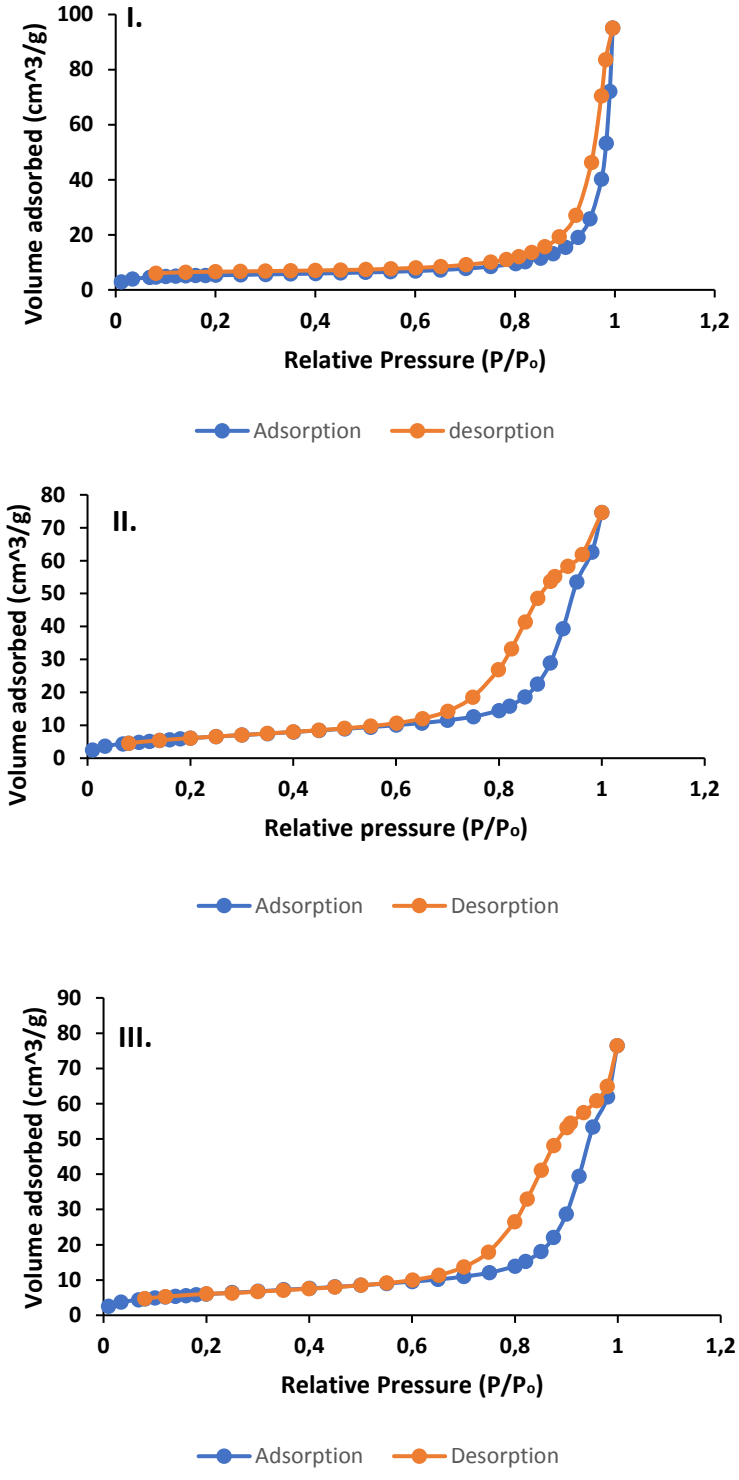

Figure 4.5: BET adsorption and desorption graphs of (I) PAN, (II) ClInOCPc/PAN and (III) MNP-ClInOCPc/PAN.

4.6 Singlet Oxygen quantum yield

For the determination of Φ_Δ of ClInOCPc/PAN, ClInOPyPc/PAN, ClInOMePyPc/PAN and MNP-ClInOCPc/PAN embedded in fiber, the direct chemical method was employed due to lack of standards. The studies were carried out in an aqueous solution, using ADMA as a chemical quencher for singlet oxygen in aqueous media. The modified fiber (using 10 mg for all compounds) was suspended in the solution containing ADMA, and irradiated using the photolysis setup described in the experimental section. The quantum yield of ADMA (Φ_{ADMA}) was calculated using eq. 1.9. The photodegradation of ADMA is shown in Fig. 4.6. Both ClInOCPc and ClInOMePyPc/PAN did not leach out of the fiber even though both are water soluble. For MNP-ClInOCPc/PAN, ClInOCPc/PAN, ClInOPyPc/PAN and ClInOMePyPc/PAN suspended in water, the Φ_Δ values are 0.22, 0.36, 0.18 and 0.17, respectively. The Φ_Δ values were larger for ClInOCPc compared to MNP-ClInOCPc for reasons explained in chapter 3.

Table 4.1: Summary of the characterization of polymer embedded complexes.

Sample	BET area (m^2/g)[a]	BET pore size (Å)	Q band (nm)[b]	Φ_Δ [c]
PAN	17.0 (0.11)	204.6	-	-
ClInOCPc/PAN	22.6 (0.11)	247.5	702 (689)	0.36
MNP-ClInOCPc/PAN	37.3 (0.18)	261.9	702 (689)	0.22
ClInOPyPc/PAN	25.3 (0.13)	250.6	722 (712)	0.18
ClInOMePyPc/PAN	-	-	722 (699)	0.17

a –are BT values (cm^3/g)

b – values in brackets in DMF

c- values in water

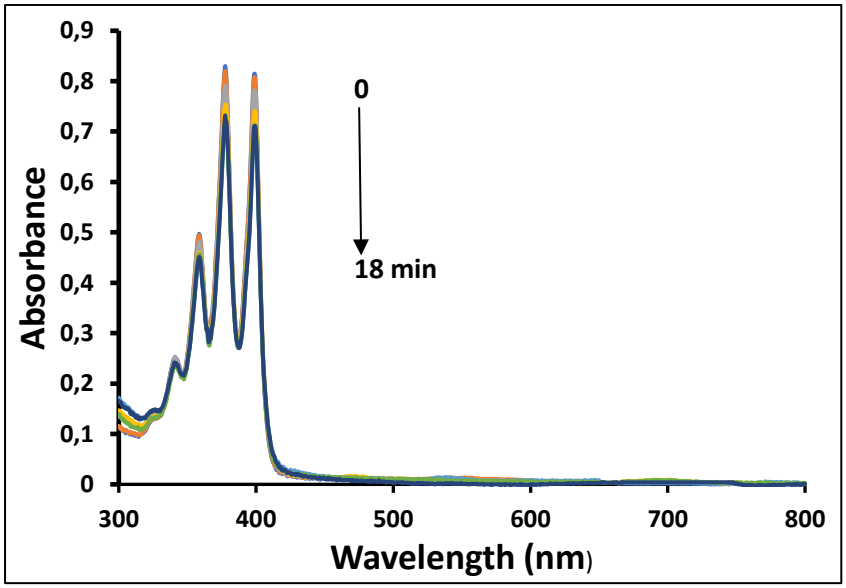

Figure 4.6: The UV-vis spectra showing changes during degradation ADMA in the presence of ClInOCPc/PAN suspended in water.

4.7 Conclusion for the chapter

This chapter discussed the characterization of PAN fiber and modified PAN fibers, these fibers were achieved by electrospinning method. The fibers were further characterized using SEM, where the fibers were unbranced and all had diameters in nanometer region (205, 370, 390, 430 and 520 for PAN, ClInOCPc/PAN, ClInOPyPc/PAN, ClInOMePyPc/PAN, and MNP-ClInOCPc/PAN, respectively). The singlet oxygen quantum yield of the fibers was completed in water, though both ClInOCPc and ClInOMePyPc are water soluble, they did not leach out. The Φ_{Δ} of the fibers followed the same trend as the compounds in solution with the ClInOCPc/PAN having the highest value, the values are as follow MNP-ClInOCPc/PAN, ClInOCPc/PAN, ClInOPyPc/PAN and ClInOMePyPc/PAN (0.22, 0.36, 0.18, 0.17, respectively).

CHAPTER FIVE

Photodynamic Antimicrobial Chemotherapy (PACT)

This chapter discusses the results of photodynamic antimicrobial chemotherapy (PACT) using neutral Pc; ClInOPyPc, ClInOCPc, MNP-ClInOCPc and cationic Pc, ClInOMePyPc. All tested in solution and when supported in PAN for the unknown water sample. For known bacteria only solution studies were done.

5.1 PACT Studies of *E.coli*, *C.albican* and *S.aurues* in solution.

Photodynamic antimicrobial studies were performed in water and 0.2% DMF (ClInOPyPc, ClInOCPc and MNP-ClInOCPc were insoluble in PBS but were soluble in the presence of 0.2% DMF followed by sonication) using ClInOPyPc and ClInOMePyPc (0.75 µg/mL each) and ClInOCPc and MNP-ClInOCPc (2.5 µg/mL each). Bacteria such as *S. aureus* are known to be resistant to DMF [139]. The survival of the microbial species was tested in PBS with 0.2% DMF (in the absence of the Pcs) to monitor the effects of the organic solvent (control in Fig. 5.1 A). The media have very low impact on the overall results. The dark toxicity studies (Fig. 5.1 A and B) showed that Pc complexes had no significant dark toxicity even at high concentration; this was done to verify that the micro-organism inactivation was due solely from the introduction of light. ClInOPyPc and MNP-ClInOCPc had slightly higher dark toxicity. The dark studies were performed for all microorganism but *S. aureus* is shown as an example (Fig. 5.1).

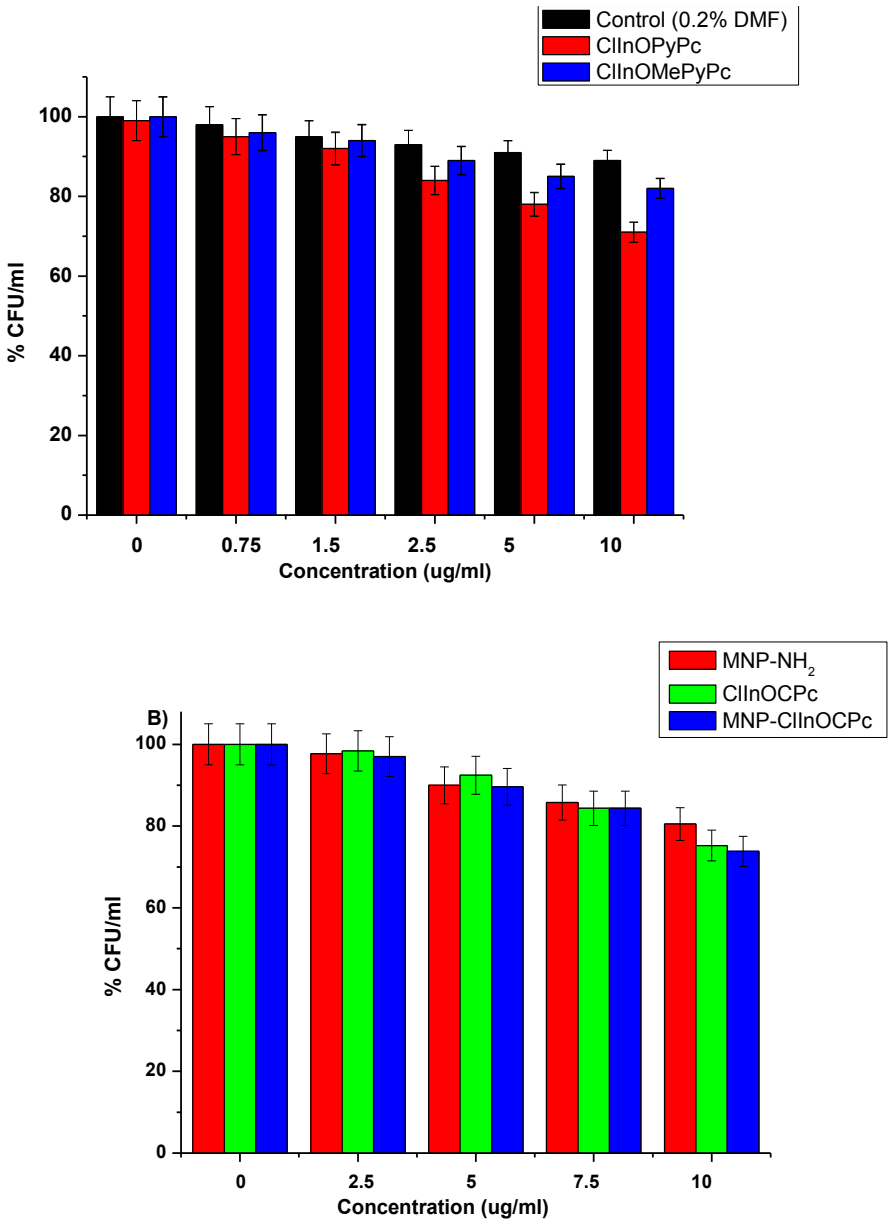

Figure 5.1: Dark toxicity studies (0.2% DMF in PBS) of *S. aureus* (A and B).

The dark toxicity studies (Fig. 5.1 B, the error bars show the standard deviation of the sample) showed that the MNPs, ClInOCPc and MNP-ClInOCPc had minimal dark toxicity up until 7.5 μg/mL.

The log plot of *S. aureus* (used as an example) showed (Fig. 5.2) that ClInOMePyPc is more effective that the ClInOPyPc with change in fluence. Log reduction values for ClInOMePyPc are higher than for ClInOPyPc for all the microorganisms, as shown in Table 5.1. This is probably due to the neutral nature of ClInOPyPc while ClInOMePyPc is positively charged. In addition, the solubility of ClInOPyPc was less than that of ClInOMePyPc in 0.2% DMF (in PBS). The positively charged ClInOMePyPc gave log reduction values of 8.30 for *S. aureus* (Gram (+)), 4.21 for *E.coli* (Gram (-)) and 3.21 for *C. albicans* (Gram (+)), Table 5.1.

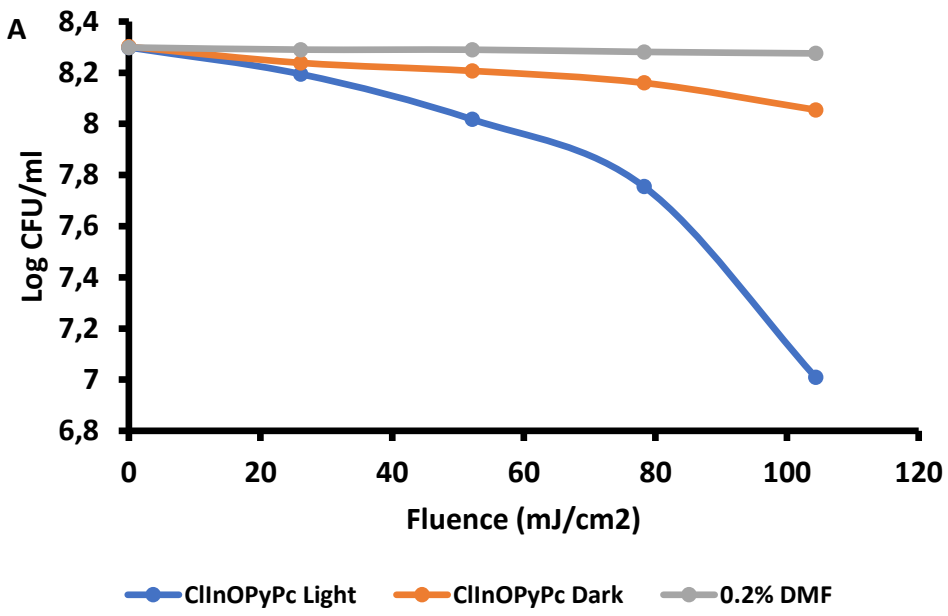

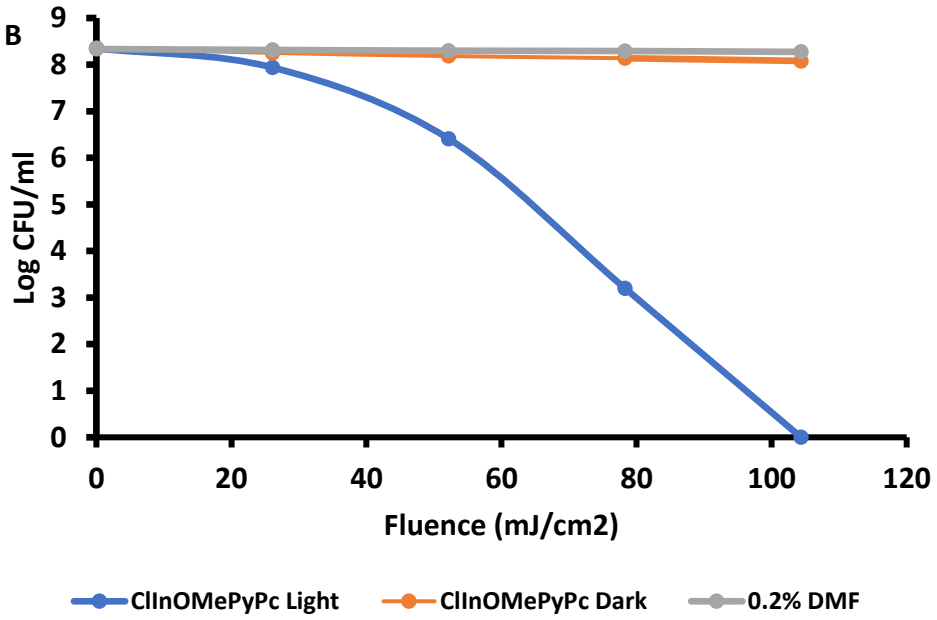

Figure 5.2: Survival curves of *S. aureus* of (A) ClInOPyPc and (B) ClInOMePyPc.

Gram (+) bacteria can easily take up photosensitisers and can therefore readily undergo photoinactivation [140, 141], hence the *S. aureus* has high log reduction values as expected. *C. albican* is also gram (+) however it has a cell wall consisting of polysaccharides and protein [142] unlike the *S. aureus* which only has the capsule and a thick peptidoglycan layer [143]. The gram negative *E. coli* cell wall consists of an outer membrane possessing a size selective porin (excluding molecules >700 Da), inner phospholipid, an outer negatively charge lipopolysaccharides (LPS), a thin peptidoglycan layer [144]. The cationic phthalocyanine may electrostatically interacts with the LPS hence in ClInOMePyPc had a higher log reduction value for *E. coli* than *C. albican.*

Table 5.1 also shows that ClInOMePyPc has lower log reduction value for *E.coli* than the reported [44, 60] complexes **1** and **2** (Fig 5.3). In terms of the number of positive charges, ClInOMePyPc has eight while **1** and **2** have three and four charges, respectively. Since **2** gives a larger log reduction value than ClInOMePyPc, it can be confirmed that charges do not

determine the log reduction activity. Comparing the reported **1** and **2**, both tetrasubstituted InPc derivatives, complex **2** having only oxo bridges gave much larger log reduction values for *E. coli*. This could suggest that the presence of sulphur bridges affect the PACT activity. All the complexes have about the same singlet oxygen quantum yield, Table 5.1, hence the difference are due to factors other than singlet oxygen quantum yield. The difference could be the interaction of *E.coli* with sulphur. It has been reported before that some sulphur containing compounds may influence the growth of *E. coli* or any organism [145-147]. The influence of the presence of sulphur is minimal on the Gram (+) *S. aureus* due to its sensitivity mentioned above. In addition, complex **1** has an amino group. Amino containing phthalocyanines have been reported show low PACT activity against *E. coli* [148].

The PACT activity of ClInOCPc improved in the presence of MNPs with high log values of 7.77 for MNP-ClInOCPc and 5.07 for ClInOCPc, showing that singlet oxygen quantum yields are not the only indicators for PACT activity, since it would be expected that ClInOCPc with a larger singlet oxygen quantum yield should show better PACT activity compared to MNP-ClInOCPc.

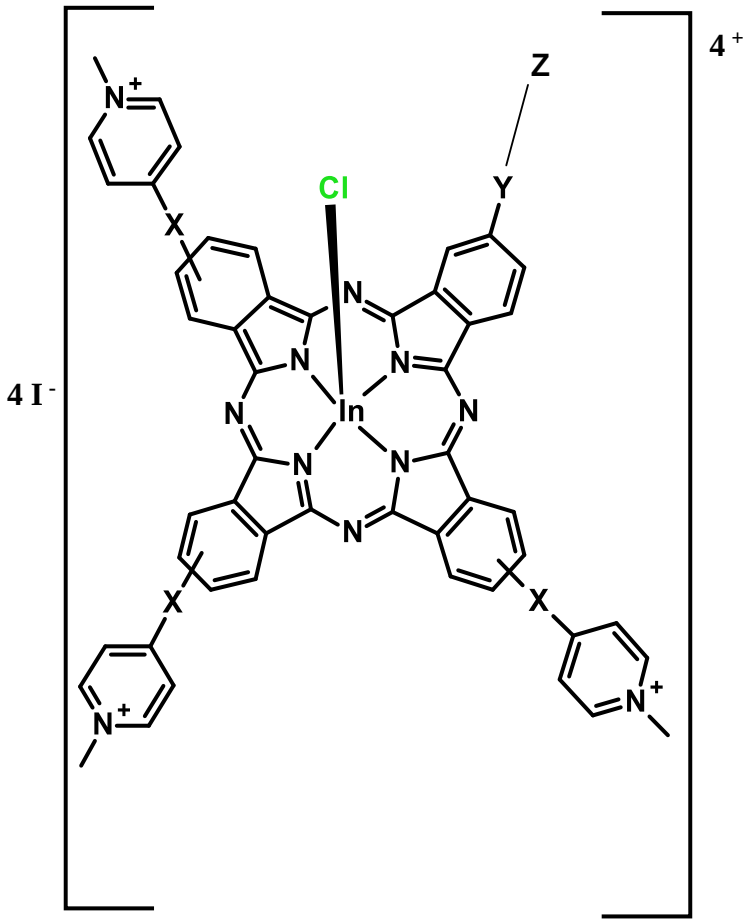

Figure 5.3: Molecular structures of complexes 1 and 2.

1: X = S; Y = O, Z = 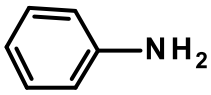

2: X=Y=O; Z = 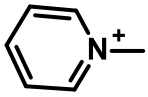

Table 5.1: Log reduction values with standard deviations in brackets

Micro-organism	Complex	Medium	Log reductions	Φ_Δ values	Reference
E. coli	**ClInOPyPc**	PBS (0.2% DMF)	0.78 ± 0.12	0.33	This work
	ClInOMePyPc	PBS (0.2% DMF)	4.21± (0.02)	0.31	This work
	1	PBS(.5 % DMSO)	4.90 ± 1.79	0.31	44
	2	PBS (1% DMSO)	8.41	0.31	60
	ClInOCPc	PBS (0.2 % DMF)	1.70 (0.04)	0.41	This work
	MNP-ClInOCPc	PBS (0.2 % DMF)	2.26 (0.01)	0.29	This work
C. albican	**ClInOPyPc**	PBS (0.2% DMF)	0.57 (0.02)	0.33	This work
	ClInOMePyPc	PBS (0.2% DMF)	3.21 (0.01)	0.31	This work
	ClInOCPc	PBS (0.2 % DMF)	1.43 (0.03)	0.41	This work
	MNP-ClInOCPc	PBS (0.2 % DMF)	1.83 (0.02)	0.29	This work
S. aureus	**ClInOPyPc**	PBS (0.2% DMF)	1.29 (0.03)	0.33	This work
	ClInOMePyPc	PBS (0.2% DMF)	8.30 (0.01)	0.31	This work
	ClInOCPc	PBS (0.2% DMF)	5.07	0.41	This work
	MNP-ClInOCPc	PBS (0.2% DMF)	7.77	0.29	This work

5.2 Antimicrobial Studies of unknown bacteria in the water sample

The water sample was collected from a local stream shown in Fig. 5.4.

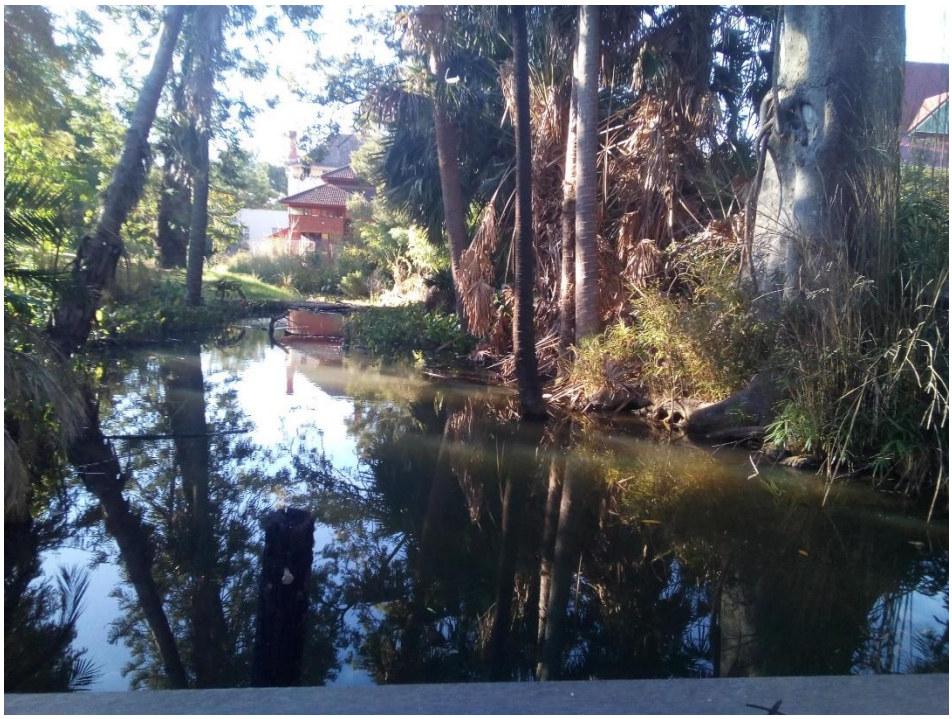

Figure 5.4: Site for the used sample.

5.2.1 Optimizations for the water sample from the stream

The heat sensitivity of different microorganism differs and the optimal temperature was determined by incubating the sample at different temperatures of 20, 25, 27, 30, 37, 40 °C for 24 and 48 h. pH sensitivities of the water sample were determined by adding buffer (PBS) of pHs 2, 4, 6, 7.4, 9 and 14. The samples were inoculated at 30°C for 24 h.

The optimization of temperature and pH was adapted from previous studies [149]. The ideal temperature was determined to be 30 °C for both at 24 h and 48 h incubation, Fig. 5.5a, but 24 h gave larger CFU (colony forming-unit) hence employed for further studies. The optimum temperature was then used to optimize the pH, Fig. 5.5b. The pH of the water sample from

the stream was found to be 6.3 and was adjusted by using acidic and basic PBS. The maximum colony count was obtained at pH 7.4 shown in Fig. 5.5b, hence pH 7.4 was employed.

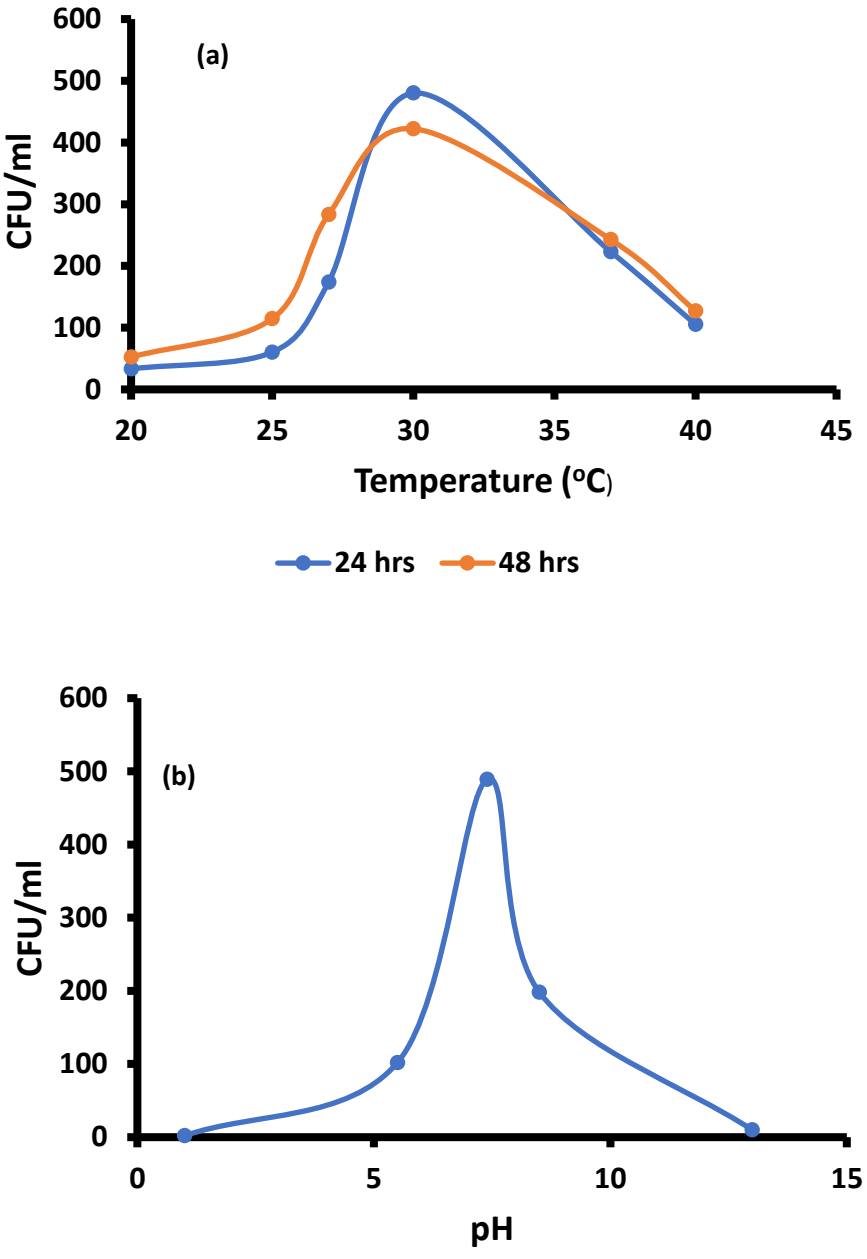

Figure 5.5: Optimization studies of a) temperature and b) pH (at 30 °C) unknown water sample.

5.2.2 PACT activity of ClInOCPc, MNP-ClInOCPc, ClInOPyPc and ClInOMePyPc in solution

The photosensitizers were dissolved in DMF (0.2 %) and further diluted with 7.4 PBS to make a final concentration of 0.75 µg/mL for ClInOPyPc and ClInOMePyPc and 2.5 µg/mL for ClInOCPc and MNP-ClInOCPc. The control sample (0.2% DMF in PBS) was exposed in the same irradiation conditions, but without a photosensitizer shown in Fig. 5.6, and there is an insignificant change on the control as was also observed above, the Photodynamic Antimicrobial Chemotherapy studies are often reported in logarithmic reduction values to manage the high population in the stock solution and to manage the bacteria growth on the agar not to clump up. The water samples exhibited maximum CFU/ml of 1000 and therefore only 1 aliquot dilution was performed hence they are reported in reduction percentage, eq. 5.1.

$$\frac{Total\ colony\ count\ on\ the\ embedded\ fibre}{Total\ colony\ count\ on\ the\ control} \times 100 \qquad 5.1$$

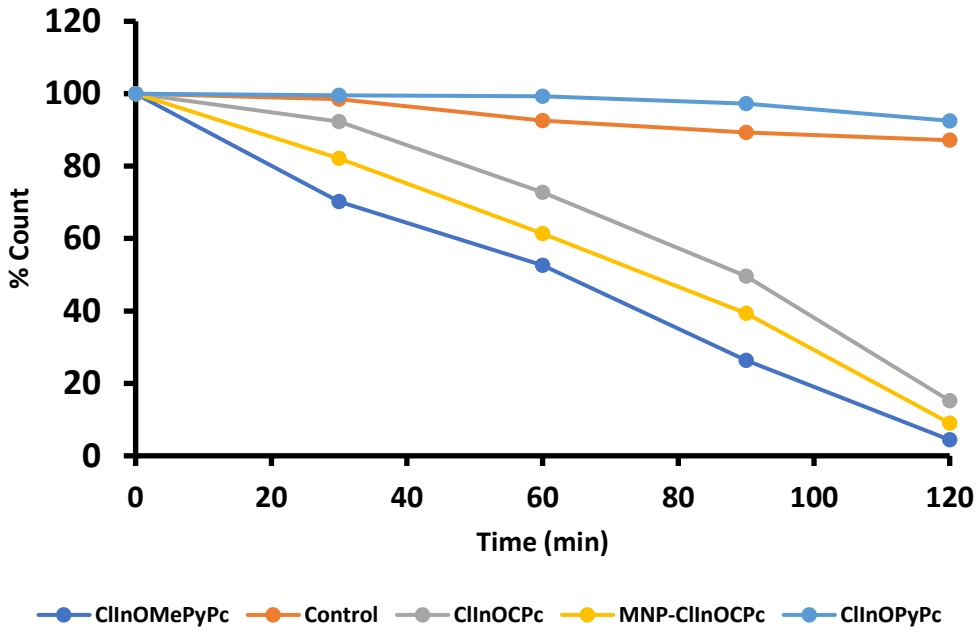

Figure 5.6: Survival curve of the unknown incubated with 0.75 µg/ml of ClInOPyPc and ClInOMePyPc and 2.5 µg/ml of ClInOCPc and MNP-ClInOCPc.

The results obtained are illustrated in Fig. 5.6 and summarised in Table 5.2. In solution the ClInOPyPc was the least effective phthalocyanine with only 7.5 % bacterial death. The ClInOMePyPc had a reduction percentage of 95.5 %, though it had a lower singlet quantum yield compared to ClInOPyPc due to the cationic nature of the former. There was major improvement for MNP-ClInOCPc at 90.5%, compared to ClInOCPc at 84.8 % alone showing the advantage on MNPs. ClInOCPc produced a higher singlet oxygen quantum yield than the MNP-ClInOCPc, but the latter had higher PACT activity. ClInOCPc showed less stability compared with MNP-ClInOCPc, Fig. 5.7. This could explain the better PACT activity for the latter. In this work, the concentration used for the photosensitizers did not influence efficiency for PACT, since ClInOCPc and MNP-ClInOCPc's concentration was three times higher at 2.5 µg/mL than the concentration of ClInOMePyPc at 0.75 µg/mL, yet the latter shows better PACT activity.

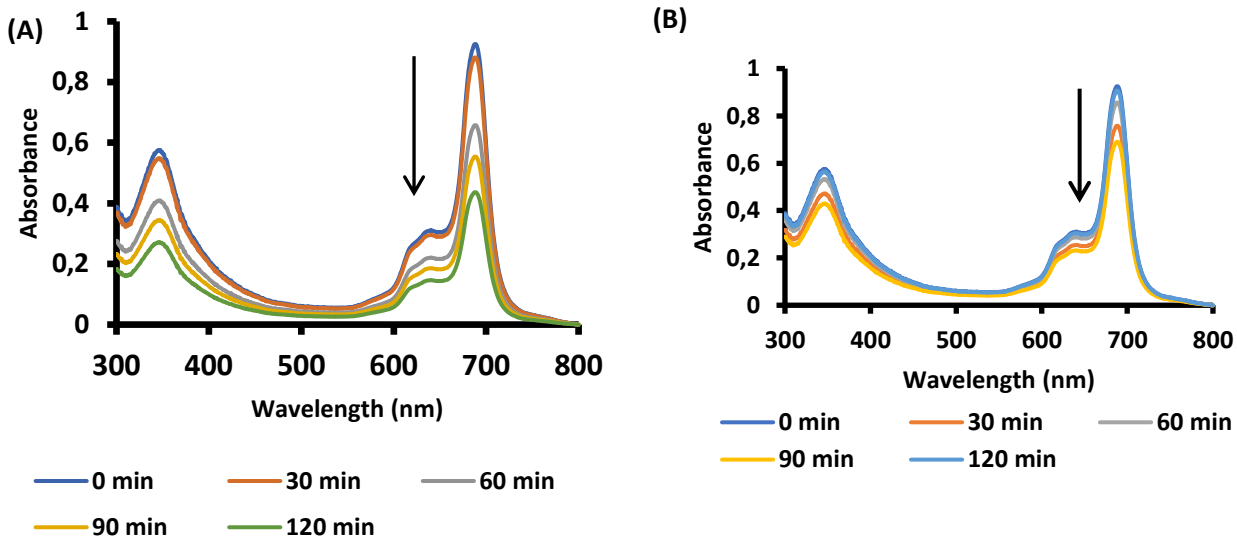

Figure 5.7: UV-Vis spectra during irradiation for PACT (A) ClInOCPc and (B) MNP-ClInOCPc in 0.2 % DMF in PBS.

5.2.3 PACT activity in PAN fiber

The embedded phthalocyanines were placed in the same agar plate as the PAN which was used as a control, the same amount of sample was inoculated and irradiated for 1 h and the reduction percentage was estimated by eq. 5.1. The results followed a similar trend as in solution, where the ClInOPyPc/PAN was the least efficient even though it had the highest singlet oxygen quantum yield. ClInOCPc/PAN is less efficient compared to MNP-ClInOCPc, Table 5.2 with the ClInOMePyPc being the most efficient.

Table 5.2: Photodynamic antimicrobial results of the unknown sample solution and fiber.

Sample	Population inactivation (%) in solution	Population inactivation (%) in PAN
PAN (control)	-	1.8
Control (0.2 % DMF)	12.9	-
ClInOCPc	84.8	48.0
MNP-ClInOCPc	90.6	63.7
ClInOPyPc	7.5	12.4
ClInOMePyPc	95.5	83.4

5.3 Conclusion for the chapter

This chapter discussed the PACT activities of ClInOPyPc, ClInOMePyPc, ClInOCPc and MNP-ClInOCPc in solution and when they are embedded in PAN fibers (the latter only for unknown water samples). The studies were completed for *E. coli*, *C. albican* and *S. aurues*, as well as an unknown micro-organism from a water sample. The results in solution were represented as log reductions, the ClInOMePyPc being the most efficient compound with values as high as 8.30 (for *S. aureus*). Furthermore, the effect of charge was studied and the results obtained for ClInOMePyPc (8 positive charges) were compared to **1** (3 positive charges) and **2** (4 positive charges)**.** The log reduction results for *E. coli* showed that **2** was more effective with the of 8.41 compared to 4.21 for ClInOMePyPc suggesting that charge does not influence log reduction values. For the unknown sample, the results were represented in reduction percentage with the ClInOMePyPc eliminating 95.5% microbes and for the Pc/PAN studies, a similar trend was observed where the ClInOMePyPc had 83.4% clearance.

CHAPTER SIX

Photodegradation of methyl red

6. Photodegradation of methyl red

The photodegradation of methyl red was attempted for all but ClInOMePyPc leached out from the fiber during the adsorption by stirring, so it is left out. ClInOCPc, MNP-ClInOCPc and ClInOPyPc were embedded in PAN nanofibers.

6.1 UV-vis studies

The photodegradation of the methyl red was monitored by viewing the spectral changes of methyl red at 8 min intervals with ClInOCPc/PAN and CiInOPyPc/PAN as examples in Fig. 6.1. From this figure, the MNP-ClInOCPc/PAN has a faster degradation than ClInOPyPc/PAN at the same concentration of 4.5×10^{-5} mol/L of methyl red.

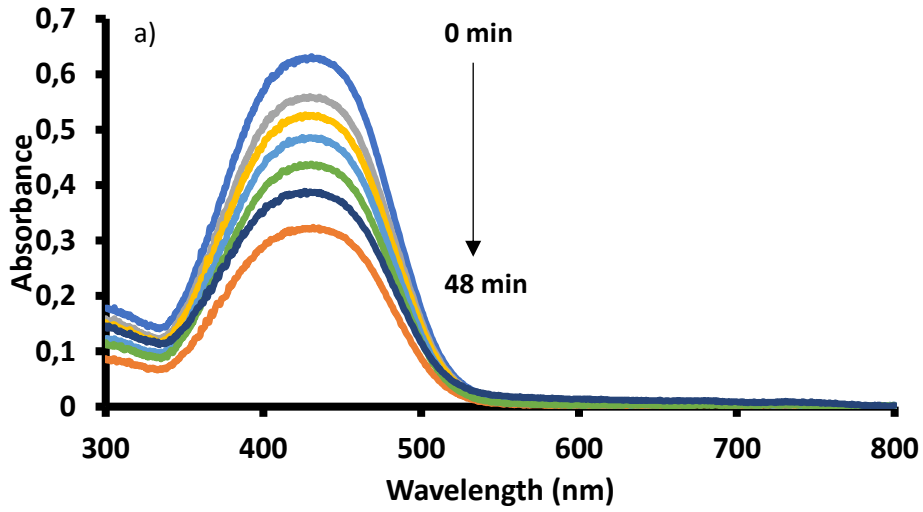

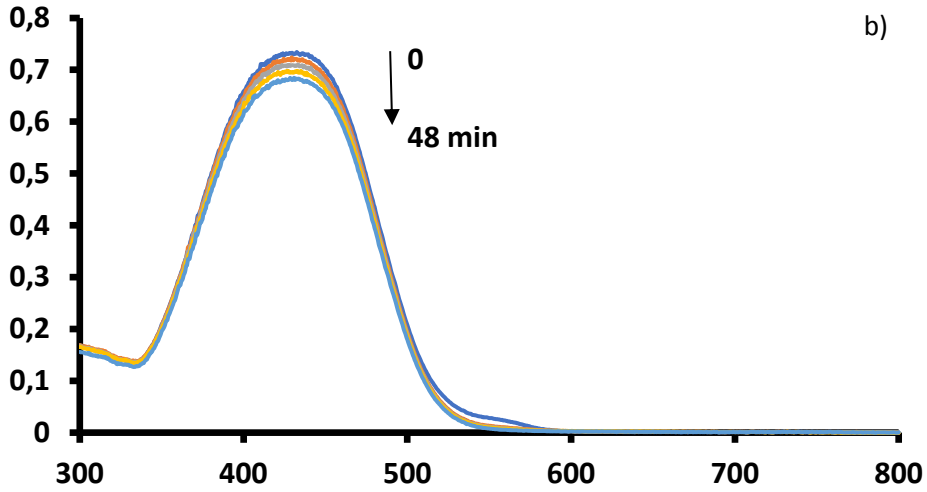

Figure 6.1: Electronic absorption spectra changes 4.5 × 10^{-5} mol/L methyl red during visible light photocatalysis in the presence of a) ClInOCPc/PAN and b) ClInOPyPc/PAN. The spectra recorded at 8 min intervals in water (pH 7.4).

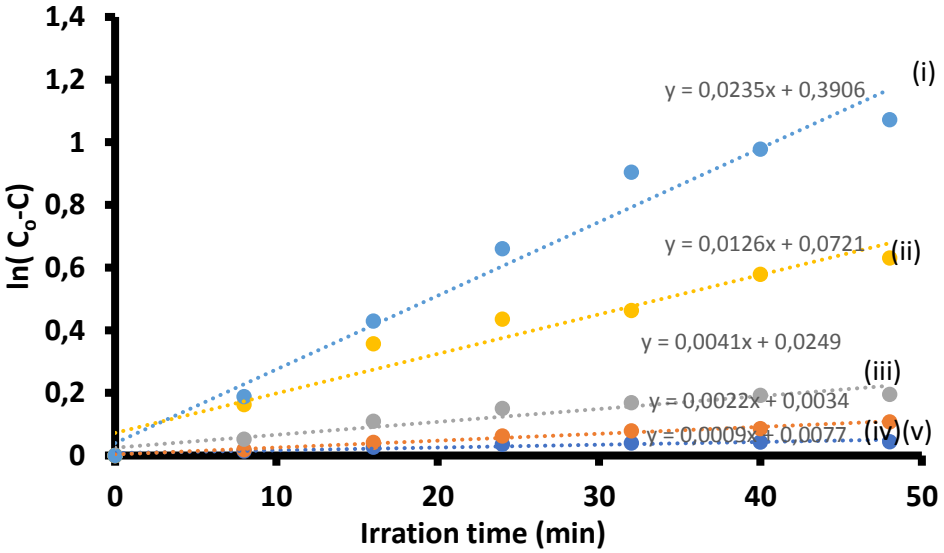

Figure 6.2: First order kinetic plots for degradation methyl red: (i) 4.5 ×10^{-5}, (ii) 7.9 ×10^{-5}, (iii) 12.7 ×10^{-5}, (iv) 15.3 ×10^{-5} and (v) 17.2 ×10^{-5} using MNP-ClInOCPc/PAN as a catalyst in pH 7.4.

There was a decrease in the methyl red absorption peak with irradiation time. The Q-band of the conjugate at the 689 nm region was not present in the spectra (Fig. 6.1 a) for water soluble ClInOCPc suggesting that the phthalocyanine did not leach out. The studies were performed at pH 7.4. Methyl red has a maximum absorbance at 425 nm, this peak has been reported as the characteristic for the dye at a pHs greater than 5.6 [150]. When the unmodified fibres were irradiated in the presence of the dye solution, there was no degradation of the methyl red (no change in absorbance), showing that the unmodified fibre does not degrade methyl red. For modified fibres, the methyl red concentration versus irradiation time plots were used to determine the kinetics, Fig. 6.2. The plots in Fig. 6.2 indicate pseudo -first order kinetics. Table 6.1 summarizeds the kinetics results. There was an increase in k_{obs} with decrease of methyl red concentration for the ClInOCPc/PAN, MNP-ClInOCPc/PAN, ClInOPyPc/PAN and MNP-ClInOCPc/PAN re-used catalyst. The MNP-ClInOCPc/PAN had a faster rate and higher k_{obs} values than ClInOCPc/PAN with ClInOPyPc/PAN with the least rate.

A similar trend observed for the half-lives where the values for the MNP-ClInOCPc/PAN were lower compared to the ClInOCPc/PAN, showing faster activity for the former. The MNP-ClInOCPc/PAN fibre was retrieved, washed with ethyl acetate, dried and re-immersed in the MR solution. The morphology of the re-used fibre was partially distorted with visible particles present (Fig 6.3 b). The rate of the recycled fibers was faster than that of ClInOPyPc/PAN and ClInOCPc/PAN in some cases. The probable methyl red degradation products are shown in Scheme 6.1, with CO_2 and H_2O are predicted to be the products (Adapted from methyl orange) [151].

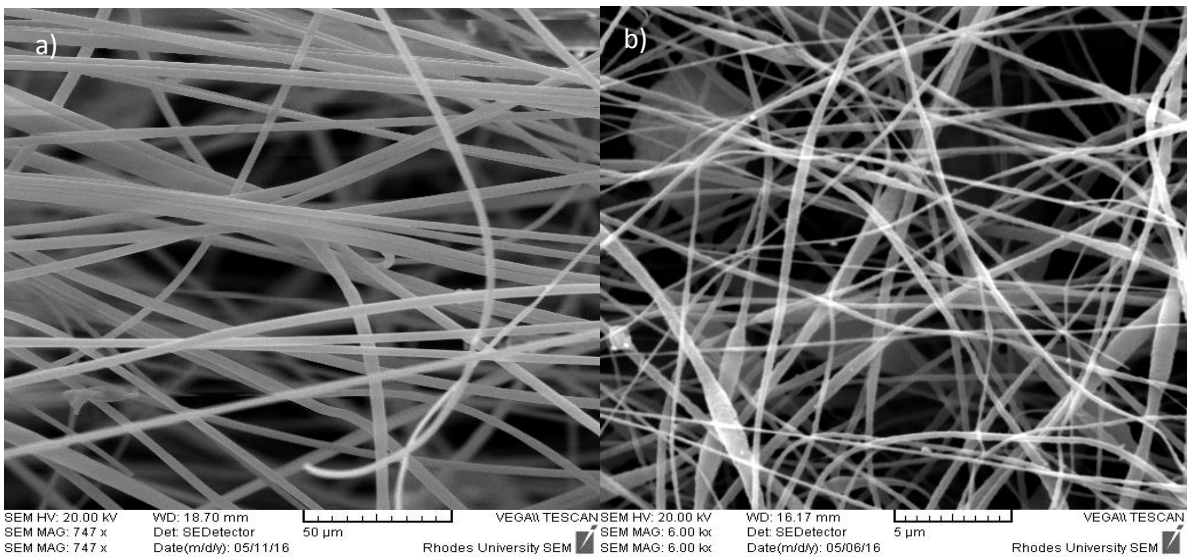

Figure 6.3: The SEM of a) MNP-ClInOCPc/PAN and b) re-used MNP-ClInOCPc/PAN fiber.

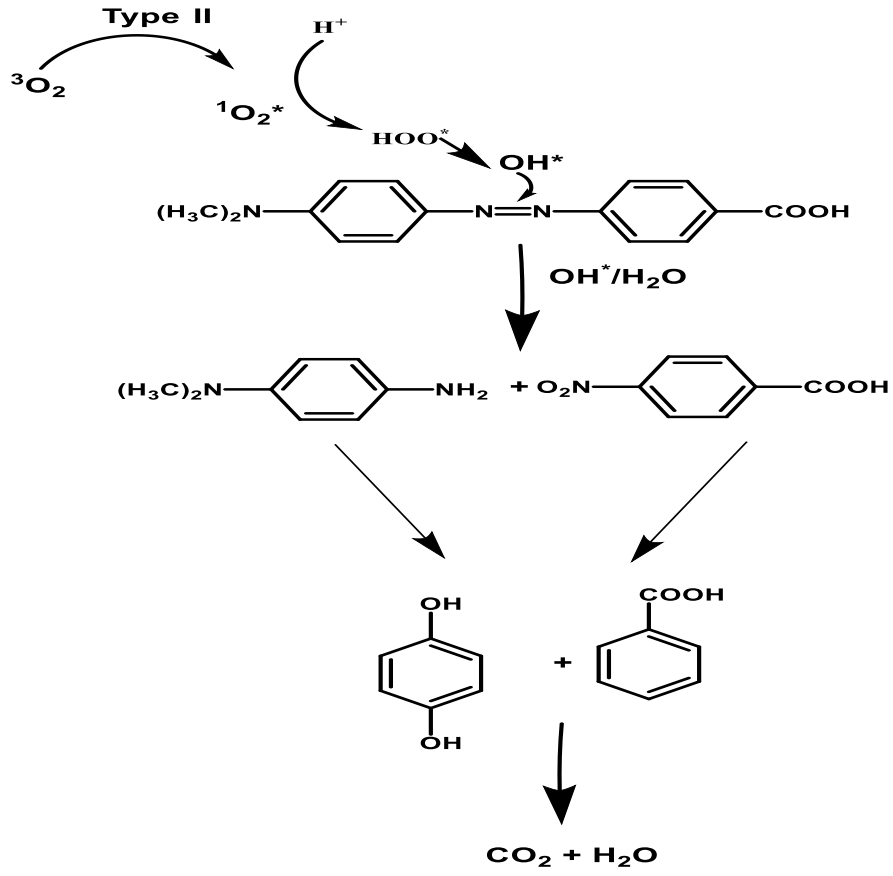

Scheme 6.1: Probable MR degradation products.

Table 6.1: The rate, rate constant (k_{obs}) and half-life of methyl red using ClInOCPc/PAN, MNP-ClInOCPc/PAN and ClInOPyPc/PAN.

[MR] $\times10^{-5}$ mol/ L	K_{obs} (min^{-1})				Initial rate ($\times10^{-7}$ mol L^{-1} min^{-1})					Half-life (min)		
	ClInOCPc /PAN	MNP-ClInOCPc /PAN	ClInOPyPc /PAN	MNP-ClInOCPc/ PAN (re-used)	ClInOCPc /PAN	MNP-ClInOCPc /PAN	ClInOPyPc /PAN	MNP-ClInOCPc /PAN (re-used)	ClInOCPc /PAN	MNP-ClInOCPc /PAN	ClInOPyPc /PAN	MNP-ClInOCPc /PAN (re-used)
4.5	0.0166	0.0235	0.0084	0.0183	7.5	10.6	3.8	8.3	41.8	29.5	82.5	37.9
7.9	0.009	0.0126	0.0034	0.0094	7.1	9.9	2.7	7.4	77.0	55.0	203.9	73.7
12.7	0.0023	0.0041	0.0011	0.0032	2.9	5.2	1.4	4.1	301.4	169.1	630.1	216.6
15.3	0.002	0.0022	0.0005	0.0017	3.1	3.8	0.8	2.6	346.6	315.1	1386.3	407.7
17.2	0.0011	0.0009	0.0001	0.0012	1.9	1.5	0.2	0.7	630.1	770.2	6931.5	577.6

6.2 Conclusion for the chapter

The photodegradation of methyl red was successfully achieved using ClInOCPc/PAN, MNP-ClInOCPc/PAN and re-used MNP-ClInOCPc/PAN. The MNP-ClInOCPc/PAN was the most efficient in degrading MR with a rate of 10.6 $\times 10^{-7}$ mol L^{-1} min^{-1} with the half-life of 29.5 min^{-1} at 4.5 mol/L. The same fiber was washed and re-used, the initial rate was smaller but performed better than ClInOPyPc/PAN and ClInOCPc/PAN in some cases. The ClInOPyPc/PAN produced the least rate, with a rate of 3.8 $\times 10^{-7}$ mol L^{-1} min^{-1} and long half-life of 82.5 min^{-1} for the lowest concentration (4.5 mol/L) of MR. Probable degradation products of methyl red are predicted to be CO_2 and H_2O.

CHAPTER SEVEN

Conclusions

Conclusions

The photophysical behaviour of quaternised (positively charged) octa-pyridylsulfanyl substituted indium (III) phthalocyanine ClInOMePyPc and the neutral ClInOPyPc were studied. ClInOPyPc showed high efficiency as photosensitizers in the photodynamic antimicrobial chemotherapy inactivation of *E. coli*, gram-positive *S. aureus* and *C. albican* with log reductions of 4.21, 8.30 and 3.21, respectively. ClInOMePyPc (containing eight positive charges) gave lower log reduction values than complexes **1** (containing 3 positive charges) and **2** (containing 4 positive charges). In turn complex **2** gave the largest log reduction values (almost twice those of ClInOMePyPc and **1**), and this is attributed to the bridging atoms linking the ring substituents to the phthalocyanine core.

The ClInOCPc, MNP-ClInOCPc, ClInOPyPc and ClInOMePyPc were successfully embedded to the PAN to produce ClInOCPc/PAN, MNP-ClInOCPc/PAN, ClInOPyPc/PAN and ClInOMePyPc/PAN, respectively. The electrospun fibres were determined to have a diameter ranging from 370 nm to 520 nm. The photochemical and physical parameters were determined and the ClInOCPc/PAN produced high singlet oxygen in water using ADMA as a quencher compared to MNP-ClInOCPc. A water sample from a local stream was tested for microbes and the fibres were applied with the MNP-ClInOCPc/PAN producing the highest reduction percentage compared ClInOCPc/PAN due to its ability to interact with the membrane of the microbes. The fibres were further used to degrade methyl red where the highest initial rates and k_{obs} were obtained from the MNP-ClInOCPc/PAN fibres with pseudo-first-order kinetics. These complexes have exhibited positive results in both applications and have potential in water purification.

References

1. von Braun, A., Tscherniac, J., 1907, Über die Produkte der Einwirkung von Acetanhydrid auf Phthalamid, *Ber. Deut. Chem. Ges.*, 40, 2709-2714.
2. McKeown, N.B., 1998, Phthalocyanine Materials: Synthesis, Structure and Function, Cambridge University Press, United Kingdom.
3. Lomax, S.Q., 2005, Phthalocyanine and quinacridone pigments: their history, properties and use, *Stud.Cons.*, 5, 19-29.
4. Dandridge, A. G., Drescher, H. A. E., Thomas, J., 1929, Dyes British Patent, 322, 169.
5. Robertson, J. M., Linstead, R. P., 1936, The Stereochemistry of Metallic Phthalocyanines, *J. Chem. Soc.,* 383, 1736-1738.
6. Robertson, J. M., 1936, An X-Ray Study of the Phthulocyanines, Part II. Quantitative Structure Determination of the Metal-free Compound, *J. Chem. Soc.,* 255, 1195-1209.
7. Linstead, R. P., Lowe, A. R., 1936, Phthlocyanines. Part III. Preliminary Experiments on thePreparation of Phthalocyanines from Phthalonitrile, *J. Chem. Soc.,* 214, 1022-1027.
8. Mondal, D., Bera, S., 2014, Porphyrins and phthalocyanines: promising molecules for light-triggered antibacterial nanoparticles, *Adv. Nat. Sci. Nanosci. Nanotechnol.,* 5, 033002 (14 pp).
9. Nemykin, V. N., Lukyanets, E. A., 2010, Synthesis of substituted phthalocyanines, *ARKIVOC*, (i), 136-208.
10. Minnes, R., Weitman, H., Lee, H.-J., Gorun, S.M., Ehrenberg, B., 2006, Enhanced Acidity, Photophysical Properties and Liposome Binding of Perfluoroalkylated Phthalocyanines Lacking C-H Bonds, *Photochem. Photobiol.*, 82, 593-599.

11. Wöhrle, D., Buck, T., Schneider, G., Schulz-Ekloff, G., Fischer, H., 1991, Low molecular weight, polymeric, and covalently bound cobalt(II)-phthalocyanines for the oxidation of mercaptans, *J. Inorg. Metallorg. Polym.,* 1, 115-130.
12. Tolbin, A.Y., Tomilova, L.G., 2007, Synthesis and spectroscopic properties of new water-soluble phthalocyanines containing pyridinium hydrochloride fragments, *Russ. Chem. Bull.*, 56, 2433-2437.
13. Moeno, S., Nyokong, T., 2009, Opposing responses elicited by positively charged phthalocyanines in the presence of CdTe quantum dots, *J. Photochem. Photobio A: Chem.*, 201, 228-236.
14. Sakamoto, K., Ohno, E., 1997, Synthesis and electron transfer property of phthalocyanine derivatives, *Prog. Org. Coat.*, 31, 139-145.
15. Mack, J., Stillman, M. J., 1994, Photochemical Formation of the Anion Radical of ZincPhthalocyanine and Analysis of the Absorption and Magnetic Circular Dichroism Spectral Data. Assignment of the Optical Spectrum of $[ZnPc(-3)]^{-}$, *J. Am. Chem. Soc.,* 116, 1292-1304.
16. Lutsenko, O. G., Kulinich, V. P., Shaposhnikov, G. P., Lyubomtsev, A. V., 2004, Synthesis and Study of Carboxysulfo Derivatives of Phthalic Acid and Octasubstituted Metal Phthalocyanines Based Thereon, *Russ. J. Gen.l Chem.,* 74, 286-291.
17. Josefsen, L. B., Boyle, R. W., 2012, Unique diagnostic and therapeutic roles of porphyrins and phthalocyanines in photodynamic therapy, imaging and theranostics, *Theranostics*, 2, 916–966.
18. Weiss, D.S., 2016, The History and Development of Organic Photoconductorsfor Electrophotography, *J. Imaging Sci. Technol.*, 60, 030505-1-030505-24.

19. Bouvet, M., Gaudillat, P., Suisse, J-M., 2013, Phthalocyanine-based hybrid materials for chemo-sensing, *J. Porphyrins Phthalocyanines,* 17, 913–919.
20. Pandey, R. K., Kessel, D., Dougherty, T. J. (Eds.), 2016, Handbook of Photodynamic Therapy – Updates on Recent Applications of Porphyrin-Based Compounds, World Scientific, New Jersey, p. 237.
21. Ragoussi, M-E., Ince, M., Torres, Y., 2013, Recent Advances in Phthalocyanine-Based Sensitizers for Dye-Sensitized Solar Cells, *Eur. J. Org. Chem.*, 29, 6475-6489.
22. Ali, F., Khan, S. B., Kamal, T., Anwar, Y., Alamry, K. A., Asiri, A. M., 2017, Anti-bacterial chitosan/zinc phthalocyanine fibers supported metallic and bimetallic nanoparticles for the removal of organic pollutants, *Carbohydrates Polymers,* 173, 676-689.
23. Maliszewska, I., Kalas, W., Wysokinska, E., Tylus, W., Pietrzyk, N., Popko, K., Palewska, K., 2017, Enhancement of photo-bacterial effect of tetrasulfonated hydroxyaluminum phthalocyanine on *Pseudomonas aeruginosa*, *Lasers Med. Sci.,* 1-10.
24. Astruc, D., 2008, Nanoparticles and Catalysis, vol.1, Wiley-VCH, Weinheim.
25. Lead, J. R., Wilkinson, K. J., 2006, Aquatic Colloids and Nanoparticles: Current Knowledge and Future Trends, *Environ. Chem.,* 3, 159-171.
26. Iravani, S., 2011, Green synthesis of metal nanoparticles using plants, *Green Chemistry,* 13, 2638-2650.
27. Choi, W. K., Liew, T. H., Chew, H. G., Zheng, F., Thompson, C. V., Wang, Y., Hong, M. H., Wang, X. D., Li, L., Yun, J., 2008, A Combined Top-Down and Bottom-UpApproach for Precise Placement of Metal Nanoparticles on Silicon, *Small*, 4, 330-333.

28. Verma, S., Gokhale, R., Burgess, D. J., 2009, A comparative study of top-down and bottom-up approaches for the preparation of micro/nanosuspensions, *Int. J. Pharm.,* 380, 216-222.

29. Wang, Y., Xia, Y., 2004, Bottom-Up and Top-Down Approaches to the Synthesis of Monodispersed Spherical Colloids of Low Melting-Point Metals, *Nano Letters*, 4, 2045-2050.

30. Chou, L. Y., Ming, K., Chan, W. C., 2011, Strategies for the intracellular delivery of nanoparticles, *Chem. Soc. Rev.*, 40, 233–245.

31. Elghanian, R., Storhoff, J. J., Mucic, R. C., Letsinger, R. L., Mirkin, C. A., 1997, Selective Colorimetric Detection of Polynucleotides Based on the Distance-Dependent Optical Properties of Gold Nanoparticles, *Science,* 277, 1078–1081.

32. De, M., Rana, S., Akpinar, H., Miranda, O. R., Arvizo, R. R.,Bunz, U. H., Rotello, V. M., 2009, Sensing of proteins in human serum using conjugates of nanoparticles and green fluorescent protein, *Nat. Chem.,*1, 461–465.

33. Lu, Y., Yin, Y., Mayers, B. T., Xia, Y., 2002, Modifying the Surface Properties of Superparamagnetic Iron Oxide Nanoparticles through A Sol−Gel Approach, *Nano Letters*, 2 (3), 183–186.

34. Boisselier, E., Astruc, D., 2009, Gold nanoparticles in nanomedicine: preparations, imaging, diagnostics, therapies and toxicity, *Chem. Soc. Rev.,* 38, 1759–1782.

35. Moyano, D. F., Rotello, V. M., 2011, Nano Meets Biology: Structure and Function at the Nanoparticle Interface, *Langmuir*, 27, 10376–10385.

36. Mout, R., Moyano, D. F., Rana, S., Rotello, V. M, 2012, Surface functionalization of nanoparticles for nanomedicine, *Chem. Rev. Soc.,* 41, 2539–2544.

37. Lu, A-H., Salabas, E. L., Schuth, F., 2007, Magnetic Nanoparticles: Synthesis, Protection, Functionalization, and Application, *Angew. Chem. Int. Ed.*, 46, 1222 – 1244.

38. Berry, C. C., Curtis, A. S. G., 2003, Functionalisation of magneticnanoparticles for applications in biomedicine, *J. Phys. D: Appl. Phys.*, 36, R198–R206.

39. Bean, C. P., Livingston, J. D., 1959, Super paramagnetism, *J. Appl. Phys.,* 30, 120S-129S.

40. Joubert, J. C., 1997, Magnetic micro composites as vectors for bioactive agents: the state of art, *Anales de Quimica Int Ed.* 93, 70-76.

41. Indira, T.K., Lakshmi, P.K., 2010, Magnetic Nanoparticle-a Review, *Int. J. Pharm. Sci. Nanotechnol.,* 3, 1035-1042.

42. Zhao, Y., Qiu, Z., Huang, J., 2008, Preparation and Analysis of Fe_3O_4 magnetic Nanoparticles used as Targeted- drug carriers*, Chinese J. Chem. Eng.,*16, 451-455.

43. Gupta, A.K., Gupta, M., 2005, Synthesis and surface engeering of iron oxide nanoparticles for biomedical applications, *Biomaterials*, 26, 3995-4021.

44. Osifeko, O. L., Uddin, I., Mashazi, P. N., Nyokong, T., 2016, Physicochemical and antimicrobial photodynamic chemotherapy of unsymmetrical indium phthalocyanines alone or in the presence of magnetic nanoparticles, *New J. Chem.,* 40, 2710-2721.

45. Modisha, P., Antunes, E., Mack, J., Nyokong, T., 2013, Improvement of the photophysical parameters of zinc octacarboxy phthalocyanine upon conjugation to magnetic nanoparticles, *Int. J. Nanosci.,* 12, 1350010-10.

46. Modisha, P., Nyokong, T., Antunes, E., 2013, Photodegradation of Orange-G using zinc octacarboxyphthalocyanine supported on Fe3O4 nanoparticles, *Chemical*, 380, 131-138.

47. Tshangana, C., Nyokong, T., 2015, Improved triplet state parameters for indium octacarboxy phthalocyanines when conjugated to quantum dots and magnetite nanoparticles, *J. Mol. Str.*, 1089, 161-169.

48. Tshangana, C., Nyokong, T., 2014, The Photophysical Properties of Multi-Functional Quantum Dots-Magnetic Nanoparticles—Indium Octacarboxyphthalocyanine Nanocomposite, *J. Flouresc.*, 25, 199-210.

49. Feuser, P. E., Fernandes, A. C., Nele, M., Viegas, A. d-C., Ricci-Junior, E., Tedesco, A. C., Sayer, C., de Araújo, P. H. H., 2015, Simultaneous encapsulation of magnetic nanoparticles and zinc phthalocyanine in poly(methyl methacrylate) nanoparticles by miniemulsion polymerization and in vitro studies, *Colloids surf. B: Biointerfaces*, 135, 357-364.

50. Feuser, P. E., Gaspar, P. C., Jacques, A. V., d-C., Tedesco, A. C., dos Santos Silva, M. C., Ricci-Junior, E., Sayer, C., de Araújo, P. H. H., 2015, Synthesis of ZnPc loaded poly(methyl methacrylate) nanoparticles via miniemulsion polymerization for photodynamic therapy in leukemic cells, *Mat. Sci. Eng.: C,* 60, 458-466.

51. Chen, J., Chen, N., Zhang, Y., Zhou, S., Wang, J., Chen, N., Huang, J., Yan, F., Huang, M., 2011, Substituted zinc phthalocyanine as an antimicrobial photosensitizer for periodontitis treatment, *J. Porphyr. Phthalocyanines, 15*, 293-299.

52. Wainwright, M., 1998, Photodynamic antimicrobial chemotherapy, *J. Antimic. Chemother.,* 42,13-28.

53. Green, B. N., Johnson, C. D., Egan, J. T., Rosenthal, M., Griffith, E.A., Evans M. W., 2012, Methicillin-resistant Staphylococcus aureus: an overview for manual therapists, *J. Chiropr. Med*.,11, 64–76.

54. Ryskova, L., Buchta, V., Slezak, R., 2010, Photodynamic Antimicrobial Therapy, *Cent. Eur. J. Biol.,* 5, 400–406.

55. https://www.redbubble.com/people/stanleyillust/works/21341791-gram-positive-vs-gram-negative-bacteria, accessed: 16/11/2017

56. Gow, N. A. R., van de Veerdonk, F. L., Brown, A. J. P., Netea, M. G., 2011, Candida albicans morphogenesis and host defence: discriminating invasion from colonization, *Nat. Rev. Microbiol.,* 10, 112–122.

57. Nombona, N., Antunes, E., Chidawanyika, W., Kleyi, P., Tshentu, Z., Nyokong, T., 2012, Synthesis, photophysics and photochemistry of phthalocyanine-ε-polylysine conjugates in the presence of metal nanoparticles against Staphylococcus aureus, *J. Photochem. Photobiol., A: Chemistry,* 233, 24-33.

58. Mantareva, V., Kussovski, V., Angelov, I., Borisova, E., Avramov, L., Schnurpfeild, G., Wohrle, D., 2007, Photodynamic activity of water-soluble phthalocyanine zinc(II) complexes against pathogenic microorganisms, *Bioorganic Med. Chem.*, 15, 4829-4835.

59. Scalise, I., Durantini, E. N., 2005, Synthesis, properties, and photodynamic inactivation of Escherichia coli using a cationic and a noncharged Zn(II) pyridyloxyphthalocyanine derivatives, *Bioorganic Med. Chem.,* 13, 3037-3045.

60. Osifeko, O. L., Durmus, M., Nyokong, T., 2015, Physicochemical and photodynamic antimicrobial chemotherapy studies of mono- and tetra-pyridyloxy substituted indium(III) phthalocyanines, *J. Photochem. Photobiol., A: Chemistry*, 301, 47–54.

61. Zheng, B.-Y., Ke, M.-R., Lan, W.-L., Hou, L., Guo, J., Wan, D.-H., Cheong, L.-Z., Huang, J.-D., 2016, Mono- and tetra-substituted zinc(II) phthalocyanines containing morpholinyl

moieties: Synthesis, antifungal photodynamic activities, and structure-activity relationships,*Eur. J. Med. Chem.,* 114, 380-389.

62. Osifeko, O. L., Nyokong, T., 2014, Applications of lead phthalocyanines embedded in electrospun fibers for the photoinactivation of Escherichia coli in water, *Dyes Pigm*., 111, 8-15.
63. Masilela, N., Nyokong, T., 2013, The interaction of silver nanoparticles with low symmetry cysteinyl metallophthalocyanines and their antimicrobial effect, *J. Photochem. Photobiol., A*: *Chemistry*, 255, 1– 9.
64. Van de Winckel, E., David, B., Simoni, M. M., Gonzalez-Delgado, J. A., de la Escosura, A., Cunha, A., Torres, T., 2017, Octacationic and axially di-substituted silicon (IV) phthalocyanines for photodynamic inactivation of bacteria, *Dyes Pigm.*, 145, 239-245.
65. Managa, M., Idowu, M. A., Antunes, E., Nyokong, T., 2014, Photophysicochemical behavior and antimicrobial activity of dihydroxosilicon tris(diaquaplatinum)octacarboxyphthalocyanine, *Spectrochim. Acta A. Mol. Biomol. Spectrosc.,* 125, 147–153.
66. Andreozzi, R., Caprio, V., Insola, A., Marotta, R., 1999, Advanced oxidation processes (AOP) for water purification and recovery, *Catal. Today,* 53, 51-59.
67. Pera-Titus, M., Garćıa-Molina, V., Baños, M.A., Giméneza, J., Esplugas, S., 2004, Degradation of chlorophenols by means of advanced oxidation processes: a general review*, Appl. Catal. B*, 47, 219-256.
68. Chan, P.Y., El-Din, M.G., Bolton, J.R., 2012, A solar-driven UV/Chlorine advanced oxidation process, *Water Res.*, 46, 5672-5682.

69. Mishra, V.S., Mahajani, V.V., Joshi, J.B., 1995, Wet air oxidation. *Ind. Eng Chem. Res.,* 34, 2–48.

70. Fenton, H.J.H., 1894. Oxidation of tartaric acid in the presence of iron. *J. Chem. Soc.,* 65, 899-910.

71. Kiwi, J., Pulgarin, C., Peringer, P., Gratzel, M., 1993, Beneficial effect of homogeneous photo-Fenton pretreatment upon the biodegradation of anthraquinone sulfonate in wastewater treatment, *Appl. Catal. B: Environ.,* 3, 85-99.

72. Pulgarin, C., Kiwi, J., 1996. Overview on photocatalytic and electrocatalytic pretreatment of industrial non-biodegradable pollutants and pesticides, *Chimia,* 50, 50-55.

73. Ollis, D., Al-Ekabi, H. (Eds.), 1993, Photocatalytic Purification of Water and Air, Elsevier, New York.

74. Gabriel, D., Zualaga, M.-F., Martinez, M.-N., Campo, M., Lange, N., 2009, Urokinase-plasminogen-activator sensitive polymeric photosensitizer prodrugs: design, synthesis and in vitro evaluation, *J. Drug Deliv. Sci. Technol.,* 19, 15-24.

75. Munter, R., 2001, Advanced oxidation processes–current status and prospects, *Proc. Estonian Acad. Sci. Chem., 5*0, 59-80.

76. Tarr, M., Valenzeno, D. P., 2003, Singlet oxygen: the relevance of extracellular production mechanisms to oxidative stress in vivo, *Photochem. Photobiol. Sci.,*2, 355-361.

77. Daneshvar, N., Salari, D., Khataee, A.R., 2003, Photocatalytic degradation of azo dye acid red 14 in water on ZnO as an alternative catalyst to TiO2, *J. Photochem. Photobiol. A,* 157, 111–116.

78. Lachheb, H., Puzenat E., Houas, A., Ksibi, M., Elaoui, E., Guillard, C., Herrmann, J.M., 2002, Photocatalytic degradation of various types of dyes (Alizarin S, Crocein Orange G, Methyl Red, Congo Red, Methylene Blue) in water by UV-irradiated titania, *Appl. Catal. B: Environ.,* 39, 75–90.
79. Pierce, J., 1994, Colour in textile effluents-the origins of the problem, *J. Soc. Dyes Colour,* 110, 131–134.
80. Medvedev, Z.A., Crowne, H.M., Medvedeva, M.N., 1988, Age related variations of hepatocarcinogenic effect of azo dye (3'-MDAB) as linked to the level of hepatocyte polyploidization, *Mech. Ageing Dev.,* 46, 159–167.
81. Zugle, R., Nyokong, T., 2013, Zin(II) 2,9,16,23-tetrakis[4-(N-methylpyridyloxy)]-phthalocyanine anchored on an electrospun polysulfone polymer fiber: Application for photosensitized conversion of methyl orange, *J. Mol. Catal. A: Chem.,* 366, 247-253.
82. Tombe, S., Antunes, E., Nyokong, T., 2013, Electrospun Fibers functionalized with phthalocyanine-gold nanoparticle conjugates for photocatalytic applications, *J. Mol. Catal. A: Chem.,* 371, 125-134.
83. Khoza, P., Nyokong, T., 2014, Photocatalytic behaviour of phthalocyanine-silver nanoparticle conjugates supported on polystyrene fibers, *J. Mol. Catal. A: Chem.*,395, 34-41.
84. Khoza, P., Nyokong, T., 2015, Photocatalytic behaviour of zinc tetraamino phthalocyanine-silver nanoparticles immobilized on chitosan beads, *J. Mol. Catal. A: Chem.,* 399, 25-32.
85. Ledwaba, M., Masilela, N., Nyokong, T., Antunes, E., 2015, Surface modification of silica-coated gadolinium oxide nanoparticles with zinc tetracarboxyphenoxy

phthalocyanine for the photodegradation of Orange G, *J. Mol. Catal. A: Chem.,*403, 64-76.

86. Yao, Y., Haung, Z., Zheng, B., Zhu, S., Lu, W., Chen, W., Chen, H., 2013, Photocalytic degradation of dyes using dioxygen activated by supported metalophthalocyanine under visible light irradiation, *Curr. Appl. Phys.,* 13, 1738-1742.
87. Zhu, Z., Chen, Y., Gu, Y., Wu, F., LU, W., Xu, T., Chem, W., 2016, Catalytic degradation of recalcitrant pollutants by Fenton-like process using polyacrylonitrile-supported iron (II) phthalocyanine nanofibers: Intermediates and pathway, *Water Res.,* 93, 296-305.
88. Mapukata, S., Chindeka, F., Sekhosana, K.E., Nyokong, T., 2017, Laser induced photodegradation of Orange G usinh phthalocyanine-cobalt ferrite magnetic nanoparticle conjugates electrospun in polystyrene nanofibers, *Mol. Catal.*, 439, 211-223.
89. Badr, Y., El-Wahed, M. G. A., Mahmoud, M. A., 2008, Photocatalytic degradation of methyl red dye by silica nanoparticles*, J. Hazard Mater.,* 154, 245-253.
90. Sharma, S. C. D., Sun, Q., Li, J., Wang, Y., Suanon, F., Yang, J., Yu, C-P., 2016, Decolorization of azo dye methyl red by suspended and co-immobilized bacteria cells with mediators anthraquinone-2,6-disulfonate and Fe_3O_4 nanoparticles, *Int. Biodeterior Biodegradation,* 112, 88-97.
91. Al-Saleh, M. H., Sundararaj, U., 2011, Review of the mechanical properties of carbon nanofiber/polymer composites, *Composites: Part A*, 42, 2126–2142.
92. Paul, D.R., Robeson, L.M., 2008, Polymer nanotechnology: nanocomposites, *Polymer,* 49, 3187–204.

93. Frenot, A., Chronakis, I. S., 2003, Polymer nanofibers assembled by electrospinning, *Curr. Opin. Colloid Interface Sci.*, 8, 64–75.

94. Agarwal, S., Greiner, A., Wendorff, J. H., 2013, Functional materials by electrospinning of polymers, *Prog. Polym. Sci.*, 38, 963–991.

95. Ondarcuhu, T., Joachim, C., 1998, Drawing a single nanofibre over hundreds of microns*, Europhys. Lett.*, 42, 215–20.

96. Feng, L., Li, S., Li, H., Zhai, J., Song, Y., Jiang, L., Zhu, D., 2002, Super-Hydrophobic Surface of Aligned Polyacrylonitrile Nanofibers, *Angew. Chem. Int. Ed.* 41, 1221–1223.

97. Liu, G.J., Ding, J.F., Qiao, L.J., Guo, A., Dymov, B.P., Gleeson, J.T., Hashimoto, T., Saijo, K., 1999, Polystyrene-block-poly (2-cinnamoylethyl methacrylate) Nanofibers-Preparation, characterization, and liquid crystallineproperties. *Chem.-A European J*., 5, 2740–2749.

98. Fong, H., Reneker, D.H., 2001, Electrospinning and formation of nanofibers.In: Salem DR, editor. Structure formation in polymeric fibers. Munich: Hanser; p. 225–46.

99. Formhals A. 1934, US patent 1,975,504.

100. Huanga, Z.-M., Zhang, Y.-Z., Kotakic, M., Ramakrishna, S., 2003, A review on polymer nanofibers by electrospinning andtheir applications in nanocomposites.*Compos. Sci. Technol.,* 63, 2223–2253.

101. Beachley, V., Wen, X., 2009, Effect of electrospinning parameters on the nanofiber diameter and length, *Mater. Sci. Eng., A,* 29, 663-668.

102. Cramariuc, B., Cramariuc, R., Scarlet, R., Manea, L. R., Lupu, L. G., Cramariuc, O., 2013, Fiber diameter in electrospinning process, *J. Electrostat.,* 71, 189-198.

103. Mogoşanu, G. D., Grumezescu, A. M., 2014, Natural and synthetic polymers for wounds and burns dressing, *Int. J. Pharm.*, 463, 127-136.

104. Hu, X., Liu, S., Zhou, G., Huang, Y., Xie, Z., Jing, X., 2014, Electrospinning of polymeric nanofibers for drug delivery applications, *J. Controlled Release*, 185, 12-21.

105. Gorji, M., Bagherzadeh, R., Fashandi, H., 2017, Electrospun Nanofibers: 21 – Electrospun nanofibers in protective clothing, Ed: Mehdi Afshari, Woodhead Publishing Series in Textiles, United Kingdom, 571–598.

106. Aussawasathien, D., Dong, J.-H, Dai, L., 2005, Electrospun polymer nanofiber sensors, *Synthetic Metals*, 154, 37-40.

107. Wang, P., Zhang, L., Xia, Y., Tong, L., Xu, X., Ying, Y., 2012, Polymer Nanofibers Embedded with Aligned Gold Nanorods: A New Platform for Plasmonic Studies and Optical Sensing, *Nano Lett*., 12, 3145–3150.

108. Deng, S., Bai, R., Chen, J. P., 2003, Aminated Polyacrylonitrile Fibers for Lead and Copper Removal, *Langmuir*, 19, 5058-5064.

109. Zhu, Z., Chen, Y., Gu, Y., Wu, F., Lu, W., Xu, T., Chen, W., 2016, Catalytic degradation of recalcitrant pollutants by Fenton-like processusing polyacrylonitrile-supported iron (II) phthalocyanine nanofibers: Intermediates and pathway, *Water Res.*, 93, 296-305.

110. Smith, W. N., 1989, US patent 07/146,847.

111. Soutis, C., 2005, Carbon fiber reinforced plastics in aircraft construction, *Mater. Sci. Eng. A,*412, 171-176.

112. Frackowiak, D., 1988, The Jablonski diagram, *J. Photochem.Photobiol. B: Biology,* 2, 399 – 408.

113. Nyokong, T., Antunes, E., 2010, Photochemical and photophysical properties of metallophthalocyanines, Eds: K. Kadish, K. Smith, R. Guilard, The handbook of pophyrin science, vol. 7, Academic Press, New York.

114. Lichtman, J. W., Conchello, J.-A., 2005, Fluorescence microscopy, *Nature Methods*, 2, 910-919.

115. DeRosa, M. C., Crutchley, R. J., 2002, Photosensitized singlet oxygen and its applications, *Coord. Chem. Rev.,* 233-234, 351-371.

116. Fery-Forgues, S., Lavabre, D., 1999, Are Fluorescence Quantum Yields So Tricky to Measure? A Demonstration Using Familiar Stationery Products, *J. Chem. Educ.,* 76, 1260-1264.

117. Ogunsipe, A., Chen, J., Nyokong, T., 2004, Photophysical and photochemical studies of zinc(II) phthalocyanine derivatives—effects of substituents and solvents, *New J. Chem.,* 28, 822-827.

118. Grossweiner, L., 1994, The Science of Phototherapy, CRC Press, Boca Raton Fla.

119. Brakenhoff, G. J., Mueller, M., Ghauharali, R.I., Visscher, K., 1995, in: Wilson, T., Cogswell, C. J. (Eds.), Proc. SPIE - Int. Soc. Opt. Eng., Society of Photo-Optical Instrumentation Engineers, San Jose, CA, USA, pp. 115-123.

120. Li, Q., Ruckstuhl, T., Seeger, S., 2004, Deep-UV Laser-Based Fluorescence Lifetime Imaging Microscopy of Single Molecules, *J. Phys. Chem. B,* 108, 8324-8329.

121. Ogunsipe, A., Nyokong, T., 2005, Photophysicochemical consequences of bovine serum albumin binding to non-transition metal phthalocyanine sulfonates, *Photochem. Photobiol. Sci.,* 4, 510-516.

122. Wilkinson, F., 1993, Quantum Yields for the Photosensitized Formation of the Lowest Electronically Excited Singlet State of Molecular Oxygen in Solution, *J. Phys. Chem. Ref. Data,*22, 113-262.

123. Ambroz, M., Beeby, A., McRobert, A. J., Simpson, M. S. C., Svensen, R. K., Phillips, D., 1991, Preparative, analytical and fluorescence spectroscopic studies of sulphonated aluminium phthalocyanine photosensitizers, *J. Photochem, Photobiol. B: Biol.,* 9, 87-95.

124. Pereira, J.B., Carvalho, E.F.A, Faustino, M. A. F., Fernandes, R., Neves, M.G.P.M.S., Cavaleiro, J. A. S., Gomes, N.C.M., Cunha, Â., Almeida, A. Tomé, J.P.C., 2012, Phthalocyanine Thio-Pyridinium Derivatives as Antibacterial Photosensitizers, *Photochem. Photobiol.,* 88, 537-547.

125. Srinivasan, N., Haney, C.A., Lindsey, J.S., Zhang, W., Chait, B.T., 1999,Investigation of MALDI-TOF Mass Spectrometry of Diverse Synthetic Metalloporphyrins, Phthalocyanines and Multiporphyrin Arrays, *J. Porphyrins Phthalocyanines,*32, 283–291.

126. Nyokong, T., 2010, In: Vol. Ed. Jiang. J. Series Ed. Mingos, D.M.P., Structure and Bonding: *Functional Phthalocyanine Molecular Materials*, Springer, vol 135, 45 -87.

127. Stillman, M.J., Nyokong T. In: P*hthalocyanines - Properties and Applications*, Edited by Lever, A.B.C. and Leznoff, C.C. VCH, New York, 1989, Vol. 1. Chapt. 3.

128. Hoo, C. M., Starostin, N., West, P., Mecartney M. L., 2008, A comparison of atomic force microscopy (AFM) and dynamic light scattering (DLS) methods to characterize nanoparticle size distributions, *J Nanopart Res.,* 10, 89-96.

129. Borker, P., Salker, A. V., 2006, Synthesis, characterization and photocatalytic studies of some metal phthalocyanines, *Indian J. Chem. Technol.,* 13,341-346.

130. Snow, A. W., Griffith, J. R., Marullo, N. P., 1984, Syntheses and Characterization of Heteroatom-Bridged Metal-Free Phthalocyanine Network Polymers and Model Compounds, *Macromolecules,*17, 1614-1624.

131. Jenkins, R., Synder, R.L., 1998 in: *Introduction to X-ray Diffractometry*. Wiley and Sons, New York.

132. Lacey, J.A., Phillips, D., 2002, Fluorescence lifetime measurements of disulfonated aluminium phthalocyanine in the presence of microbial cells, *Photochem. Photobiol. Sci.*, 1, 378-383.

133. Debacker, M.G., Deleplanque, O., Van Vlierberge, B., Sauvage, F.X., 1988,A Laser Photolysis Study of Triplet Lifetimes and of Triplet–Triplet Annihilation Reactions of Phthalocyanins in DMSO Solutions,*Laser Chem.,* 8, 1-11.

134. Sagun, E.I., Zenkevich, E.I., Knyukshuto, V.N., Shulga, A.M., Starukhin, D.A., von-Borczyskowski, C., 2002, Interaction of multiporphyrin systems with molecular oxygen in liquid solutions: extra-ligation and screening effects, *Chem Phys, 275,*211-230.

135. Auger, A., Burnham, P.M., Chambrier, I., Cook, M.J., Hughes, D.L., 2005, X-Ray crystallographic studies of three substituted indium(III) phthalocyanines: effect of ring substitution and the axial ligand on molecular geometry and packing, *J. Mat. Chem, 15,* 168-176.

136. Alagna, L. Capobianchi, A., Casaletto, M.P.,Mattogno, G.,Paoletti, A.M.,Pennesi, G., Rossi, G., 2001, Effect of molecular packing on the solid state spectraof ruthenium phthalocyanine: anomalous behaviour of a monodimensional stacked assembly, *J. Mater. Chem., 11*, 1928–1935.

137. Fong, H., Reneker, D. H., 1999, Elastomer nanofibers of styrene-butadiene-styrene tri-block copolymer, *J. Polym. Sci. B.,*37,3488-3493.

138. Brunauer, S., Deming, L. S., Deming, W. E., Teller, E., 1940,On the theory of Van der Waals adsorption of gases, *J. Am. Chem. Soc.,*62, 1723-1732.

139. Barry, A. L., Lasner, R. A., 1976, Inhibition of Bacterial Growth by the Nitrofurantoin Solvent Dimethylformamide, *Antimicrob. Agents Chemother.,* 9,549-550.

140. Malik, Z., Ladan, H., Nitzan, Y., 1992, Photodynamic inactivation of Gram-negative bacteria: Problems and possible solutions, *J. Photochem. Photobiol. B Biol.,*14, 262–265.

141. Bachmann, B. J., 1990, Linkage map of Escherichia coli K-12, *Microbiol. Rev.,* 54, 30–197.

142. Gow, N. A. R., Hube B., 2012, Importance of the Candida albicans cell wall during commensalism and infection, *Current Opinion in Microbiology*, 15, 406–412.

143. Kong, E. F.,Johnson, J.K., Jabra-Rizk, M. A., 2016,Community-Associated Methicillin-Resistant Staphylococcus aureus: An Enemy amidst Us, *PLOS Pathogens*,12, e1005837.

144. Minnock, A., Vernon, D. I., Schofield, J., Griffiths, J., Parish, J. H., Brown, S. B., 2000, Mechanism of Uptake of a Cationic Water-Soluble Pyridinium Zinc Phthalocyanine across the Outer Membrane ofEscherichia coli, *Antimicrob. Agents Chemother.*,44, 522-227.

145. Kertesz, M. A., 2000, Riding the sulfur cycle – metabolism of sulfonates and sulfate esters in Gram-negative bacteria, *FEMS Microbiology Reviews,* 24, 135–175.

146. Cowie, D. B.,Bolton, E. T. Sands, M. K., SULFUR METABOLISM IN ESCHERICHIA COLI II.Competitive Utilization of Labeled and Nonlabeled Sulfur Compounds, 1951, *J. Bact.,* 62, 63-74.

147. Wei, J., Tang, Q. X., Varlamova, O., Roche, C., Lee, R., Leyh, T. S., 2002,Cysteine Biosynthetic Enzymes Are the Pieces of a Metabolic Energy Pump,*Biochem.*, 41, 8493-8498.

148. Ben-Hur, E., Chan, W. S., 2003,in: K. Kadish, R. Guilard, K. M. Smith(Eds.), The Porphyrin Handbook, Academic Press,Boston, *Vol 19, Chpt 117, pp 1-35.*

149. Rosso, L., Lobry, J.R., Bajard, S., Flandrois, J.P., 1995, Convenient model to describe the combined effects of temperature and pH on microbial growth. *Appl. Environ. Microbio.,*61, 610-616.

150. Zhang, J-H., Liu, Q., Chen, Y-M., Liu, Z-Q., Xu, C-W., 2012, Determination of acid dissociation constant of methyl red by multi-peaks Gaussian fitting method based on Uv-visible absorption spectrum, *Acta Phys. Chim. Sin.,* 28,1030-1036.

151. Devi, L. G., Kumar, S. G., Reddy, K. M., Munikrishnappa, C., 2009, Photo degradation of Methyl Red an azo dye by Advance Fenton Process using zero valent metallic iron: Influence of various reaction parameters and its degradation mechanism, *J. Hazard Mater.,* 164, 459-467.